Supplementary material for the article:

Milošev, M. Z.; Jakovljević, K.; Joksović, M. D.; Stanojković, T.; Matić, I. Z.; Perović, M.; Tešić, V.; Kanazir, S.; Mladenović, M.; Rodić, M. V.; et al. Mannich Bases of 1,2,4-Triazole-3-Thione Containing Adamantane Moiety: Synthesis, Preliminary Anticancer Evaluation, and Molecular Modeling Studies. *Chemical Biology and Drug Design* **2017**, *89* (6), 943–952. https://doi.org/10.1111/cbdd.12920

Supporting Information

Mannich Bases of 1,2,4-Triazole-3-thione Containing Adamantane Moiety: Synthesis, Preliminary Anticancer Evaluation, and Molecular Modeling Studies

Milorad Z. Milošev,[1] Katarina Jakovljević,[2] Milan D. Joksović,[2] Tatjana Stanojković,[3] Ivana Z. Matić,[3] Milka Perović,[4] Vesna Tešić,[4] Selma Kanazir,[4] Milan Mladenović,[2] Marko V. Rodić,[5] Vukadin M. Leovac,[5] Snežana Trifunović[6] and Violeta Marković[2,*]

[1]*Faculty of Medicinal Science, University of Kragujevac, S. Markovića 69, 34000 Kragujevac, Serbia*

[2]*Faculty of Science, Department of Chemistry, University of Kragujevac, R. Domanovića 12, 34000 Kragujevac, Serbia*

[3]*Institute of Oncology and Radiology of Serbia, Pasterova 14, 11000 Belgrade, Serbia*

[4]*Institute for Biological Research "Siniša Stanković", Department of Neurobiology, University of Belgrade, Bulevar Despota Stefana 142, 11060 Belgrade, Serbia*

[5]*Faculty of Sciences, University of Novi Sad, Trg D. Obradovića 3, 21000 Novi Sad, Serbia*

[6]*Faculty of Chemistry, University of Belgrade, Studentski trg 12–16, 11000 Belgrade, Serbia*

**Corresponding author: Violeta Marković, markovicvioleta@kg.ac.rs*

Procedure for the preparation of 5a-r

To the solution of 1-adamantanecarboxylic acid **1** (0.541 g, 3.00 mmol) in dry dichloromethane (10.0 mL), $SOCl_2$ (0.9 mL, 12.00 mmol) was slowly added, followed by two drops of dimethylformamide. The resulting mixture was then stirred for 2 h at room temperature. Afterwards, the solvent was evaporated under reduced pressure, and the excess of $SOCl_2$ was removed by azeotropic distillation with toluene. To the formed 1-adamantanecarbonyl chloride **2**, thiosemicarbazide (0.301 g, 3.30 mmol) and dry tetrahydrofuran (10.0 mL) were added, and resulting mixture was stirred at room temperature for 6 h. Afterwards, the solvent was evaporated under reduced pressure, 30 mL of H_2O was added to the residue and the formed suspension was stirred for 30 minutes, filtrated and dried over $CaCl_2$. In the next step, the obtained 1-adamantoylthiosemicarbazone **3** (0.617 g, 2.44 mmol) was treated with aqueous solution of sodium hydroxide (2 M, 45.00 mmol), and the mixture was then refluxed for 3h. After cooling, the clear solution was acidified using 2M HCl until pH 1 was reached, followed with a formation of a precipitate. The mixture was left standing for 1 h at 4 °C and compound **4** was filtered off and dried over $CaCl_2$. The synthesized 5-adamantyl-1,2,4-triazole-3-thione **4** was obtained with very high purity and it is used for further synthesis without any purification. To the mixture of **4** (0.200 g, 0.85 mmol) in THF, the corresponding primary arylamine (0.85 mmol) and 36.5 % solution of formaldehyde (0.070 g, 0.85 mmol) were added and stirred at room temperature for 48 h. Then, the solvent was evaporated, and EtOH (3.0 mL) was added to the resulting residue, followed with the formation of the suspension which was left to stand overnight at 4 °C. The formed solid (**5a-r**) was then filtered off and dried over $CaCl_2$. The final compounds **5a-r** were obtained with satisfactory purity and did not require any further purification.

5-Adamantyl-2H-1,2,4-triazole-3(4H)-thione (**4**): White powder; yield: 0.52 g (90%); mp: > 250 ºC (Dec.); ^{1}H NMR (200 MHz, DMSO-d_6): 1.69, (s, 6H, Ad); 1.86, (s, 3H, Ad); 1.87, (s, 3H,Ad); 1.99, (s, 3H, Ad); 13.10, (s, 1H, NH); 13.18, (s, 1H, NH); ^{13}C NMR (50 MHz, DMSO-d_6): 27.40, 33.25, 35.89, 39.44, 159.31, 166.25; IR (KBr, cm^{-1}): 3137, 3072, 2914, 2852, 1581, 1499, 1225, 726; Anal. Calcd. For $C_{12}H_{17}N_3S$ (235.35 g/mol): C, 61.24; H, 7.28; N, 17.85; S, 13.62; Found: C, 61.35; H, 7.30; N, 17.79; S, 13.60.

2-(N-Phenylaminomethyl)-5-adamantyl-2H-1,2,4-triazole-3(4H)-thione × *H_2O* (**5a**): Light yellow powder; yield: 0.16 g (52%); mp: > 250 ºC (Dec.); ^{1}H NMR (200 MHz, DMSO-d_6): 1.77, (s, 6H, Ad); 1.93, (s, 3H, Ad); 1.94, (s, 3H,Ad); 2.09, (s, 3H, Ad); 5.19, (t, 1H, *J* = 7.8 Hz, NH-CH_2), 5.50 (d, 2H, *J* = 7.8 Hz, CH_2), 6.79, (t, 1H, *J* = 7.4 Hz, Ar-H), 6.94, (d, 2H, *J* = 8.0 Hz, Ar-H), 7.17, (d, 1H, *J* = 7.4 Hz, Ar-H), 7.21, (d, 1H, *J* = 8.0 Hz, Ar-H), 12.29, (s, 1H, NH); ^{13}C NMR (50 MHz, DMSO-d_6): 27.80, 33.92, 36.20, 40.28, 57.64, 114.23, 119.30, 129.17, 144.72, 158.39, 164.01; IR (KBr, cm^{-1}): 3355, 2910, 2850, 1605, 1569, 1472, 1253, 753; Anal. Calcd. For $C_{19}H_{24}N_4SxH_2O$ (358.51 g/mol): C, 63.66; H, 7.31; N, 15.63; S, 8.94; Found: C, 63.47; H, 7.29; N, 15.58; S, 8.92.

2-(N-(o-Tolyl)aminomethyl)-5-adamantyl-2H-1,2,4-triazole-3(4H)-thione (**5b**): White crystals; yield: 0.18 g (61%); mp: 179–180 ºC; ^{1}H NMR (200 MHz, DMSO-d_6): 1.77, (s, 6H, Ad); 1.92, (s, 3H, Ad); 1.94, (s, 3H,Ad); 2.09, (s, 3H, Ad); 2.20, (s, 3H, CH_3), 5.16, (t, 1H, *J* = 8.0 Hz, NH-CH_2), 5.55 (d, 2H, *J* = 8.0 Hz, CH_2); 6.73, (td, 1H, *J* = 7.0 and 1.6 Hz, Ar-H), 7.05, (d, 1H, *J* =

7.0 Hz, Ar-H), 7.15, (td, 2H, *J* = 8.0 and 1.6 Hz, Ar-H), 12.08, (s, 1H, NH); ^{13}C NMR (50 MHz, DMSO-d_6): 17.38, 27.83, 33.92, 36.23, 40.32, 57.62, 112.00, 119.01, 123.30, 126.95, 130.36, 142.83, 158.25, 163.97; IR (KBr, cm^{-1}): 3395, 2909, 2850, 1609, 1589, 1563, 1465, 1258, 751; Anal. Calcd. For $C_{20}H_{26}N_4S$ (354.52 g/mol): C, 67.76; H, 7.39; N, 15.80; S, 9.04; Found: C, 68.02; H, 7.41; N, 15.82; S, 9.07.

2-(N-(m-Tolyl)aminomethyl)-5-adamantyl-2H-1,2,4-triazole-3(4H)-thione x 3 H_2O (**5c**): Light yellow powder; yield: 0.18 g (52%); mp: 146–147 ºC; ^{1}H NMR (200 MHz, DMSO-d_6): 1.77, (s, 6H, Ad); 1.94, (s, 3H, Ad); 1.95, (s, 3H,Ad); 2.09, (s, 3H, Ad); 2.27, (s, 3H, CH_3), 5.15, (t, 1H, *J* = 7.6 Hz, NH-CH_2), 5.48 (d, 2H, *J* = 7.6 Hz, CH_2), 6.61, (d, 1H, *J* = 7.6 Hz, Ar-H), 6.72-6.79, (m, 2H, Ar-H), 7.07, (t, 2H, *J* = 7.6 Hz, Ar-H), 12.50, (s, 1H, NH); ^{13}C NMR (50 MHz, DMSO-d_6): 21.49, 27.83, 33.93, 36.24, 40.33, 57.70, 111.34, 115.10, 120.19, 129.03, 139.01, 144.72, 158.28, 164.07; IR (KBr, cm^{-1}): 3365, 2909, 2851, 1609, 1571, 1471, 1269, 752; Anal. Calcd. For $C_{20}H_{26}N_4Sx3H_2O$ (408.57 g/mol): C, 58.80; H, 7.89; N, 13.71; S, 7.85; Found: C, 59.03; H, 7.88; N, 13.69; S, 7.86.

2-(N-(p-Tolyl)aminomethyl)-5-adamantyl-2H-1,2,4-triazole-3(4H)-thione x 1.5 H_2O (**5d**): Light yellow powder; yield: 0.17 g (53%); mp: 177–178 ºC; ^{1}H NMR (200 MHz, DMSO-d_6): 1.77, (s, 6H, Ad); 1.93, (s, 3H, Ad); 1.94, (s, 3H,Ad); 2.09, (s, 3H, Ad); 2.22, (s, 3H, CH_3), 5.10, (t, 1H, *J* = 7.0 Hz, NH-CH_2), 5.47 (d, 2H, *J* = 7.0 Hz, CH_2), 6.84, (d, 2H, J_{AB} = 8.2 Hz, Ar-H), 6.99, (d, 2H, J_{BA} = 8.2 Hz, Ar-H), 12.47, (s, 1H, NH); ^{13}C NMR (50 MHz, DMSO-d_6): 20.41, 27.84, 33.92, 36.24, 40.32, 58.08, 114.42 (2C), 128.56, 129.69 (2C), 142.31, 158.29, 164.04; IR (KBr, cm^{-1}): 3356, 2915, 2851, 1617, 1569, 1526, 1469, 1258, 812; Anal. Calcd. For $C_{20}H_{26}N_4Sx1.5H_2O$ (381.54 g/mol): C, 62.96; H, 7.66; N, 14.68; S, 8.40; Found: C, 62.85; H, 7.64; N, 14.63; S, 8.38.

2-(N-(2-Fluorophenyl)aminomethyl)-5-adamantyl-2H-1,2,4-triazole-3(4H)-thione (**5e**): White powder; yield: 0.16 g (54%); mp: 194–195 ºC; ^{1}H NMR (200 MHz, DMSO-d_6): 1.77, (s, 6H, Ad); 1.94, (s, 3H, Ad); 1.95, (s, 3H,Ad); 2.10, (s, 3H, Ad); 5.32-5.41, (m, 1H, NH-CH_2), 5.53 (d, 2H, *J* = 7.4 Hz, CH_2), 6.66-6.77, (m, 1H, Ar-H), 6.94, (dd, 1H, *J* = 8.2 and 1.4 Hz, Ar-H), 6.97-7.03, (m, 1H, Ar-H), 7.31, (td, 1H, *J* = 8.2 and 1.4 Hz, Ar-H), 12.56, (s, 1H, NH); ^{13}C NMR (50 MHz, DMSO-d_6): 27.82, 33.98, 36.22, 40.30, 56.82, 114.30 (J_{CF} = 2.2 Hz), 114.77 (J_{CF} = 18.6 Hz), 118.99 (J_{CF} = 6.9 Hz), 124.40 (J_{CF} = 3.5 Hz), 133.25 (J_{CF} = 11.2 Hz), 151.84 (J_{CF} = 238.6 Hz), 158.60, 164.29; IR (KBr, cm^{-1}): 3363, 2909, 2851, 1623, 1571, 1529, 1467, 1195, 744; Anal. Calcd. For $C_{19}H_{23}FN_4S$ (358.48 g/mol): C, 63.66; H, 6.47; N, 15.63; S, 8.94; Found: C, 63.59; H, 6.48; N, 15.69; S, 8.91.

2-(N-(3-Fluorophenyl)aminomethyl)-5-adamantyl-2H-1,2,4-triazole-3(4H)-thione (**5f**): White powder; yield: 0.15 g (50%); mp: 198–199 ºC; ^{1}H NMR (200 MHz, DMSO-d_6): 1.77, (s, 6H, Ad); 1.94, (s, 3H, Ad); 1.95, (s, 3H,Ad); 2.10, (s, 3H, Ad); 5.28, (t, 1H, *J* = 7.8 Hz, NH-CH_2), 5.47 (d, 2H, *J* = 7.8 Hz, CH_2), 6.47, (td, 1H, *J* = 8.2 and 2.2 Hz, Ar-H), 6.64-6.77, (m, 2H, Ar-H), 7.05-7.17, (m, 1H, Ar-H), 12.42, (s, 1H, NH); ^{13}C NMR (50 MHz, DMSO-d_6): 27.81, 33.97, 36.21, 40.31, 57.37, 101.34 (J_{CF} = 25.7 Hz), 105.87 (J_{CF} = 21.4 Hz), 110.00 (J_{CF} = 2.0 Hz), 116.79 (J_{CF} = 9.9 Hz), 146.66 (J_{CF} = 10.7 Hz), 158.53, 163.88 (J_{CF} = 242.8 Hz), 164.22; IR (KBr, cm^{-1}): 3356, 2911, 2851, 1617, 1568, 1478, 1156, 765; Anal. Calcd. For $C_{19}H_{23}FN_4S$ (358.48 g/mol): C, 63.66; H, 6.47; N, 15.63; S, 8.94; Found: C, 63.56; H, 6.46; N, 15.61; S, 8.96.

2-(N-(4-Fluorophenyl)aminomethyl)-5-adamantyl-2H-1,2,4-triazole-3(4H)-thione x H_2O (**5g**): Light yellow powder; yield: 0.17 g (54%); mp: 243–244 ºC; ^{1}H NMR (200 MHz, DMSO-d_6): 1.77, (s, 6H, Ad); 1.92, (s, 3H, Ad); 1.93, (s, 3H,Ad); 2.09, (s, 3H, Ad); 5.10, (t, 1H, *J* = 6.4 Hz, NH-CH_2); 5.45, (d, 2H, *J* = 6.4 Hz, CH_2); 6.88, (d, 4H, *J* = 6.4 Hz, Ar-H); 12.16, (s, 1H, NH); ^{13}C NMR (50 MHz, DMSO-d_6): 27.86, 33.95, 36.25, 40.38, 58.44, 115.66 (2C, J_{CF} = 7.6 Hz), 115.68 (2C, J_{CF} = 22.2 Hz), 140.95, 154.66, 158.26, 159.40, 164.40; IR (KBr, cm^{-1}): 3403, 2930, 2921, 2852, 1570, 1529, 1469, 1223, 815; Anal. Calcd. For $C_{19}H_{23}FN_4SxH_2O$ (376.50 g/mol): C, 60.61; H, 6.69; N, 14.88; S, 8.52; Found: C, 60.56; H, 6.68; N, 14.86; S, 8.54.

2-(N-(2-Trifluoromethylphenyl)aminomethyl)-5-adamantyl-2H-1,2,4-triazole-3(4H)-thione x 0.5 H_2O (**5h**): White powder; yield: 0.16 g (45%); mp: 205–206 ºC; ^{1}H NMR (200 MHz, DMSO-d_6): 1.77, (s, 6H, Ad); 1.94, (s, 3H, Ad); 1.96, (s, 3H,Ad); 2.10, (s, 3H, Ad); 5.54, (d, 2H, *J* =7.6 Hz, CH_2), 5.80, (t, 1H, *J* = 7.6 Hz, NH-CH_2), 6.77-6.89, (m, 1H, Ar-H), 7.39, (d, 2H, *J* = 3.4 Hz, Ar-H), 7.46, (d, 1H, *J* = 7.6 Hz, Ar-H), 12.56, (s, 1H, NH); ^{13}C NMR (50 MHz, DMSO-d_6): 27.81, 34.00, 36.20, 40.31, 56.70, 114.04, 115.08 (J_{CF} = 29.5 Hz), 118.36, 124.77 (J_{CF} = 271.2 Hz), 126.7 (m,CF_3), 133.03, 142.79, 158.71, 164.42; IR (KBr, cm^{-1}): 3080, 2913, 2852, 1616, 1591, 1527, 1466, 1106, 755; Anal. Calcd. For $C_{20}H_{23}F_3N_4Sx0.5H_2O$ (417.50 g/mol): C, 57.54; H, 5.79; N, 13.42; S, 7.68; Found: C, 57.61; H, 5.78; N, 13.45; S, 7.70.

2-(N-(3-Trifluoromethylphenyl)aminomethyl)-5-adamantyl-2H-1,2,4-triazole-3(4H)-thione (**5i**): White powder; yield: 0.16 g (47%); mp: >250 ºC; ^{1}H NMR (200 MHz, DMSO-d_6): 1.77, (s, 6H, Ad); 1.92, (s, 3H, Ad); 1.94, (s, 3H,Ad); 2.10, (s, 3H, Ad); 5.37, (t, 1H, *J* = 7.6 Hz, NH-CH_2); 5.51, (d, 2H, *J* = 7.6 Hz, CH_2); 7.01-7.08, (m, 2H, Ar-H); 7.24-7.26, (m, 2H, Ar-H); 12.22, (s, 1H, NH); ^{13}C NMR (50 MHz, DMSO-d_6): 27.84, 33.96, 36.24, 40.32, 57.39, 110.79 (J_{CF} = 3.6 Hz), 115.91 (J_{CF} = 3.7 Hz), 119.55 (J_{CF} = 194.2 Hz), 126.91, 130.78 (m, CF_3), 145.23, 158.31, 164.52; IR (KBr, cm^{-1}): 3351, 2931, 2913, 2849, 1618, 1570, 1475, 1324, 1170, 792; Anal. Calcd. For $C_{20}H_{23}F_3N_4S$ (408.49 g/mol): C, 58.81; H, 5.68; N, 13.72; S, 7.85; Found: C, 58.98; H, 5.70; N, 13.71; S, 7.87.

2-(N-(2-Chlorophenyl)aminomethyl)-5-adamantyl-2H-1,2,4-triazole-3(4H)-thione (**5j**): White powder; yield: 0.17 g (54%); mp: 204–205 ºC; ^{1}H NMR (200 MHz, DMSO-d_6): 1.77, (s, 6H, Ad); 1.94, (s, 3H, Ad); 1.96, (s, 3H,Ad); 2.10, (s, 3H, Ad); 5.56, (d, 2H, *J* = 7.4 Hz, CH_2), 5.74, (t, 1H, *J* = 7.4 Hz, NH-CH_2); 6.72, (td, 1H, *J* = 7.6 and 1.4 Hz, Ar-H), 7.14, (td, 1H, *J* = 7.6 and 1.4 Hz, Ar-H), 7.25, (dd, 1H, *J* = 8.0 and 1.4 Hz, Ar-H), 7.32, (dd, 1H, *J* = 8.0 and 1.4 Hz, Ar-H); 12.39, (s, 1H, NH); ^{13}C NMR (50 MHz, DMSO-d_6): 27.87, 33.99, 36.25, 40.35, 56.84, 113.47, 119.47, 120.24, 127.66, 129.36, 141.17, 158.45, 164.56; IR (KBr, cm^{-1}): 3370, 2911, 2851, 1560, 1565, 1509, 1459, 1272, 747; Anal. Calcd. For $C_{19}H_{23}ClN_4S$ (374.94 g/mol): C, 60.86; H, 6.18; N, 14.94; S, 8.55; Found: C, 60.80; H, 6.19; N, 14.99; S, 8.53.

2-(N-(3-Chlorophenyl)aminomethyl)-5-adamantyl-2H-1,2,4-triazole-3(4H)-thionex 0.5 H_2O (**5k**): White powder; yield: 0.11 g (33%); mp: 192–193 ºC; ^{1}H NMR (200 MHz, DMSO-d_6): 1.77, (s, 6H, Ad); 1.94, (s, 3H, Ad); 1.95, (s, 3H,Ad); 2.10, (s, 3H, Ad); 5.24, (t, 1H, *J* = 7.8 Hz, NH-CH_2); 5.46, (d, 2H, *J* = 7.8 Hz, CH_2); 6.77, (td, 2H, *J* = 8.0 and 2.0 Hz, Ar-H), 7.00, (t, 1H, *J* = 2.0 Hz, Ar-H), 7.09, (t, 1H, *J* = 8.0 Hz, Ar-H); 12.33, (s, 1H, NH); ^{13}C NMR (50 MHz, DMSO-d_6): 27.82, 33.96, 36.22, 40.33, 57.34, 112.51, 114.37, 119.34, 130.17, 135.00, 146.02, 158.40, 164.31; IR (KBr, cm^{-1}): 3345, 2909, 2850, 1602, 1571, 1474, 1231, 770; Anal. Calcd.

For $C_{19}H_{23}ClN_4Sx0.5H_2O$ (383.95 g/mol): C, 59.44; H, 6.30; N, 14.59; S, 8.35; Found: C, 59.31; H, 6.35; N, 14.54; S, 8.36.

2-(N-(4-Chlorophenyl)aminomethyl)-5-adamantyl-2H-1,2,4-triazole-3(4H)-thione x 0.5 H_2O (**5l**): Yellow powder; yield: 0.16 g (48%); mp: 204–205 ºC (Dec.); ^{1}H NMR (200 MHz, DMSO-d_6): 1.77, (s, 6H, Ad); 1.92, (s, 3H, Ad); 1.94, (s, 3H,Ad); 2.10, (s, 3H, Ad); 5.19, (t, 1H, J = 7.8 Hz, NH-CH_2); 5.46, (d, 2H, J = 7.8 Hz, CH_2); 6.87, (d, 2H, J_{AB} = 9.0 Hz, Ar-H), 7.13, (d, 2H, J_{BA} = 9.0 Hz, Ar-H); 12.36, (s, 1H, NH); ^{13}C NMR (50 MHz, DMSO-d_6): 27.80, 33.94, 36.19, 40.31, 57.59, 115.52 (2C), 124.19, 129.07 (2C), 143.34, 158.47, 164.20; IR (KBr, cm^{-1}): 3346, 2908, 2853, 1603, 1570, 1458, 1269, 813; Anal. Calcd. For $C_{19}H_{23}ClN_4Sx0.5H_2O$ (383.95 g/mol): C, 59.44; H, 6.30; N, 14.59; S, 8.35; Found: C, 59.37; H, 6.29; N, 14.62; S, 8.33.

2-(N-(2-Nitrophenyl)aminomethyl)-5-adamantyl-2H-1,2,4-triazole-3(4H)-thione x 2 H_2O (**5m**): Yellow powder; yield: 0.18 g (50%); mp: 211–212 ºC; ^{1}H NMR (200 MHz, DMSO-d_6): 1.78, (s, 6H, Ad); 1.95, (s, 3H, Ad); 1.97, (s, 3H,Ad); 2.11, (s, 3H, Ad); 5.65, (d, 2H, J = 7.4 Hz, CH_2); 6.76-6.84, (m, 1H, Ar-H), 7.45-7.53, (m, 1H, Ar-H); 7.62, (dd, 1H, J = 8.4 and 0.8 Hz, Ar-H); 8.18, (dd, 1H, J = 8.4 and 1.6 Hz, Ar-H); 8.82, (t, 1H, J = 7.8 Hz, NH-CH_2); 12.60, (s, 1H, NH); ^{13}C NMR (50 MHz, DMSO-d_6): 27.77, 34.04, 36.17, 40.27, 55.42, 115.35, 117.71, 126.68, 133.57, 136.00, 142.83, 158.96, 164.72; IR (KBr, cm^{-1}): 3394, 2909, 2851, 1620, 1577, 1514, 1242, 741; Anal. Calcd. For $C_{19}H_{23}N_5O_2Sx2H_2O$ (421.52 g/mol): C, 54.14; H, 6.46; N, 16.61; S, 7.61; Found: C, 54.21; H, 6.44; N, 16.58; S, 7.59.

2-(N-(3-Nitrophenyl)aminomethyl)-5-adamantyl-2H-1,2,4-triazole-3(4H)-thione x 2.5 H_2O (**5n**): Light orange powder; yield: 0.20 g (55%); mp: 182–183 ºC; ^{1}H NMR (200 MHz, DMSO-d_6): 1.78, (s, 6H, Ad); 1.94, (s, 3H, Ad); 1.95, (s, 3H,Ad); 2.11, (s, 3H, Ad); 5.49-5.58, (m, 3H, NH-CH_2 and CH_2); 7.21, (ddd, 1H, J = 8.0, 2.2 and 1.0 Hz, Ar-H), 7.32, (t, 1H, J = 8.0 Hz, Ar-H); 7.63, (ddd, 1H, J = 8.0, 2.2 and 1.0 Hz, Ar-H); 7.88, (t, 1H, J = 2.2 Hz, Ar-H); 12.27, (s, 1H, NH); ^{13}C NMR (50 MHz, DMSO-d_6): 27.77, 33.97, 36.17, 40.29, 57.13, 108.63, 114.10, 120.15, 129.81, 145.92, 149.32, 158.57, 164.48; IR (KBr, cm^{-1}): 3340, 2909, 2852, 1624, 1571, 1532, 1470, 1347, 752; Anal. Calcd. For $C_{19}H_{23}N_5O_2Sx2.5H_2O$ (430.53 g/mol): C, 53.01; H, 6.56; N, 16.27; S, 7.45; Found: C, 53.16; H, 6.57; N, 16.25; S, 7.48.

2-(N-(4-Nitrophenyl)aminomethyl)-5-adamantyl-2H-1,2,4-triazole-3(4H)-thione x 0.5 H_2O (**5o**): Yellow powder; yield: 0.24 g (72%); mp: 237–238 ºC (Dec.); ^{1}H NMR (200 MHz, DMSO-d_6): 1.78, (s, 3H, Ad); 1.79, (s, 3H, Ad); 1.93, (s, 3H, Ad); 1.95, (s, 3H,Ad); 2.12, (s, 3H, Ad);); 5.55, (d, 2H, J = 7.6 Hz, CH_2); 5.75, (t, 1H, J = 7.6 Hz, NH-CH_2); 6.98, (d, 2H, J_{AB} = 9.2 Hz, Ar-H), 8.11, (d, 2H, J_{BA} = 9.2 Hz, Ar-H); 12.18, (s, 1H, NH); ^{13}C NMR (50 MHz, DMSO-d_6): 27.80, 34.03, 36.19, 40.38, 56.39, 113.12 (2C), 126.00 (2C), 140.24, 150.55, 158.67, 164.91; IR (KBr, cm^{-1}): 3339, 2906, 2852, 1603, 1508, 1466, 1330, 1110, 754; Anal. Calcd. For $C_{19}H_{23}N_5O_2Sx0.5H_2O$ (394.50 g/mol): C, 57.85; H, 6.13; N, 17.75; S, 8.13; Found: C, 57.99; H, 6.11; N, 17.69; S, 8.15.

2-(N-(2-Acetylphenyl)aminomethyl)-5-adamantyl-2H-1,2,4-triazole-3(4H)-thione x 3 H_2O (**5p**): Beige powder; yield: 0.22 g (60%); mp: 204–205 ºC (Dec.); ^{1}H NMR (200 MHz, DMSO-d_6): 1.77, (s, 6H, Ad); 1.94, (s, 3H, Ad); 1.95, (s, 3H, Ad); 2.09, (s, 3H, Ad); 2.60, (s, 3H, CH_3); 5.58, (d, 2H, J =7.2 Hz, CH_2); 6.69-6.77, (m, 1H, Ar-H); 7.35-7.49, (m, 1H, Ar-H); 7.45, (d, 1H, J = 1.4 Hz, Ar-H); 7.77, (dd, 1H, J = 8.0 and 1.4 Hz, Ar-H); 9.72, (t, 1H, J = 7.2 Hz, NH-CH_2); 12.38, (s, 1H, NH); ^{13}C NMR (50 MHz, DMSO-d_6): 27.84, 28.07, 33.96, 36.24, 40.27, 55.65,

113.60, 116.53, 119.08, 132.44, 134.89, 148.60, 158.54, 164.43, 201.04; IR (KBr, cm^{-1}): 3319, 2911, 2850, 1643, 1580, 1571, 1520, 1465, 1235, 756; Anal. Calcd. For $C_{21}H_{26}N_4OSx3H_2O$ (436.58 g/mol): C, 57.77; H, 7.39; N, 12.83; S, 7.34; Found: C, 57.90; H, 7.40; N, 12.79; S, 7.36.

2-(N-(3-Acetylphenyl)aminomethyl)-5-adamantyl-2H-1,2,4-triazole-3(4H)-thione x 0.5 H_2O (**5q**): White powder; yield: 0.23 g (69%); mp: 193–194 ºC (Dec.); ^{1}H NMR (200 MHz, DMSO-d_6): 1.76, (s, 3H, Ad); 1.77, (s, 3H, Ad); 1.93, (s, 3H, Ad); 1.94, (s, 3H,Ad); 2.10, (s, 3H, Ad); 2.51, (s, 3H, CH_3); 5.31, (d, 2H, *J* =7.0 Hz, CH_2), 5.54, (t, 1H, *J* = 7.0 Hz, NH-CH_2); 7.13, (ddd, 1H, *J* = 7.8, 2.0 and 1.0 Hz, Ar-H), 7.27, (t, 1H, *J* = 7.8 Hz, Ar-H), 7.39, (dt, 1H, *J* = 7.8 and 1.0 Hz, Ar-H); 7.56, (t, 1H, *J* = 2.0 Hz, Ar-H); 12.25, (s, 1H, NH); ^{13}C NMR (50 MHz, DMSO-d_6): 26.82, 27.77, 33.94, 36.18, 40.28, 57.30, 113.74, 118.86, 119.36, 129.37, 138.19, 145.06, 158.50, 164.28, 198.36; IR (KBr, cm^{-1}): 3343, 2914, 2849, 1685, 1589, 1569, 1468, 1241, 786; Anal. Calcd. For $C_{21}H_{26}N_4OSx0.5H_2O$ (391.54 g/mol): C, 64.42; H, 6.95; N, 14.31; S, 8.19; Found: C, 64.55; H, 6.94; N, 14.33; S, 8.22.

2-(N-(4-Acetylphenyl)aminomethyl)-5-adamantyl-2H-1,2,4-triazole-3(4H)-thione x 0.5 H_2O (**5r**): Light beige powder; yield: 0.20 g (59%); mp: 218–219 ºC (Dec.); ^{1}H NMR (200 MHz, DMSO-d_6): 1.77, (s, 3H, Ad); 1.78, (s, 3H, Ad); 1.93, (s, 3H, Ad); 1.94, (s, 3H,Ad); 2.11, (s, 3H, Ad); 2.51, (s, 3H, CH_3); 5.54, (s, 3H, NH-CH_2 and CH_2); 6.96, (d, 2H, J_{AB} = 8.8 Hz, Ar-H); 7.85, (d, 2H, J_{BA} = 8.8 Hz, Ar-H), 11.95, (s, 1H, NH); ^{13}C NMR (50 MHz, DMSO-d_6): 26.06, 27.84, 33.97, 36.23, 40.37, 56.74, 113.26 (2C), 128.95, 130.55 (2C), 149.20, 158.31, 164.86, 196.48; IR (KBr, cm^{-1}): 3346, 2910, 1653, 1598, 1469, 1265, 845; Anal. Calcd. For $C_{21}H_{26}N_4OSx0.5H_2O$ (391.54 g/mol): C, 64.42; H, 6.95; N, 14.31; S, 8.19; Found: C, 64.35; H, 6.97; N, 14.26; S, 8.17.

Copies of ^{1}H and ^{13}C NMR spectra

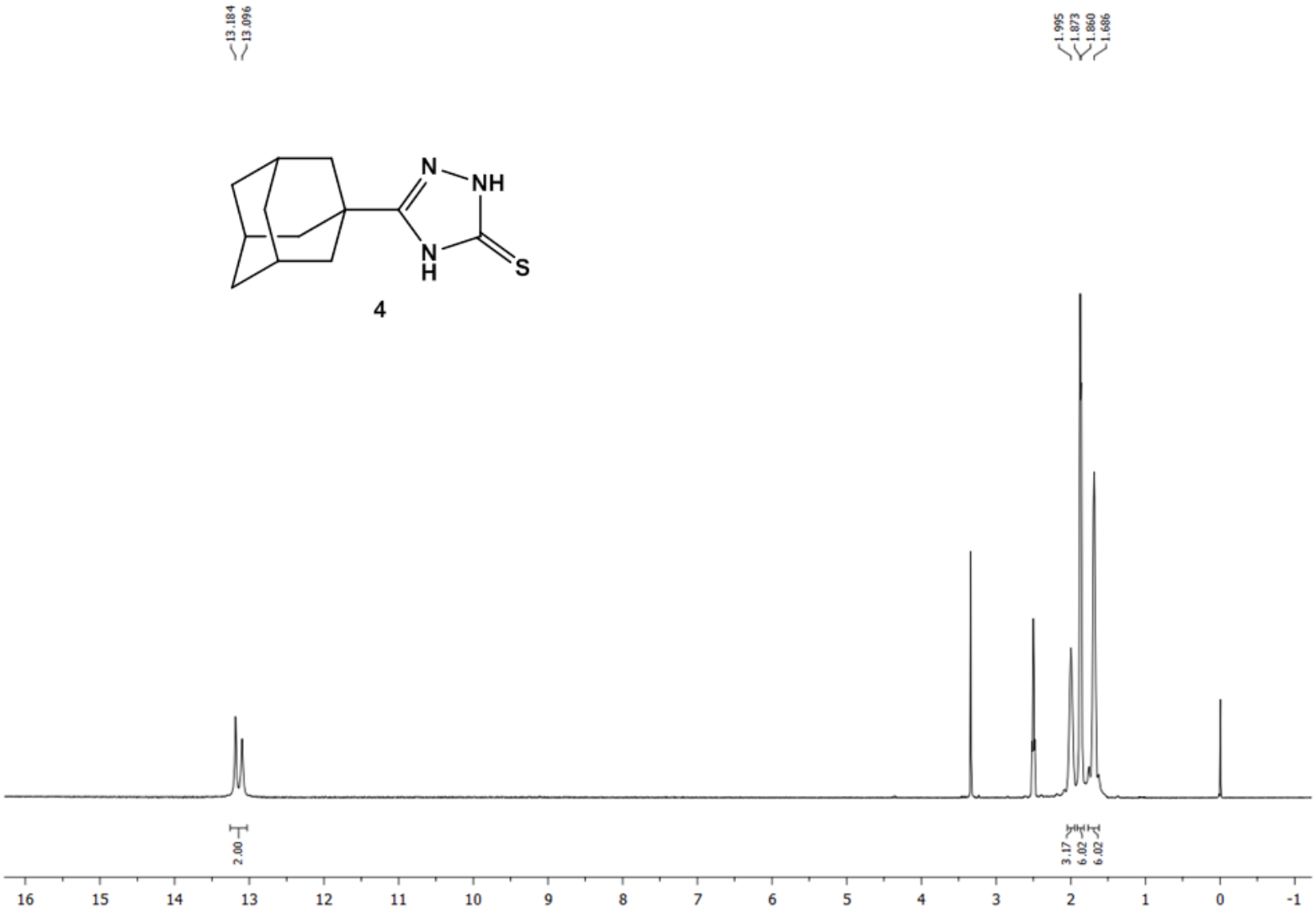

Figure S1: ^{1}H NMR spectrum of **4** in DMSO-d_6 (200 MHz).

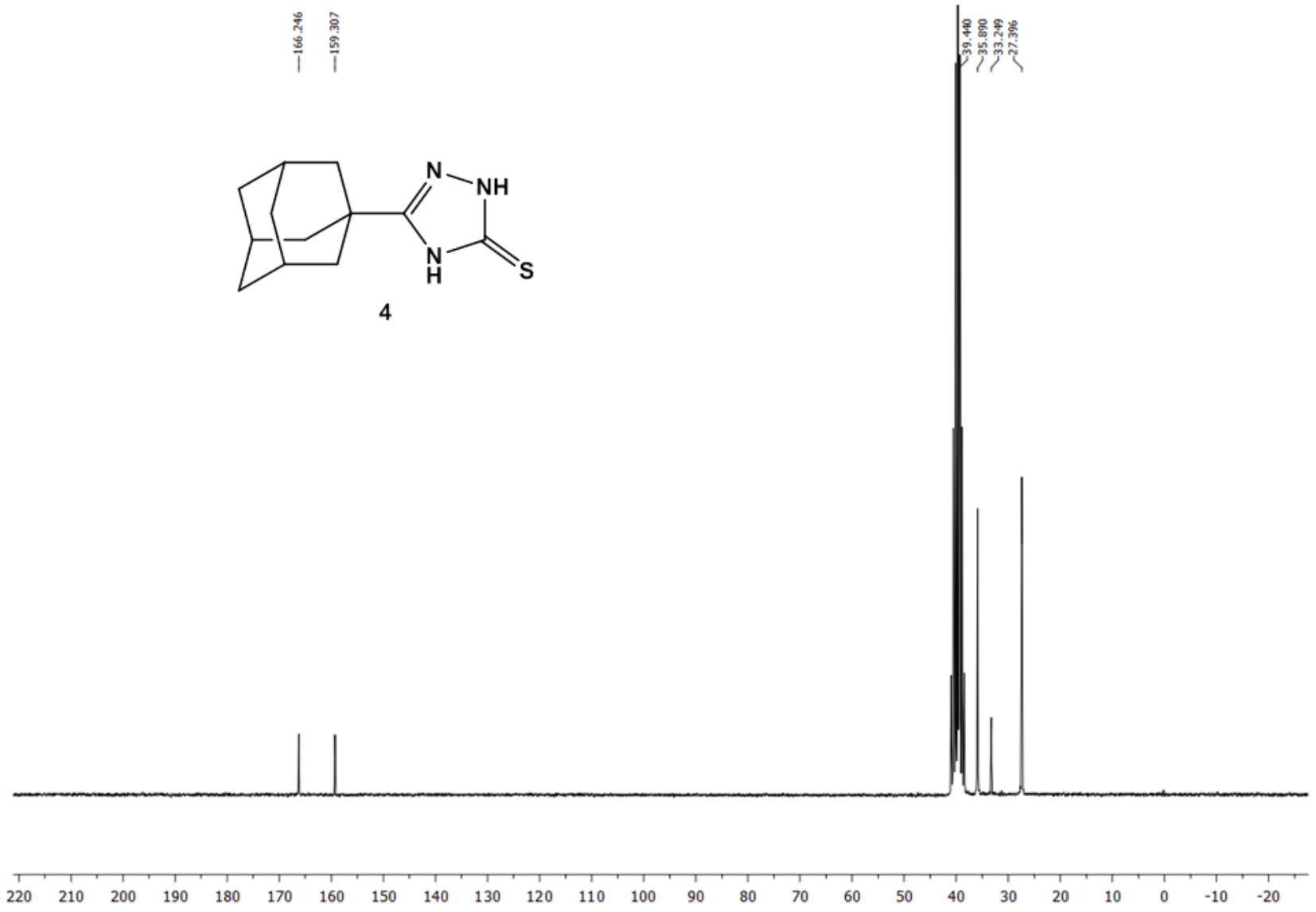

Figure S2: ^{13}C NMR spectrum of **4** in DMSO-d_6 (50 MHz).

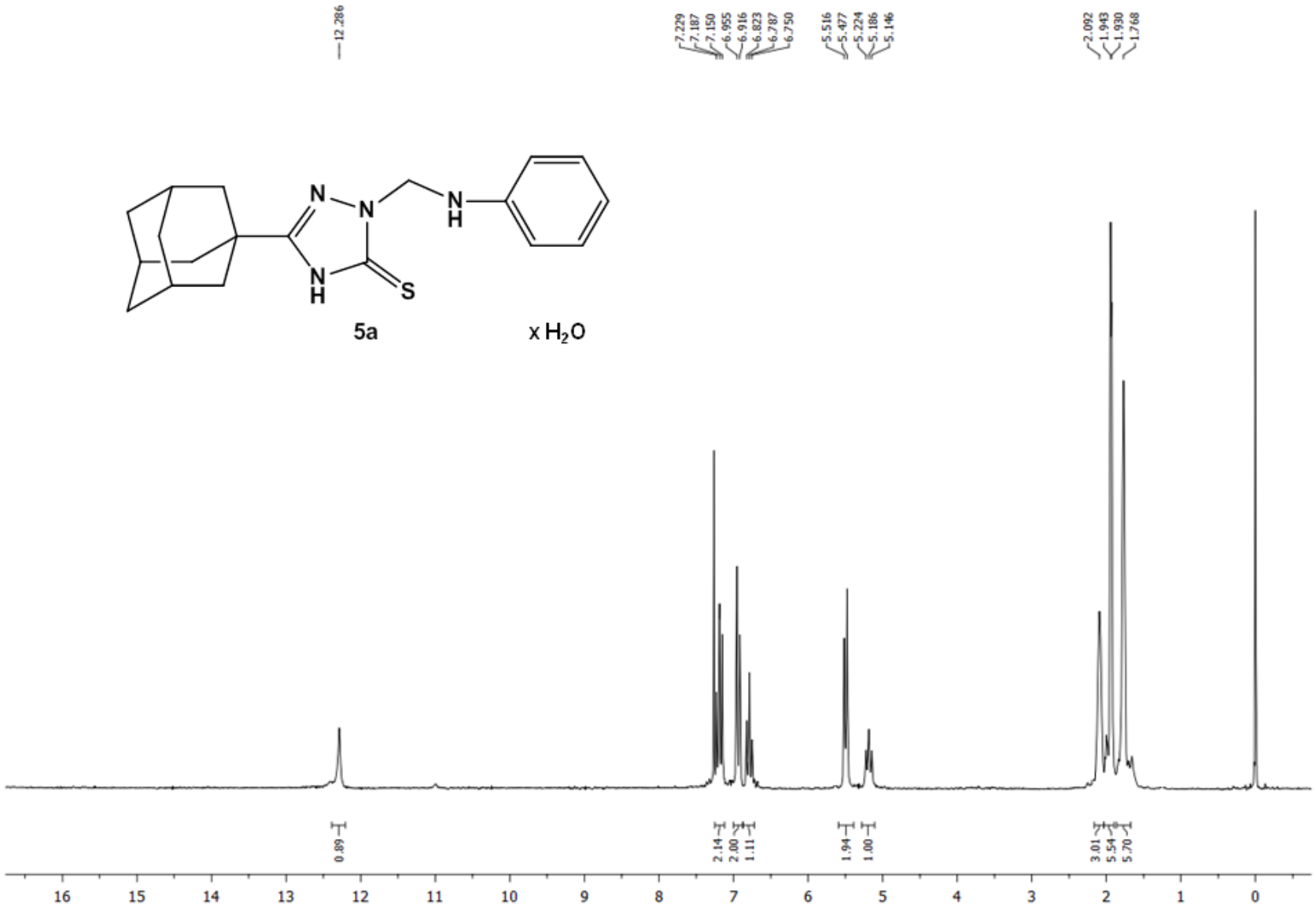

Figure S3: ^{1}H NMR spectrum of **5a** in $CDCl_3$ (200 MHz).

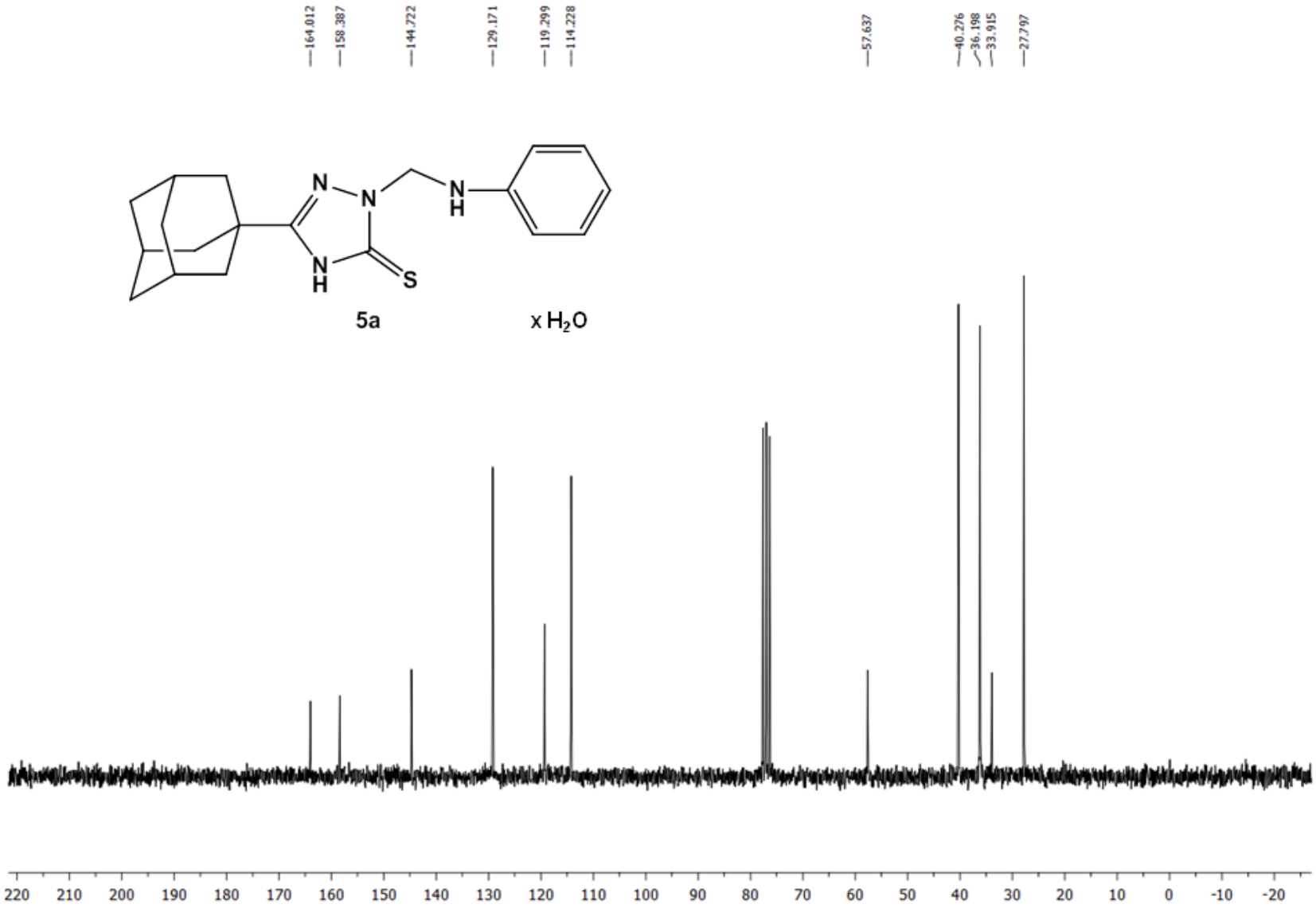

Figure S4: ^{13}C NMR spectrum of **5a** in $CDCl_3$ (50 MHz).

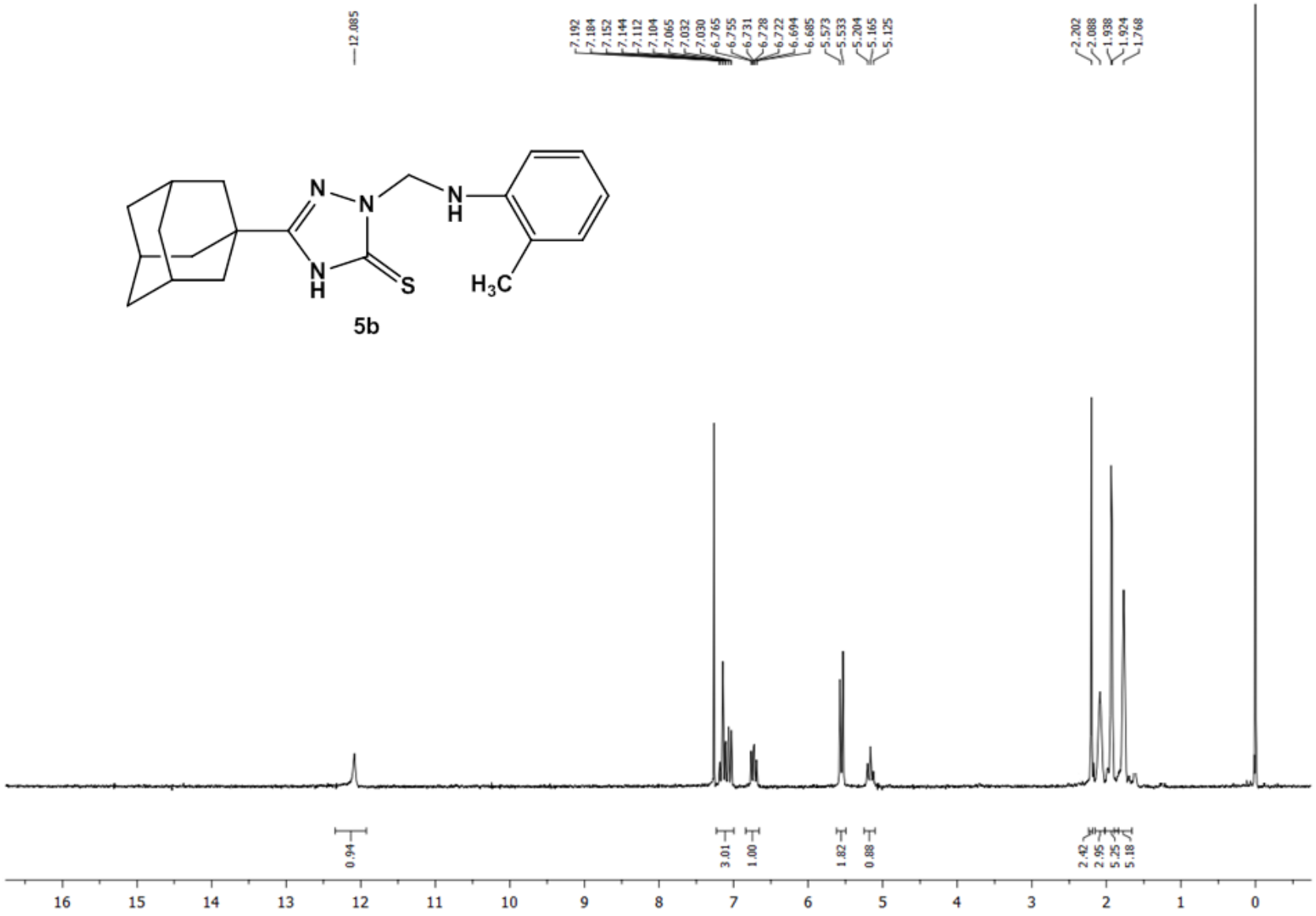

Figure S5: ^{1}H NMR spectrum of **5b** in $CDCl_3$ (200 MHz).

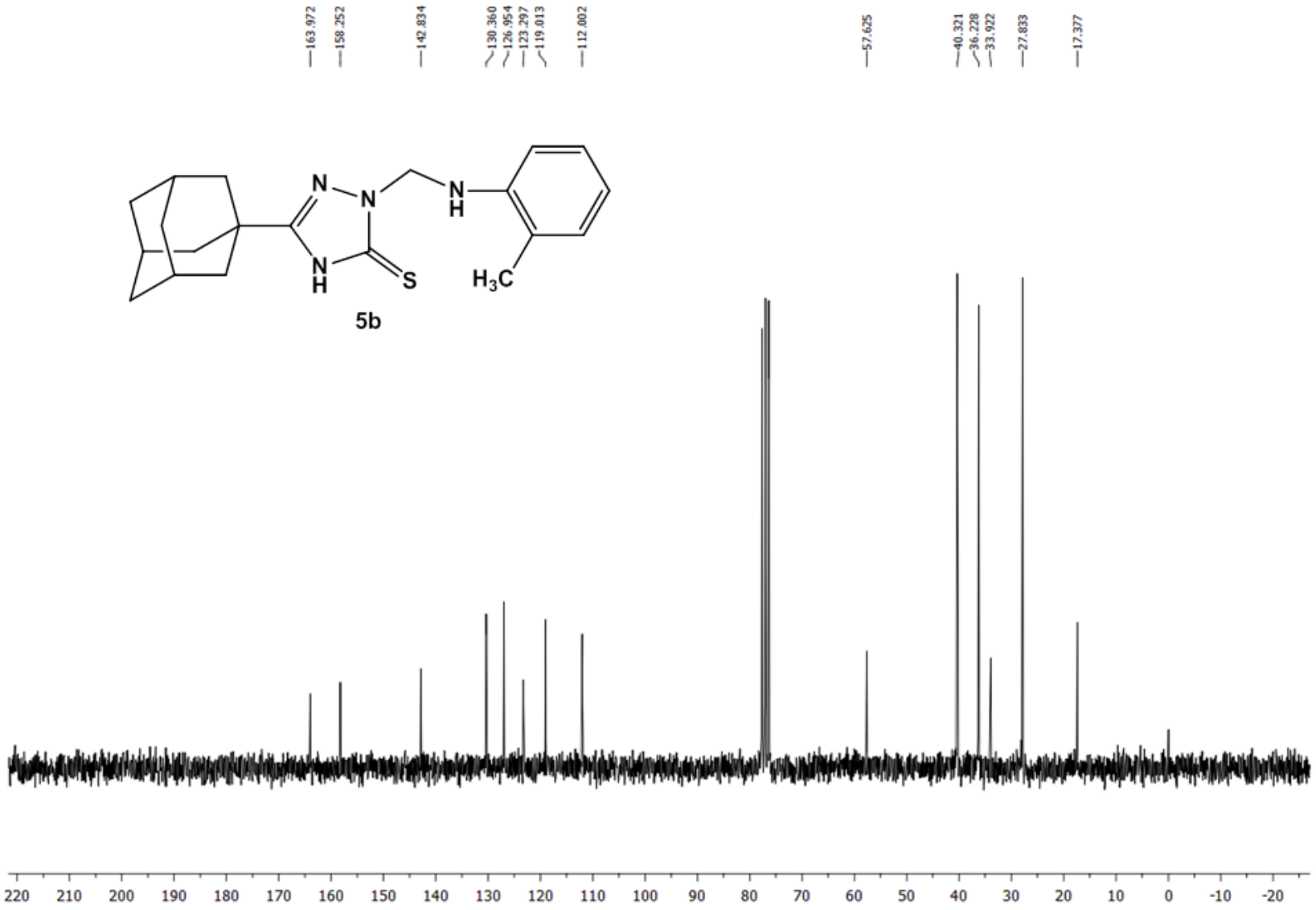

Figure S6: ^{13}C NMR spectrum of **5b** in $CDCl_3$ (50 MHz).

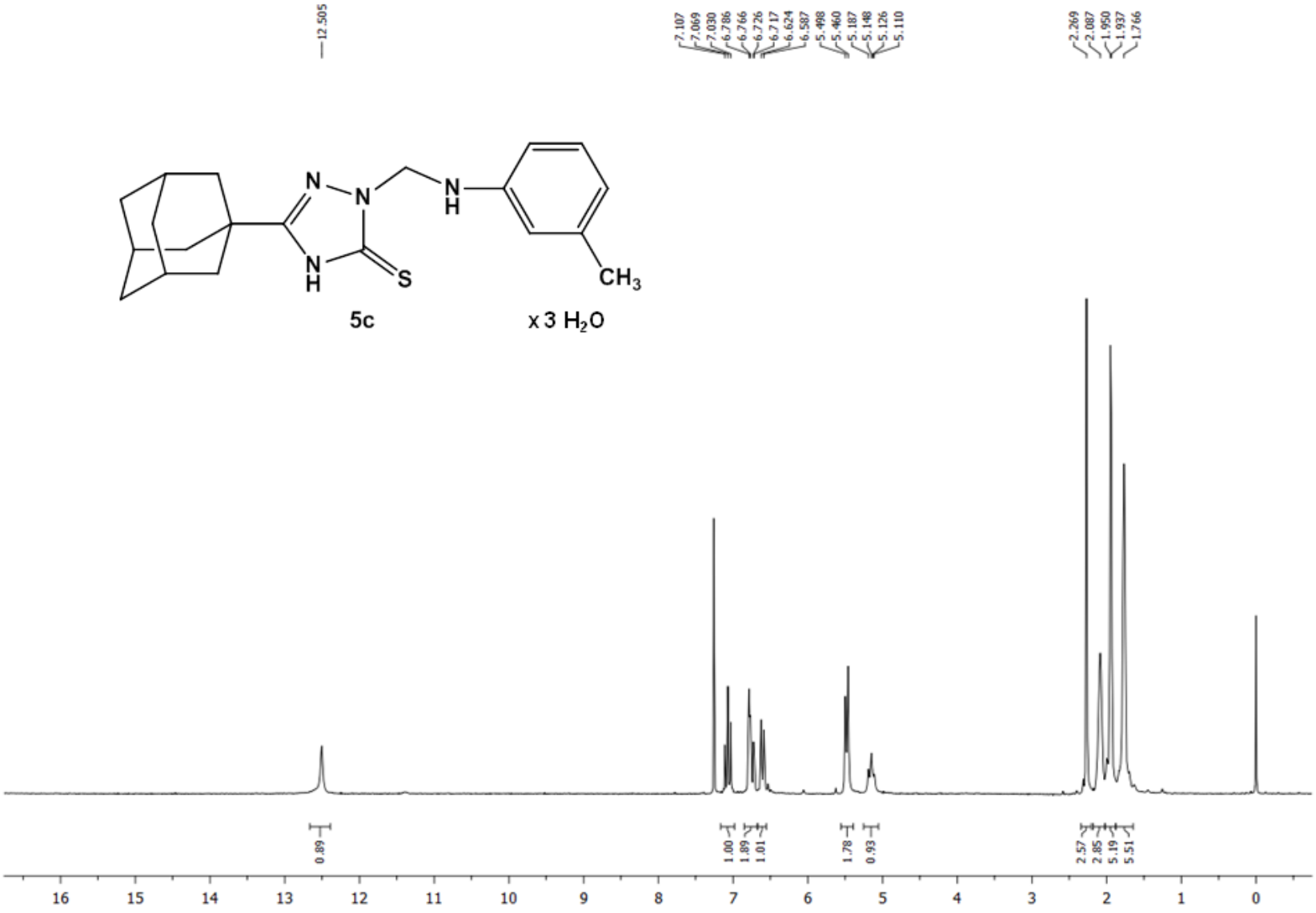

Figure S7: ^{1}H NMR spectrum of **5c** in $CDCl_3$ (200 MHz).

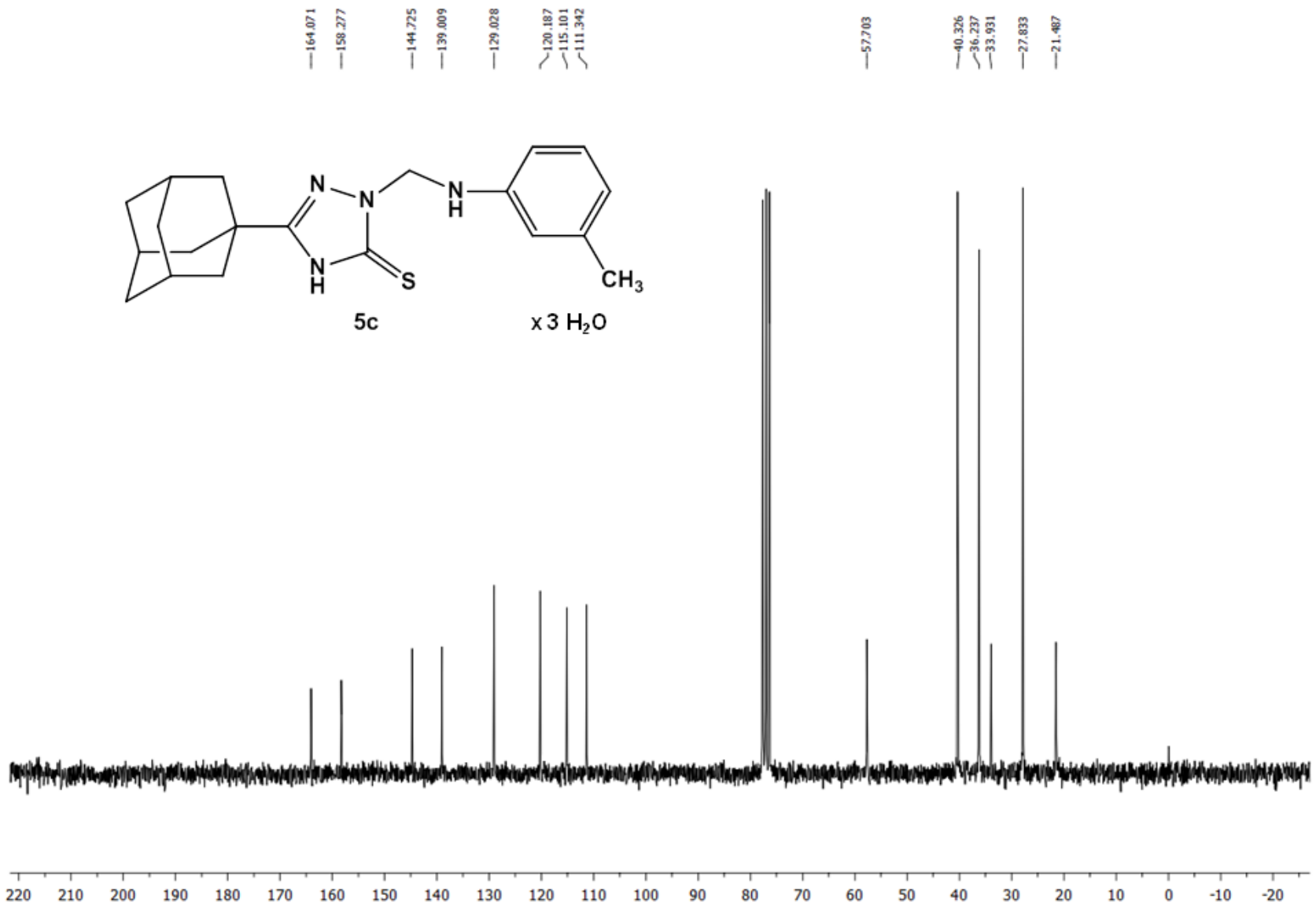

Figure S8: ^{13}C NMR spectrum of **5c** in $CDCl_3$ (50 MHz).

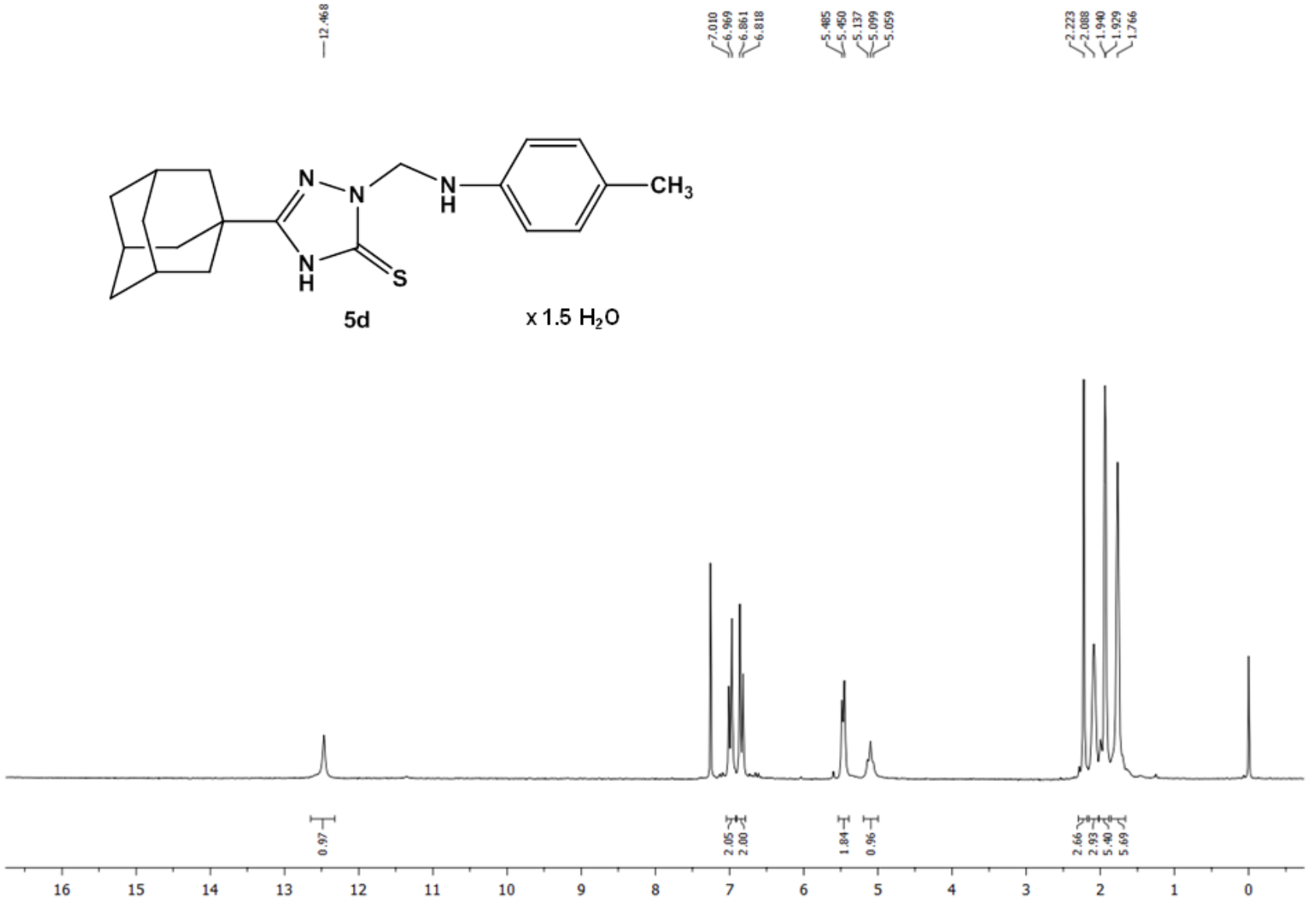

Figure S9: ^{1}H NMR spectrum of **5d** in $CDCl_3$ (200 MHz).

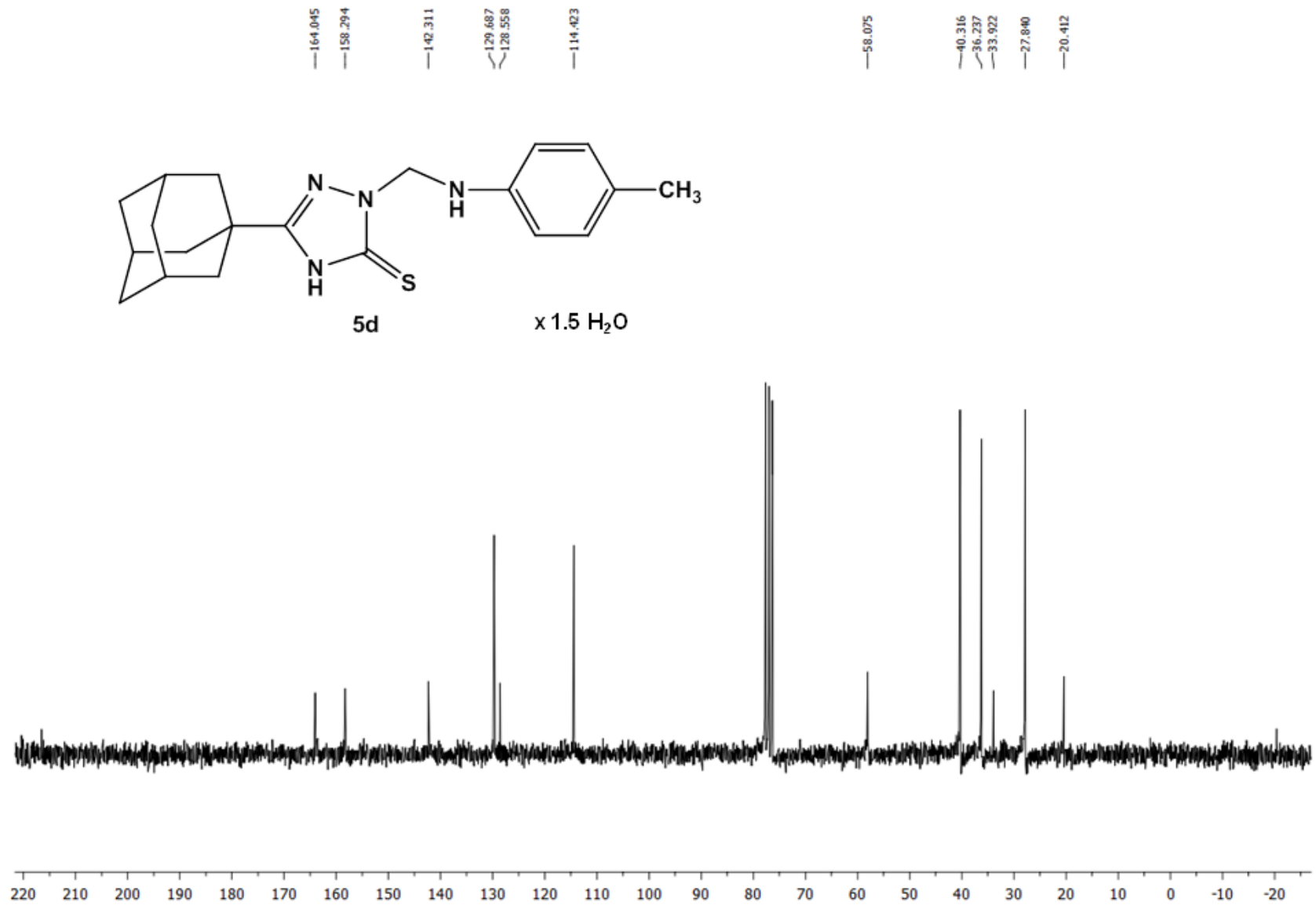

Figure S10: ^{13}C NMR spectrum of **5d** in $CDCl_3$ (50 MHz).

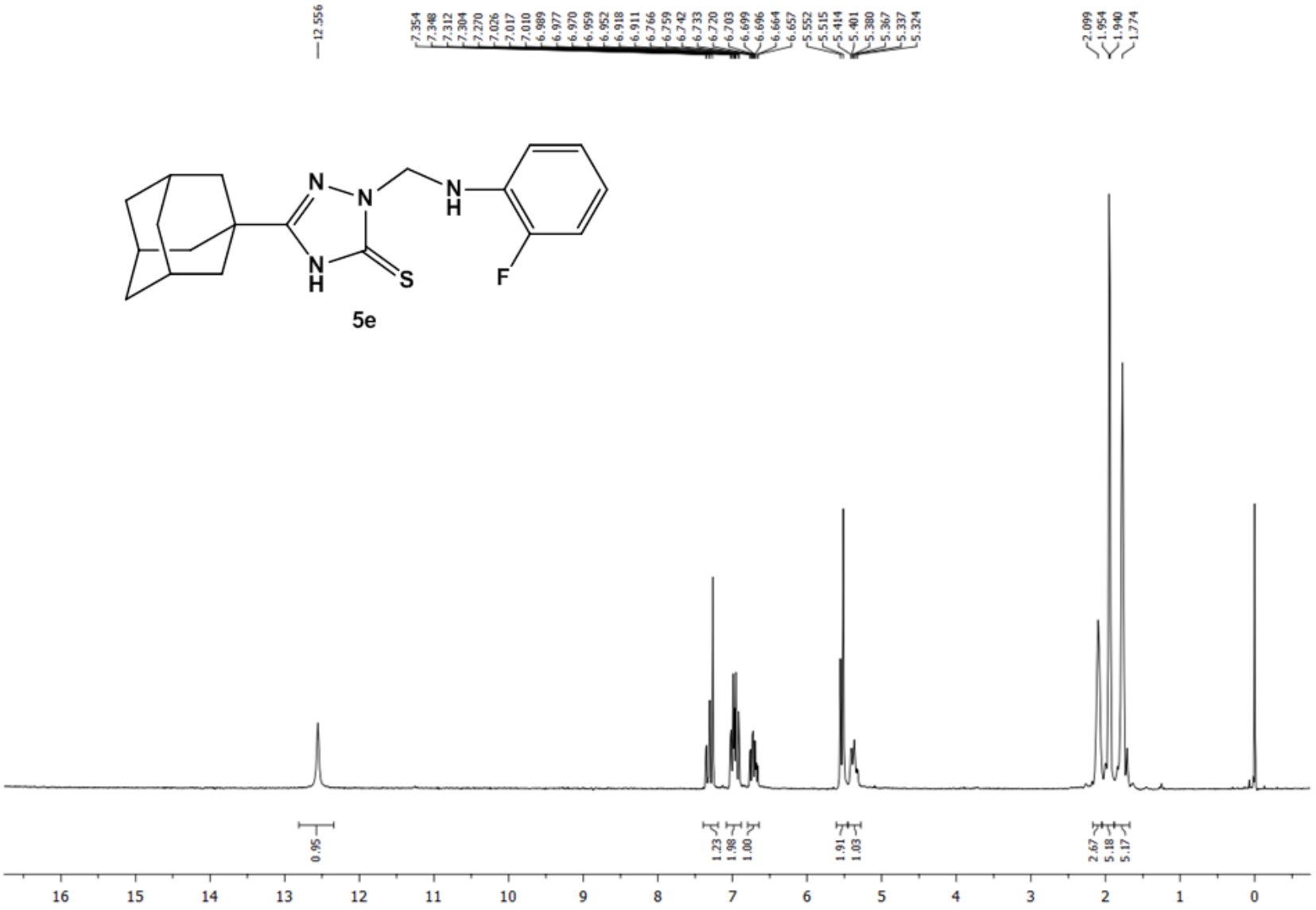

Figure S11: ^{1}H NMR spectrum of **5e** in $CDCl_3$ (200 MHz).

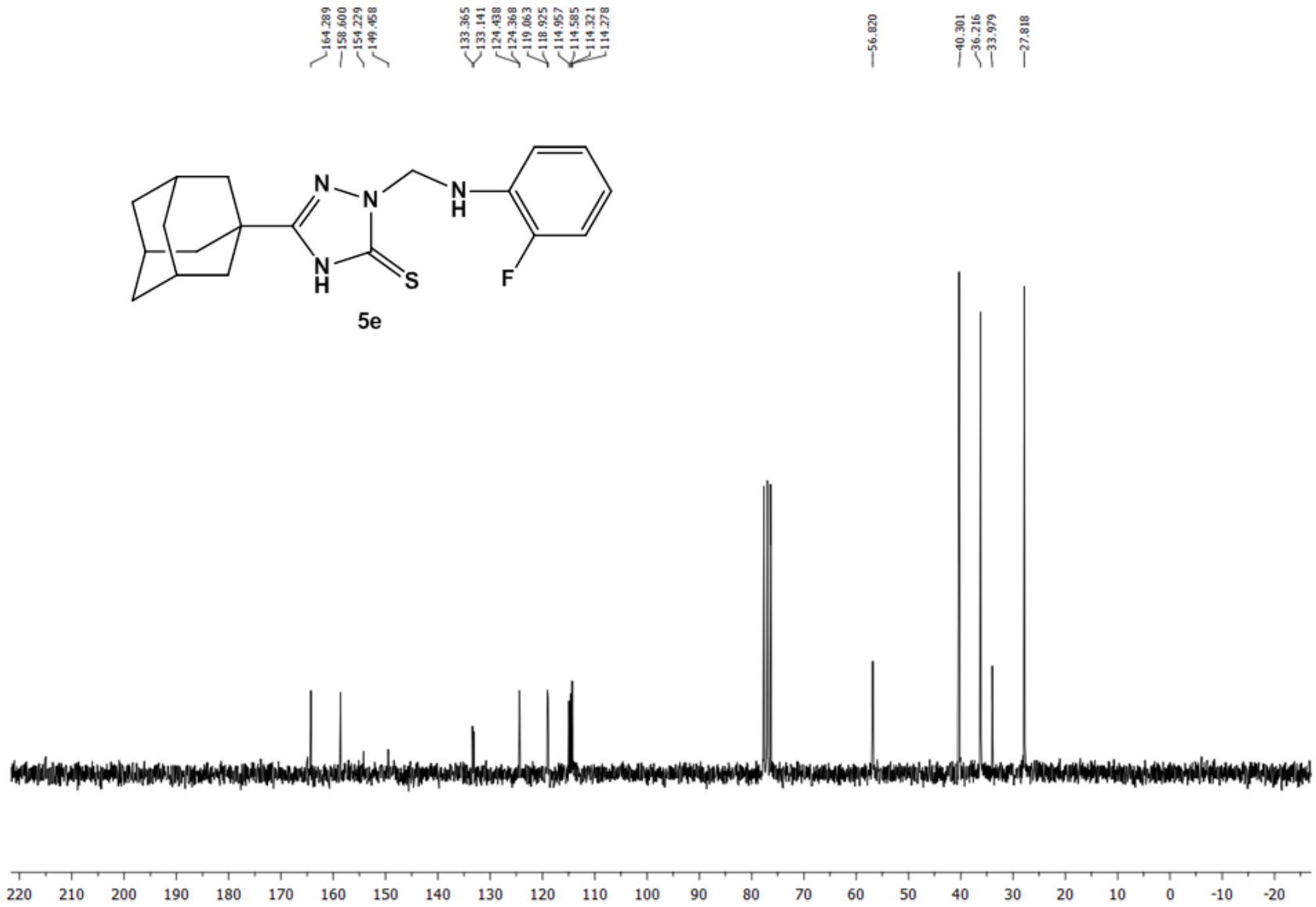

Figure S12: ^{13}C NMR spectrum of **5e** in $CDCl_3$ (50 MHz).

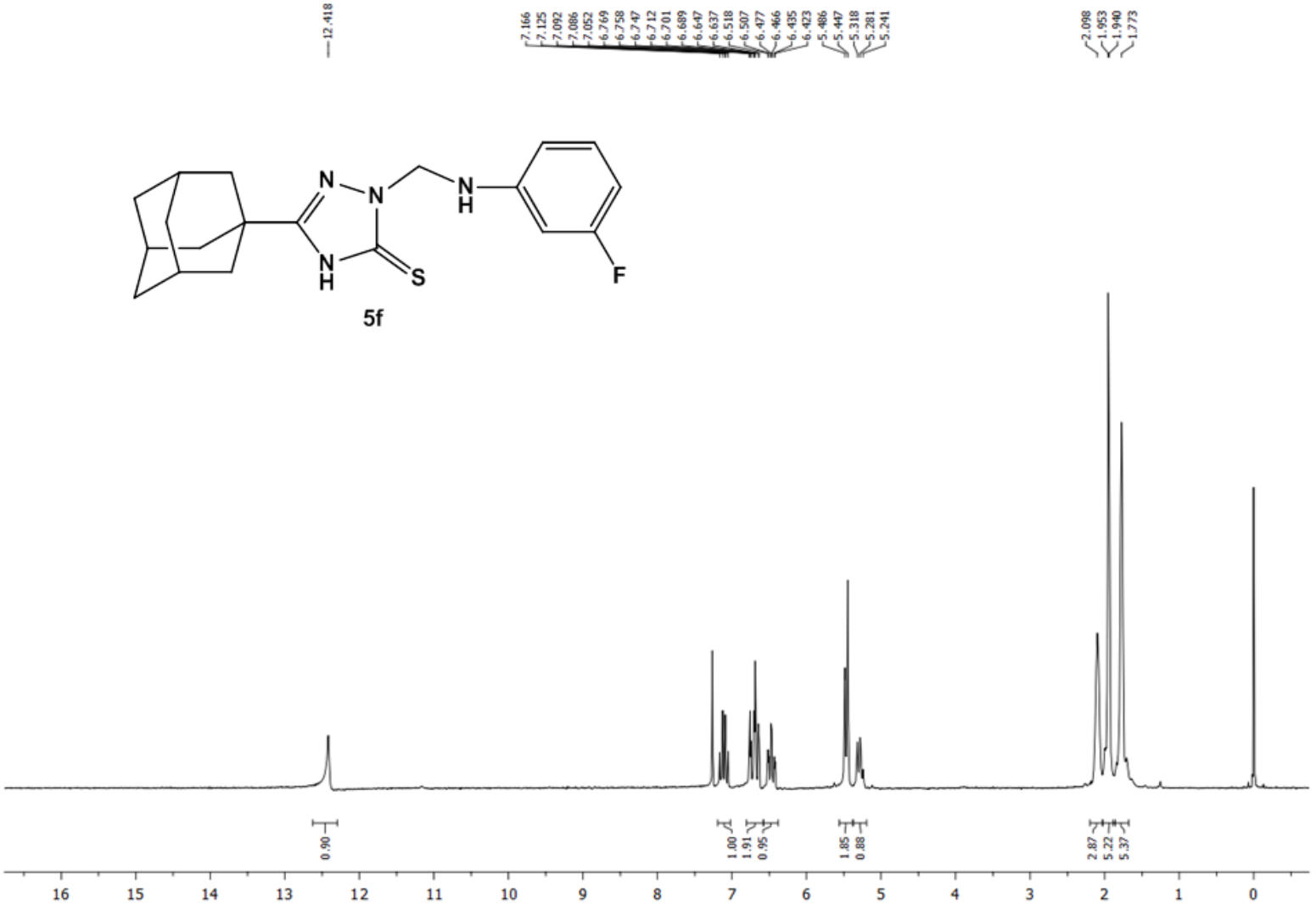

Figure S13: ^{1}H NMR spectrum of **5f** in $CDCl_3$ (200 MHz).

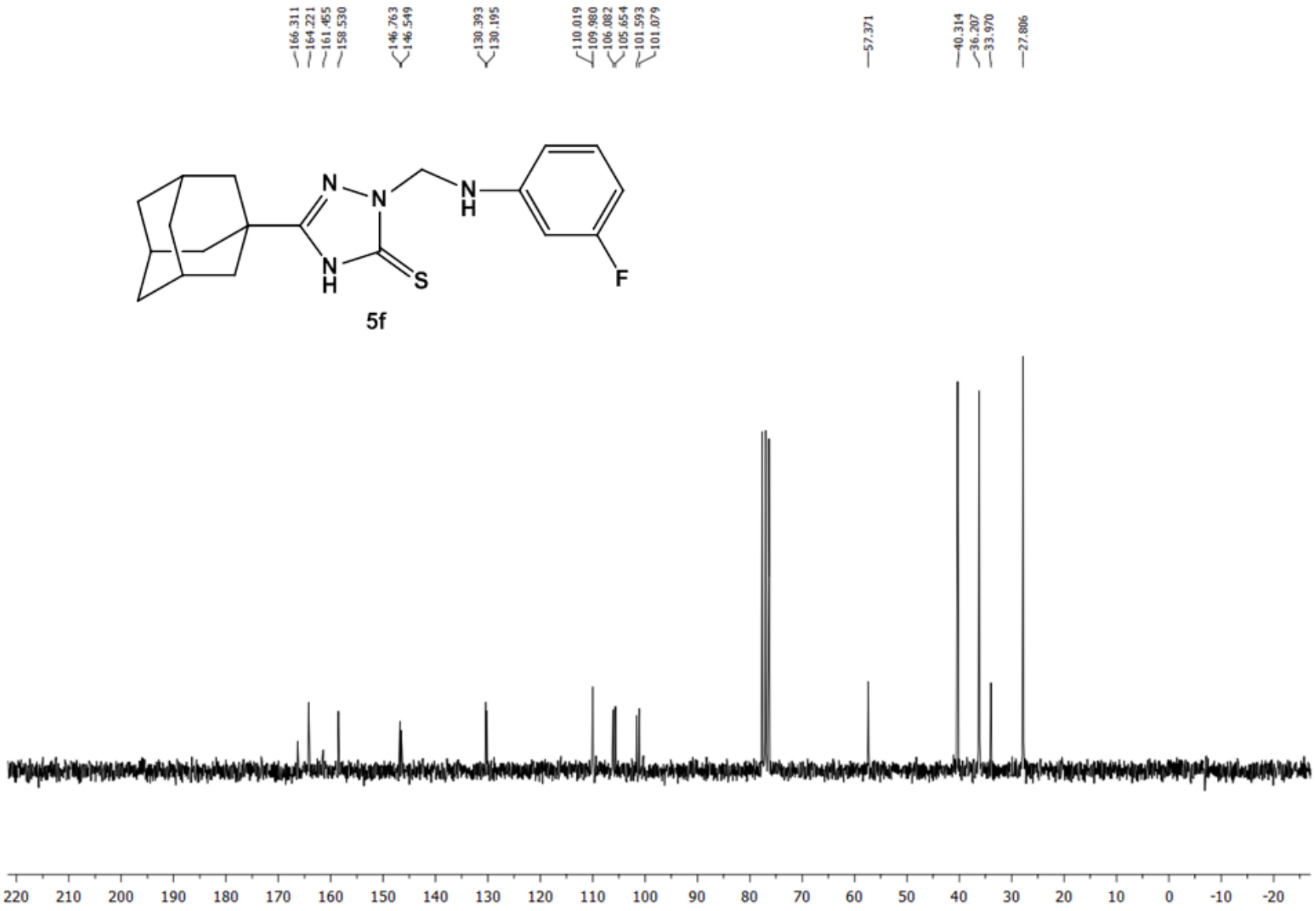

Figure S14: ^{13}C NMR spectrum of **5f** in $CDCl_3$ (50 MHz).

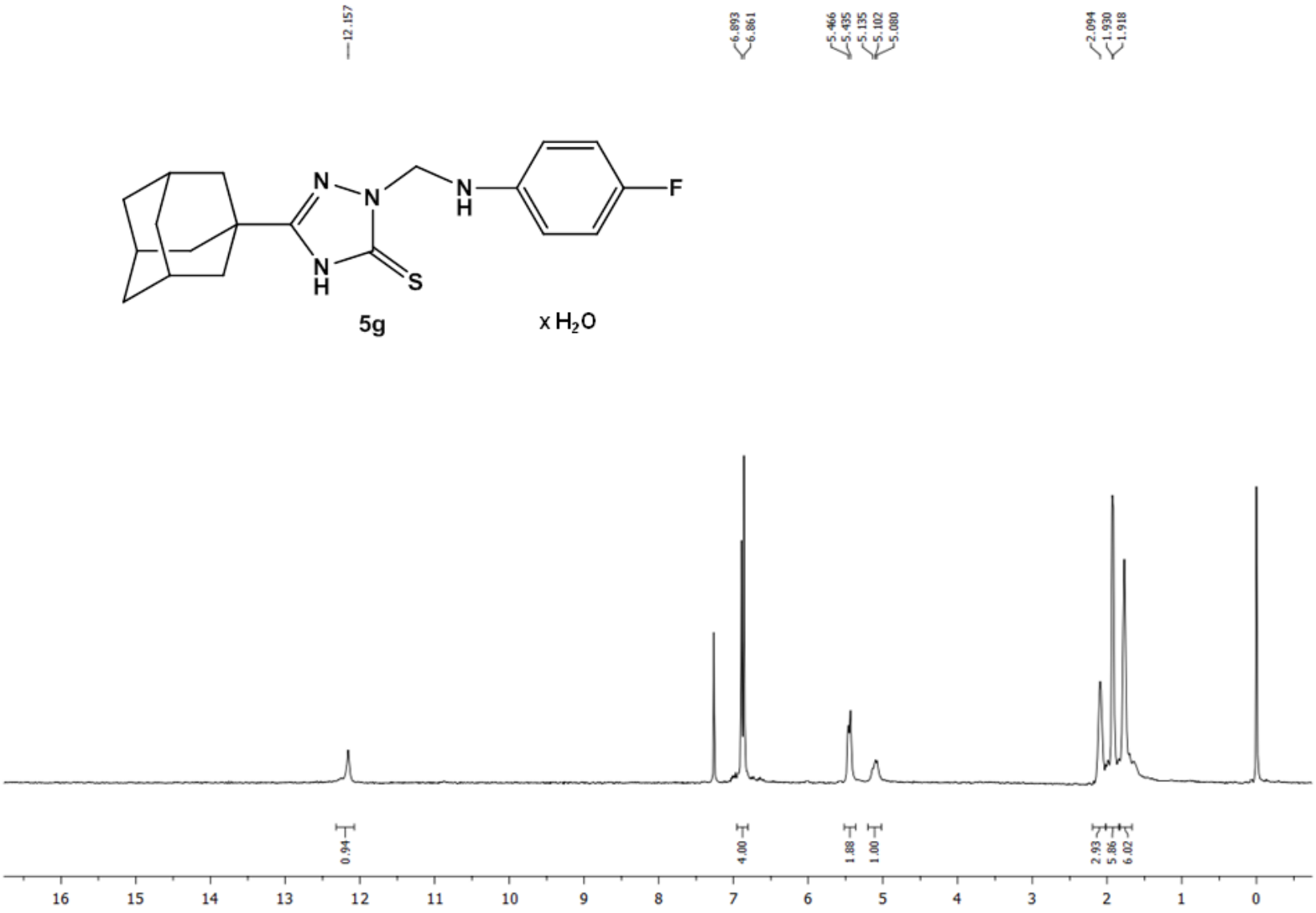

Figure S15: ^{1}H NMR spectrum of **5g** in $CDCl_3$ (200 MHz).

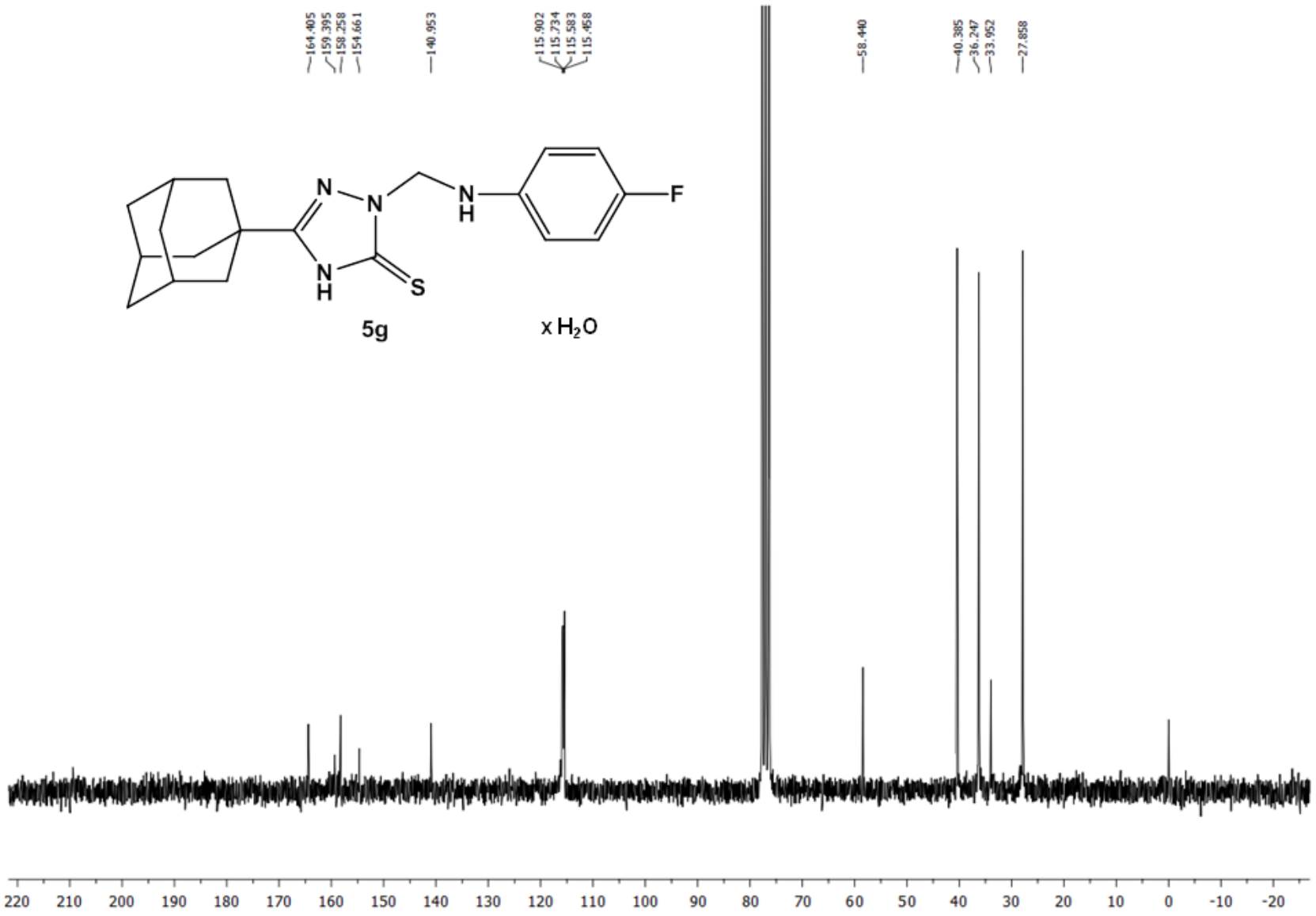

Figure S16: ^{13}C NMR spectrum of **5g** in $CDCl_3$ (50 MHz).

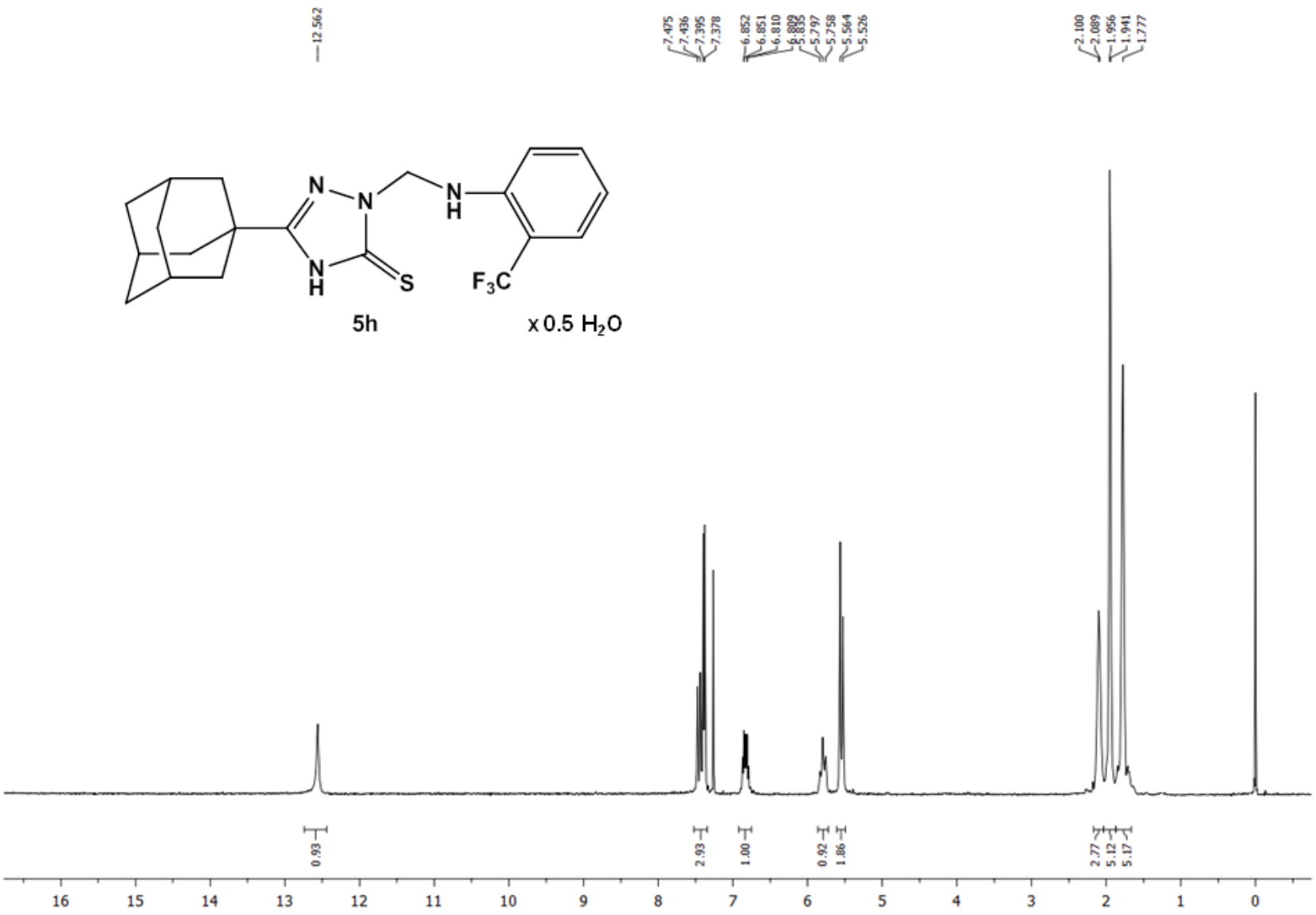

Figure S17: ^{1}H NMR spectrum of **5h** in $CDCl_3$ (200 MHz).

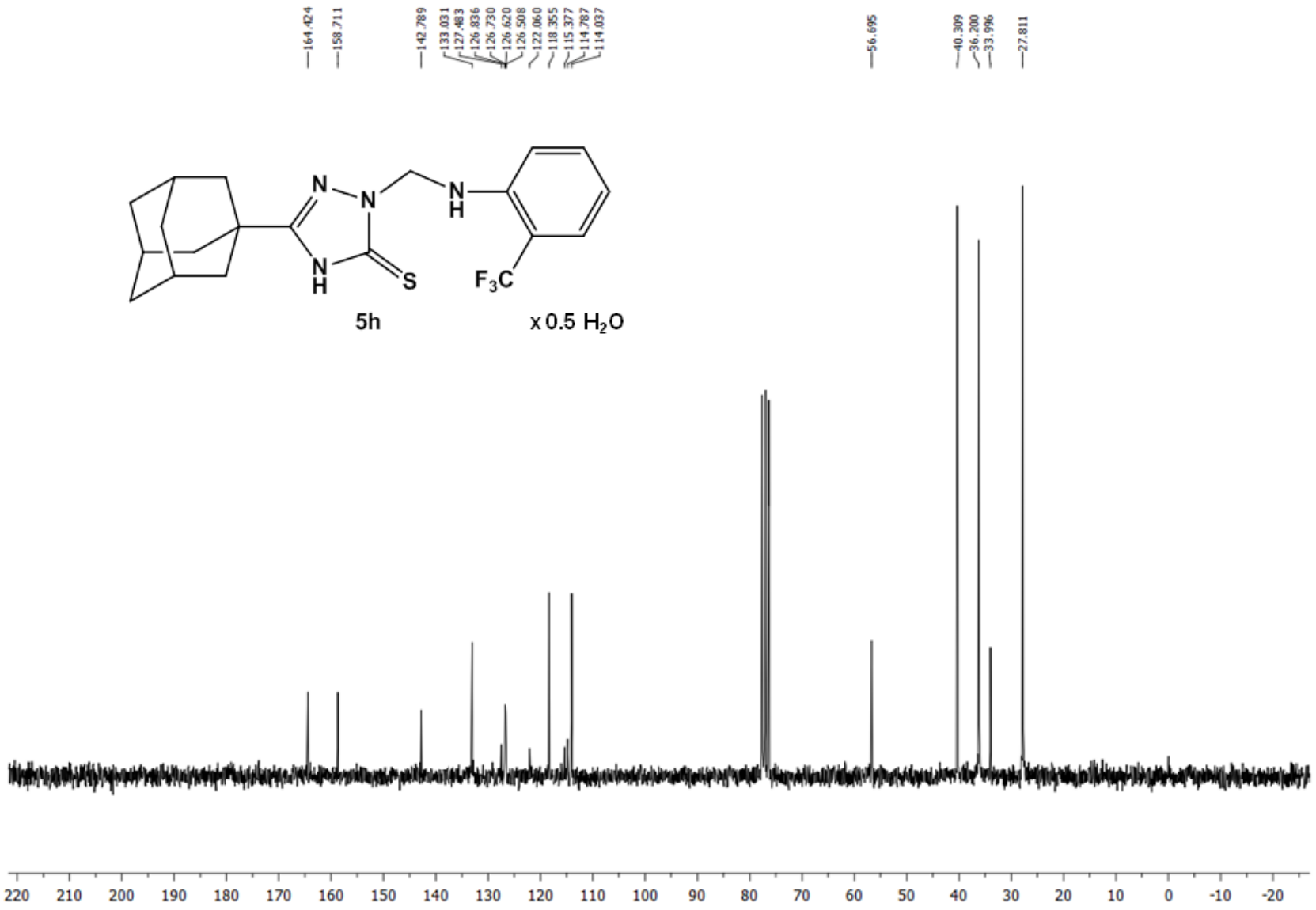

Figure S18: ^{13}C NMR spectrum of **5h** in $CDCl_3$ (50 MHz).

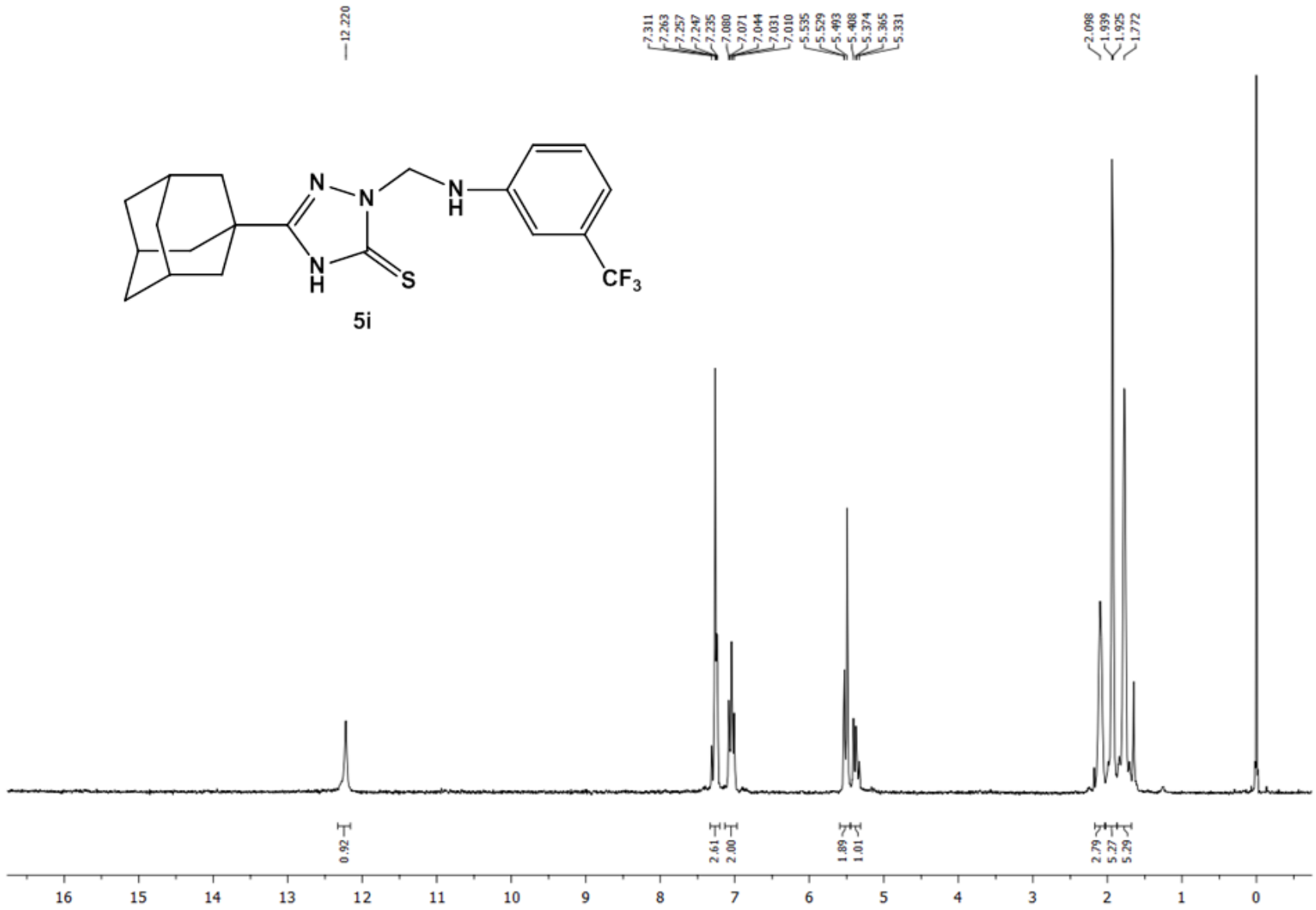

Figure S19: ^{1}H NMR spectrum of **5i** in $CDCl_3$ (200 MHz).

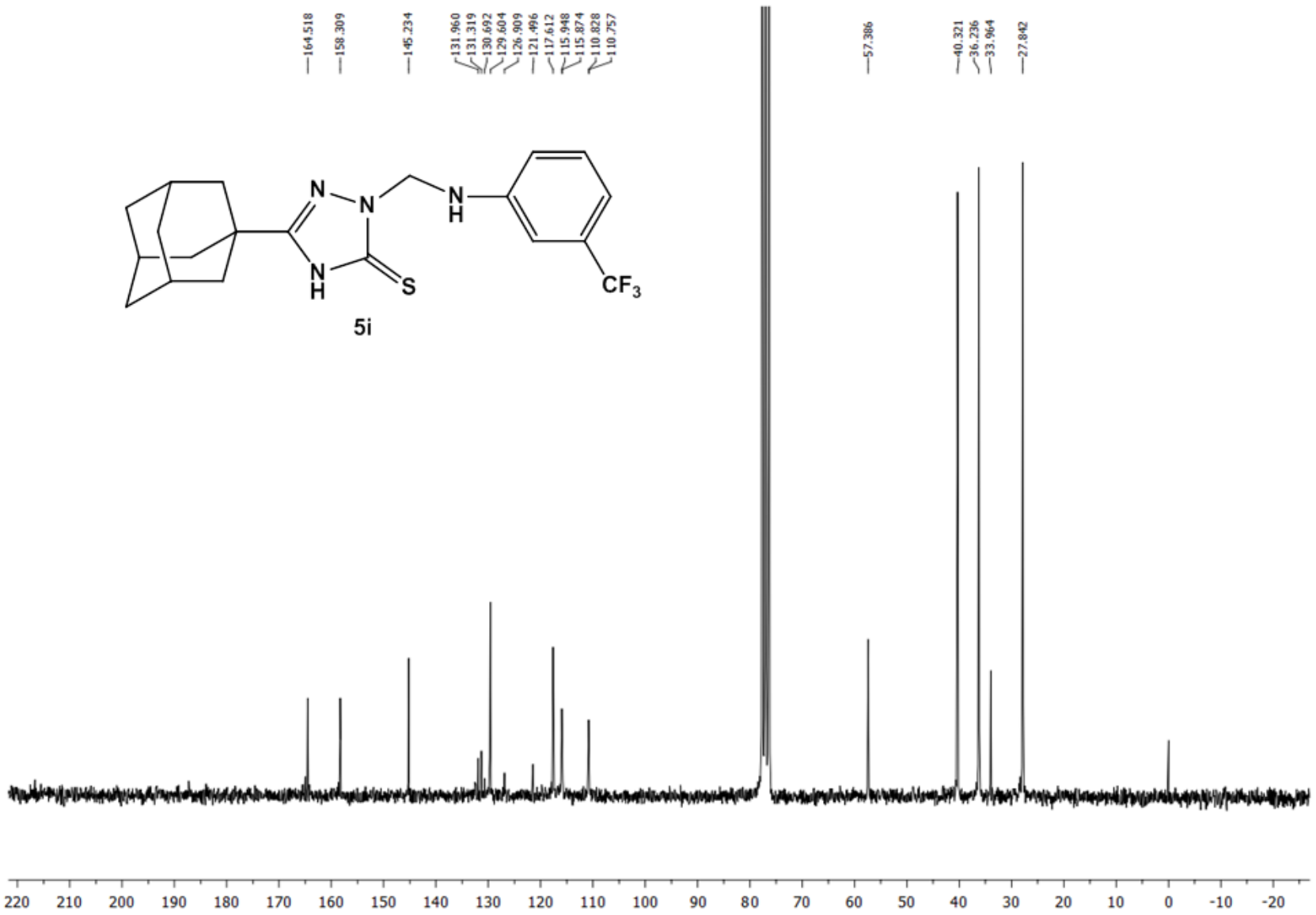

Figure S20: ^{13}C NMR spectrum of **5i** in $CDCl_3$ (50 MHz).

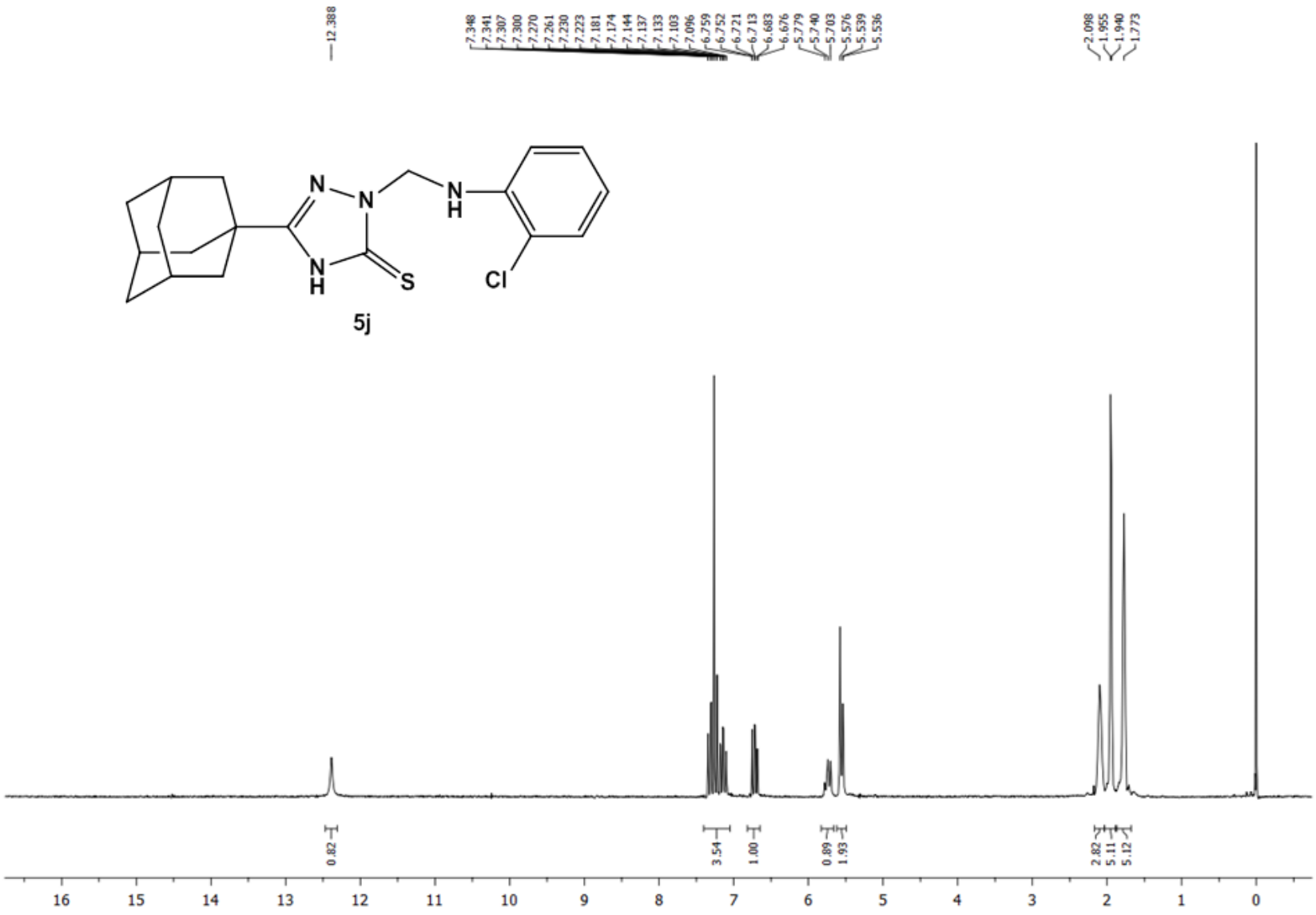

Figure S21: ^{1}H NMR spectrum of **5j** in $CDCl_3$ (200 MHz).

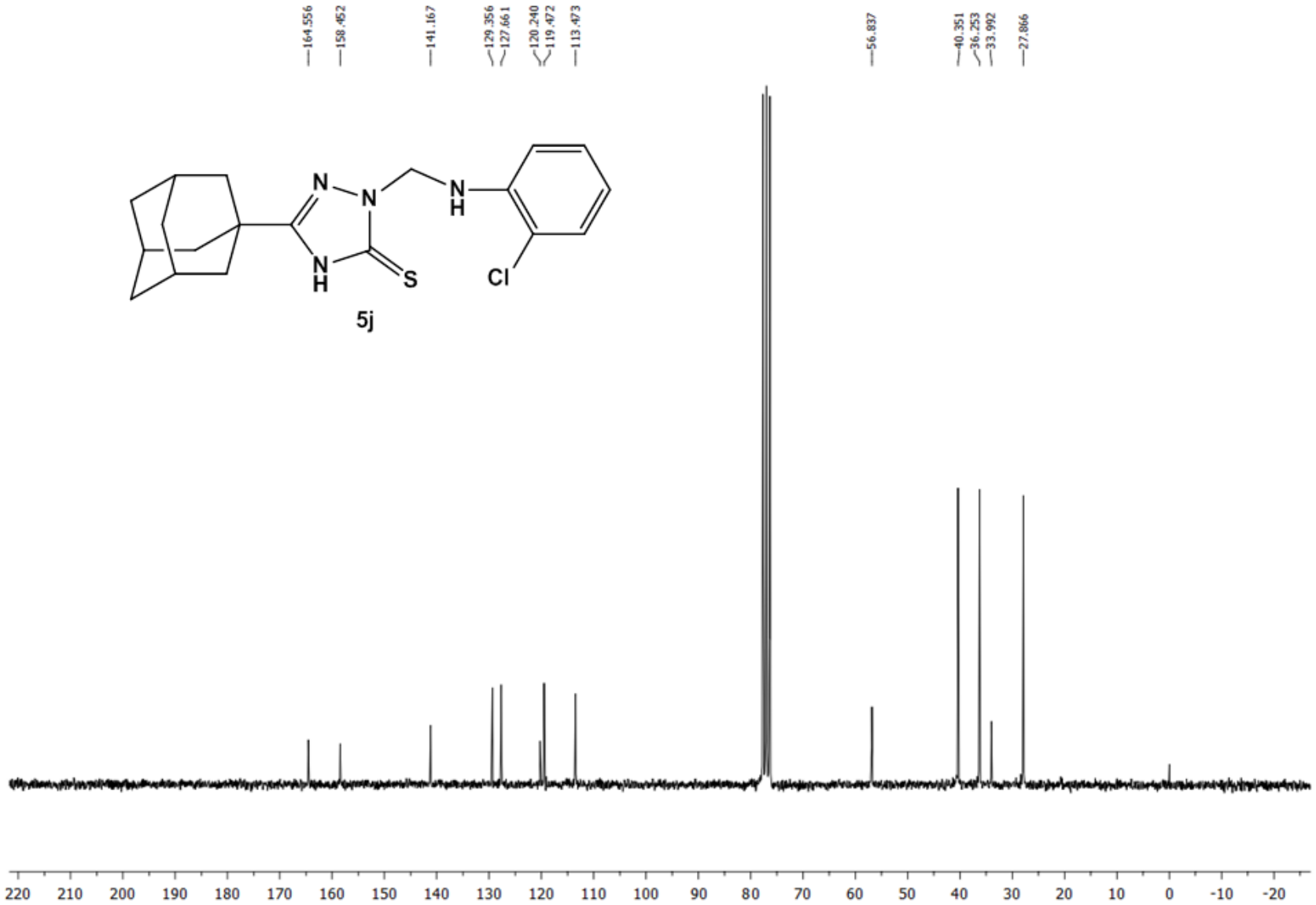

Figure S22: ^{13}C NMR spectrum of **5j** in $CDCl_3$ (50 MHz).

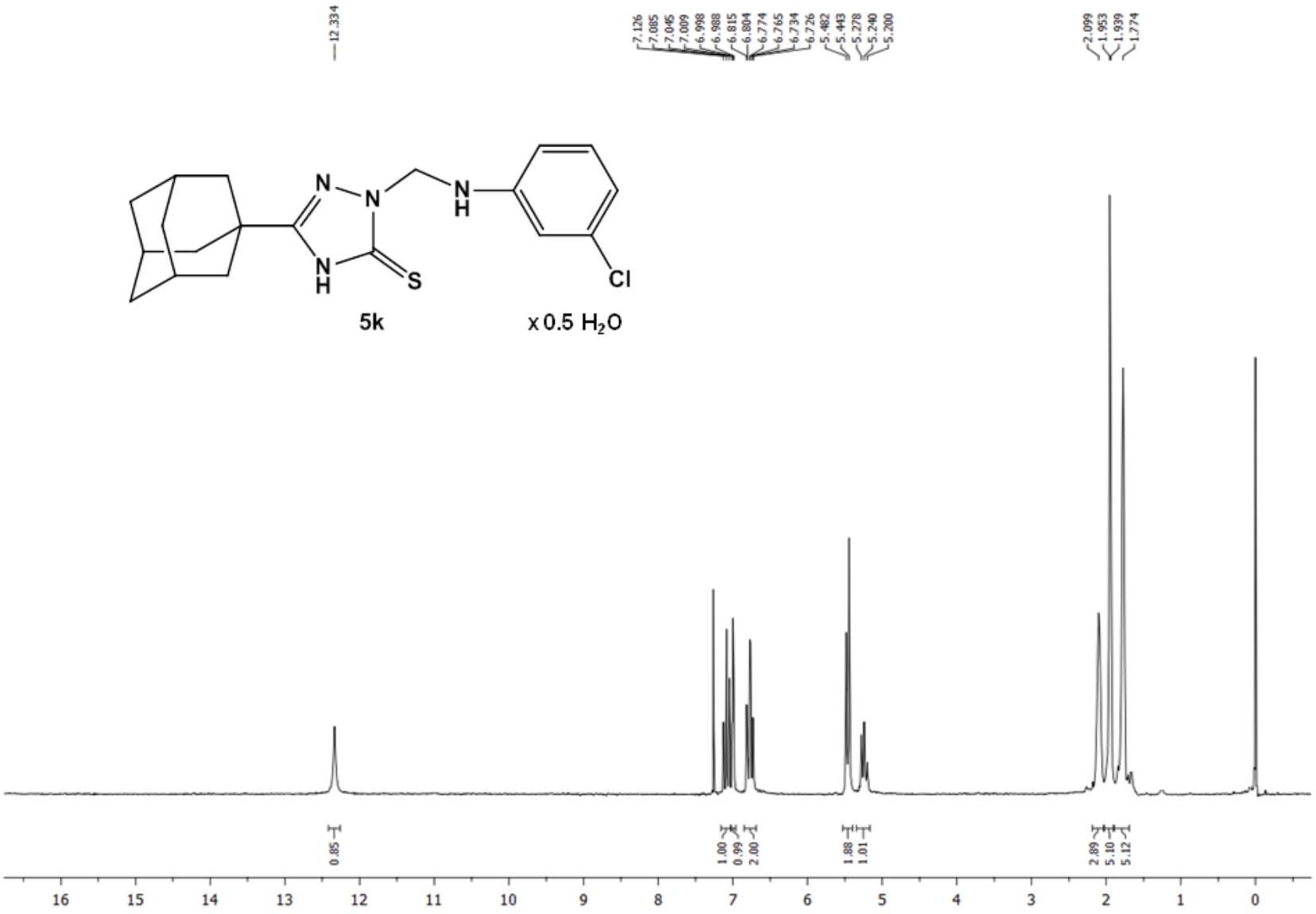

Figure S23: ^{1}H NMR spectrum of **5k** in $CDCl_3$ (200 MHz).

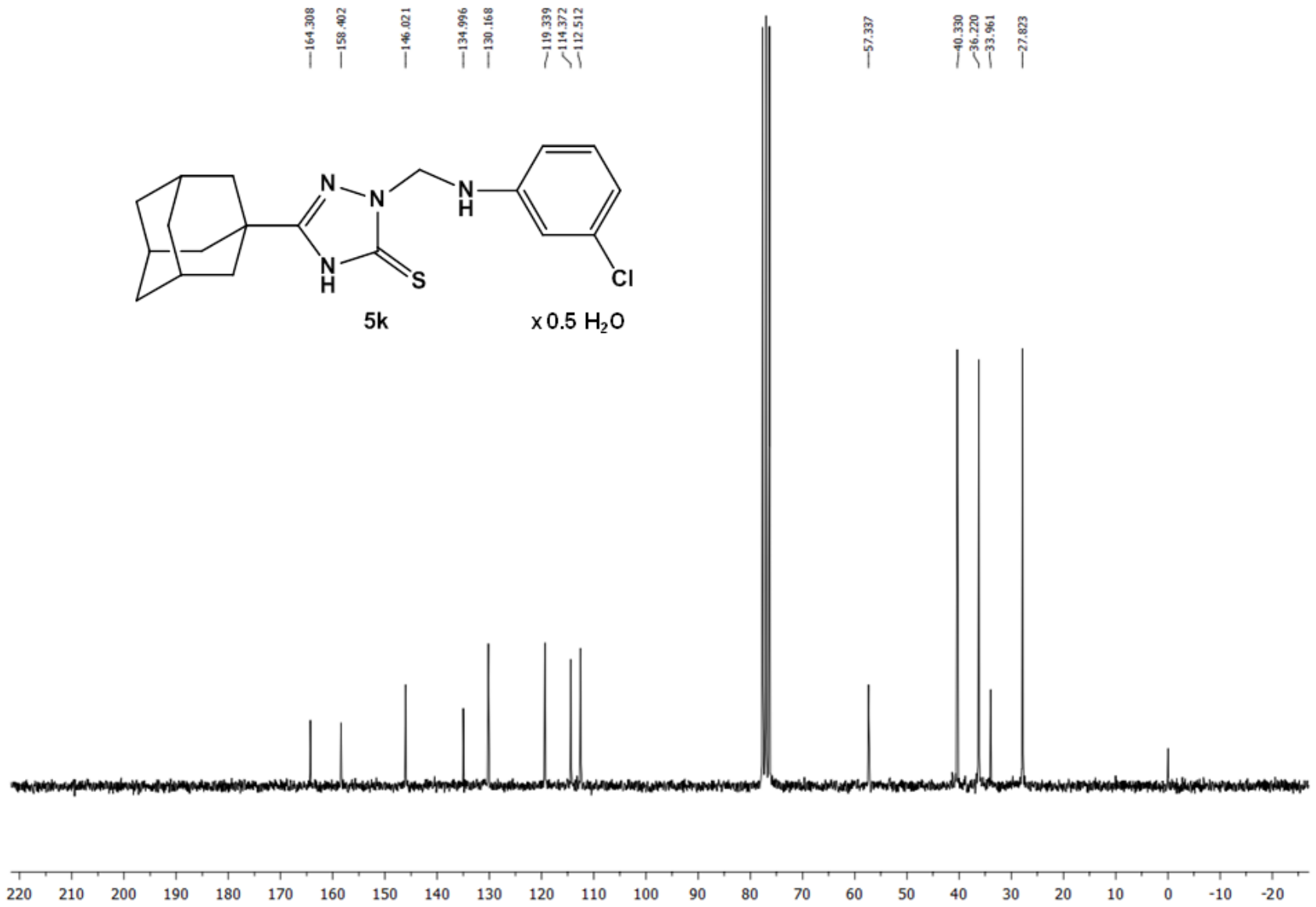

Figure S24: ^{13}C NMR spectrum of **5k** in $CDCl_3$ (50 MHz).

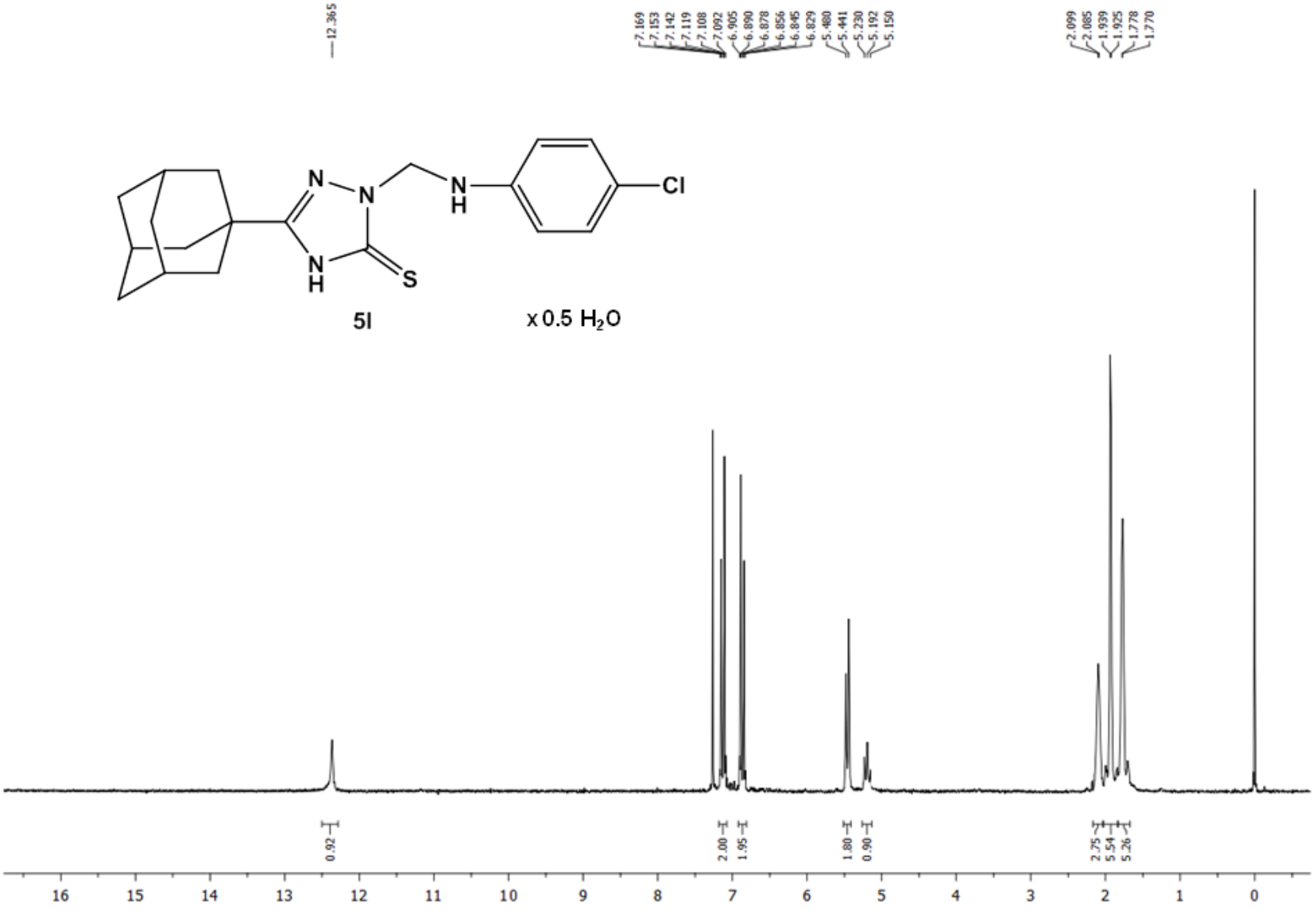

Figure S25: ^{1}H NMR spectrum of **5l** in $CDCl_3$ (200 MHz).

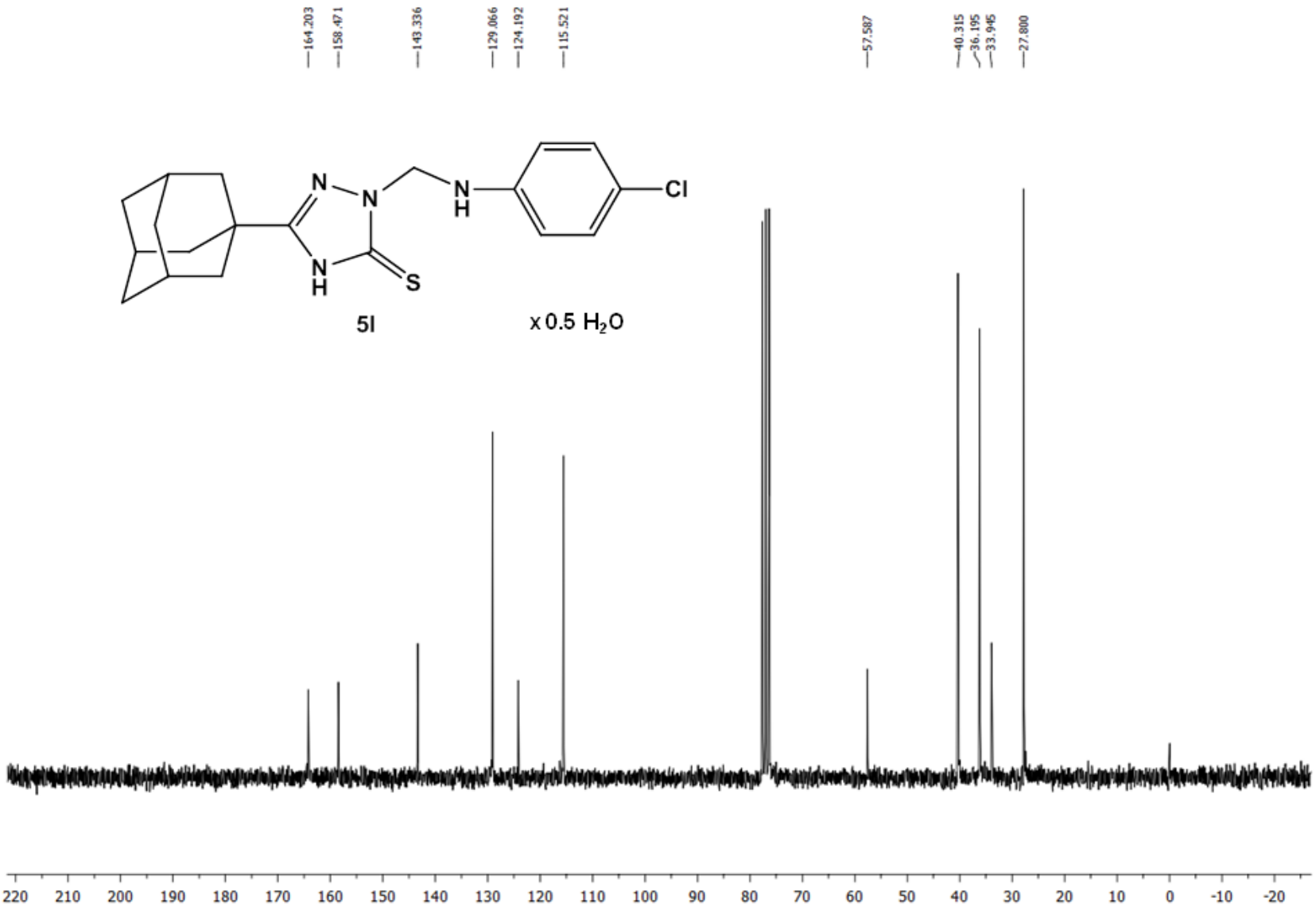

Figure S26: ^{13}C NMR spectrum of **5l** in $CDCl_3$ (50 MHz).

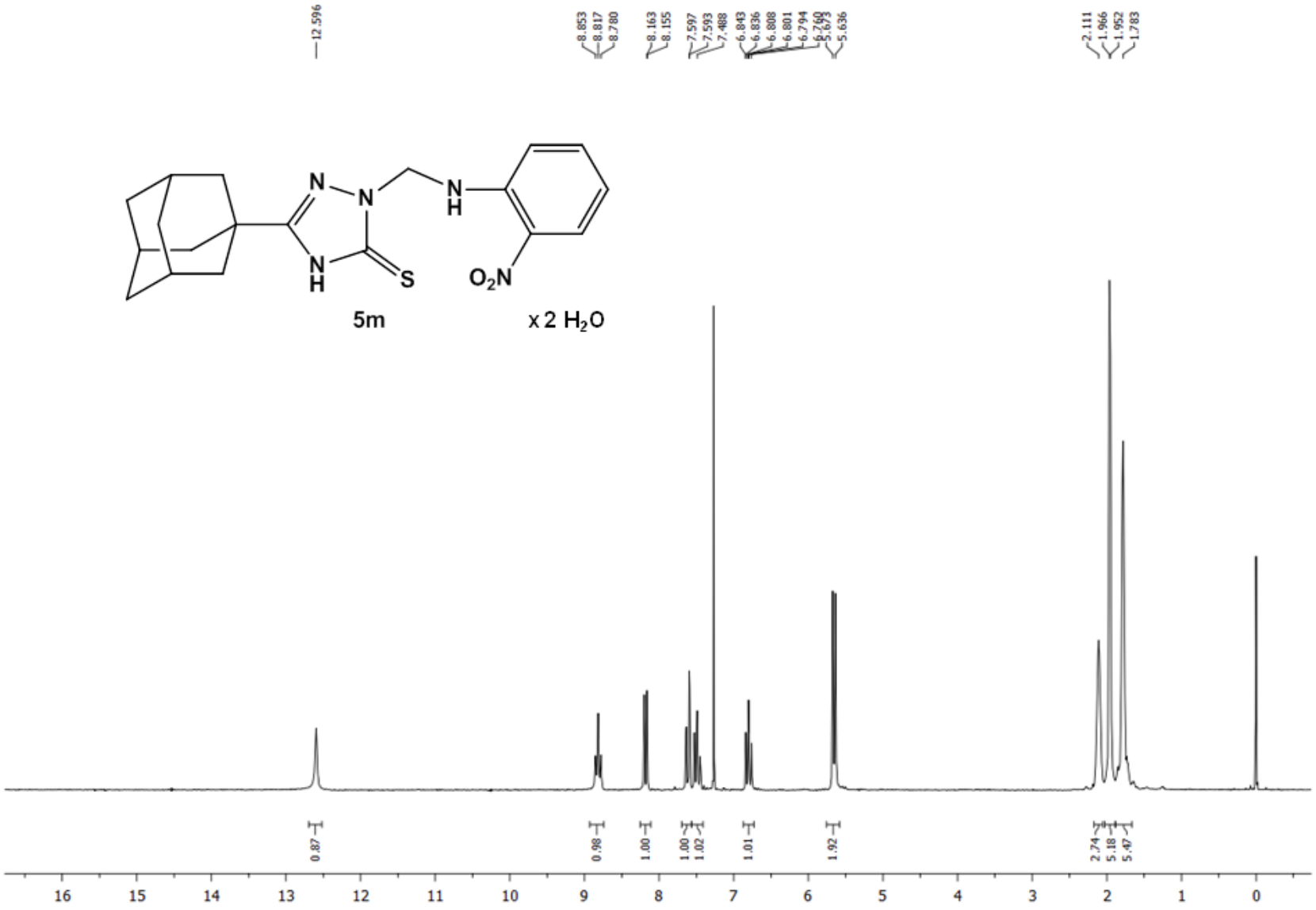

Figure S27: ^{1}H NMR spectrum of **5m** in $CDCl_3$ (200 MHz).

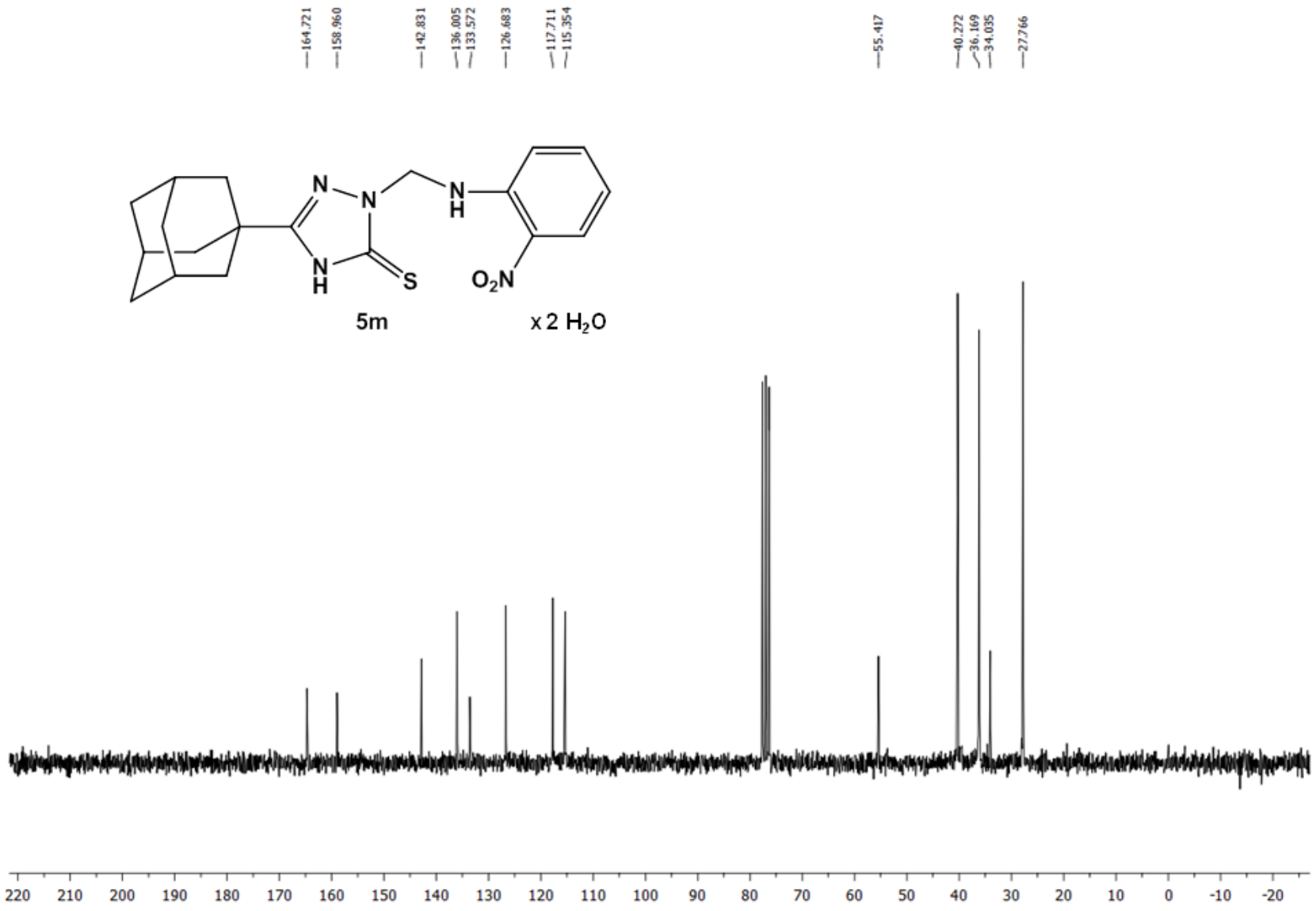

Figure S28: ^{13}C NMR spectrum of **5m** in $CDCl_3$ (50 MHz).

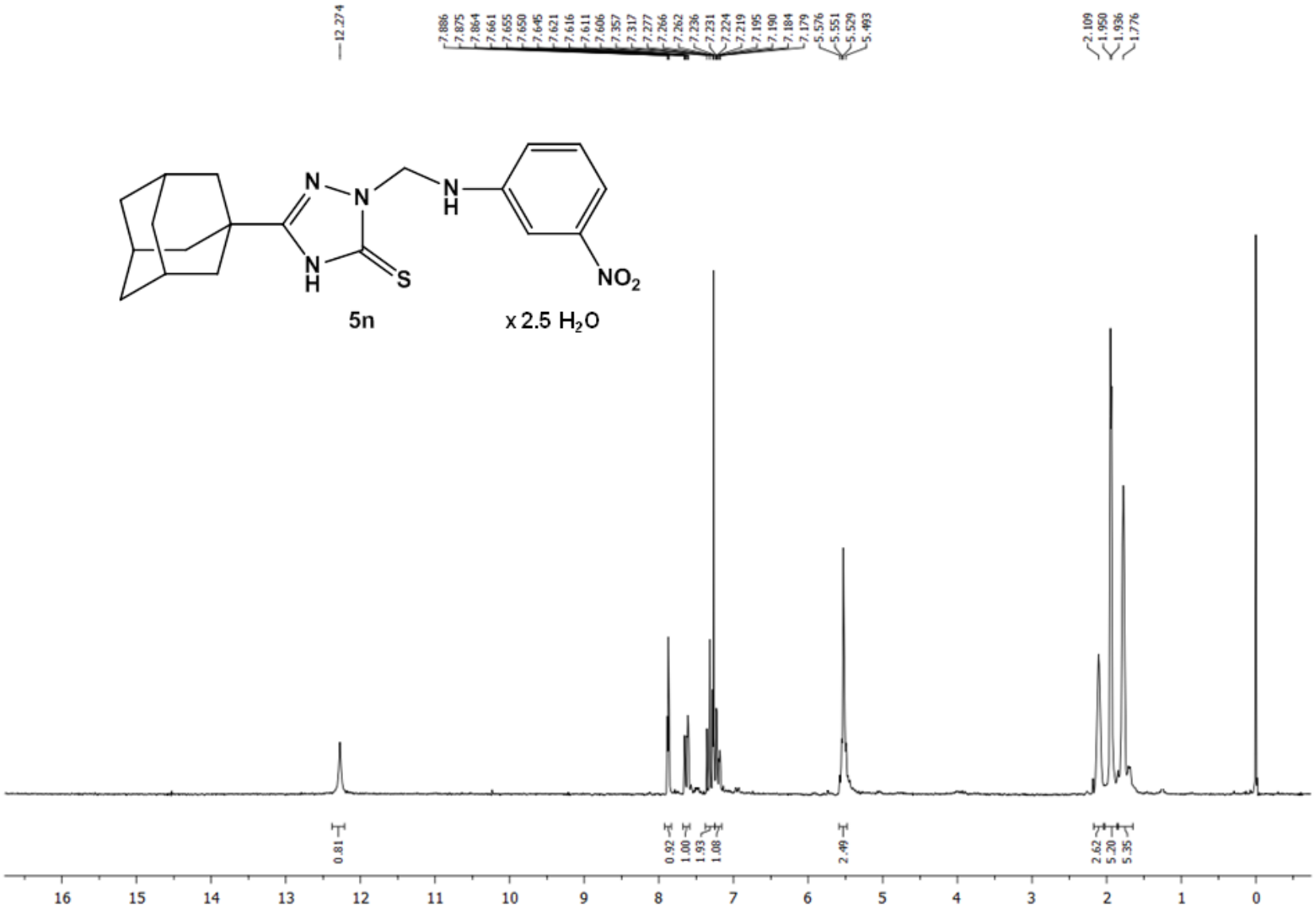

Figure S29: ^{1}H NMR spectrum of **5n** in $CDCl_3$ (200 MHz).

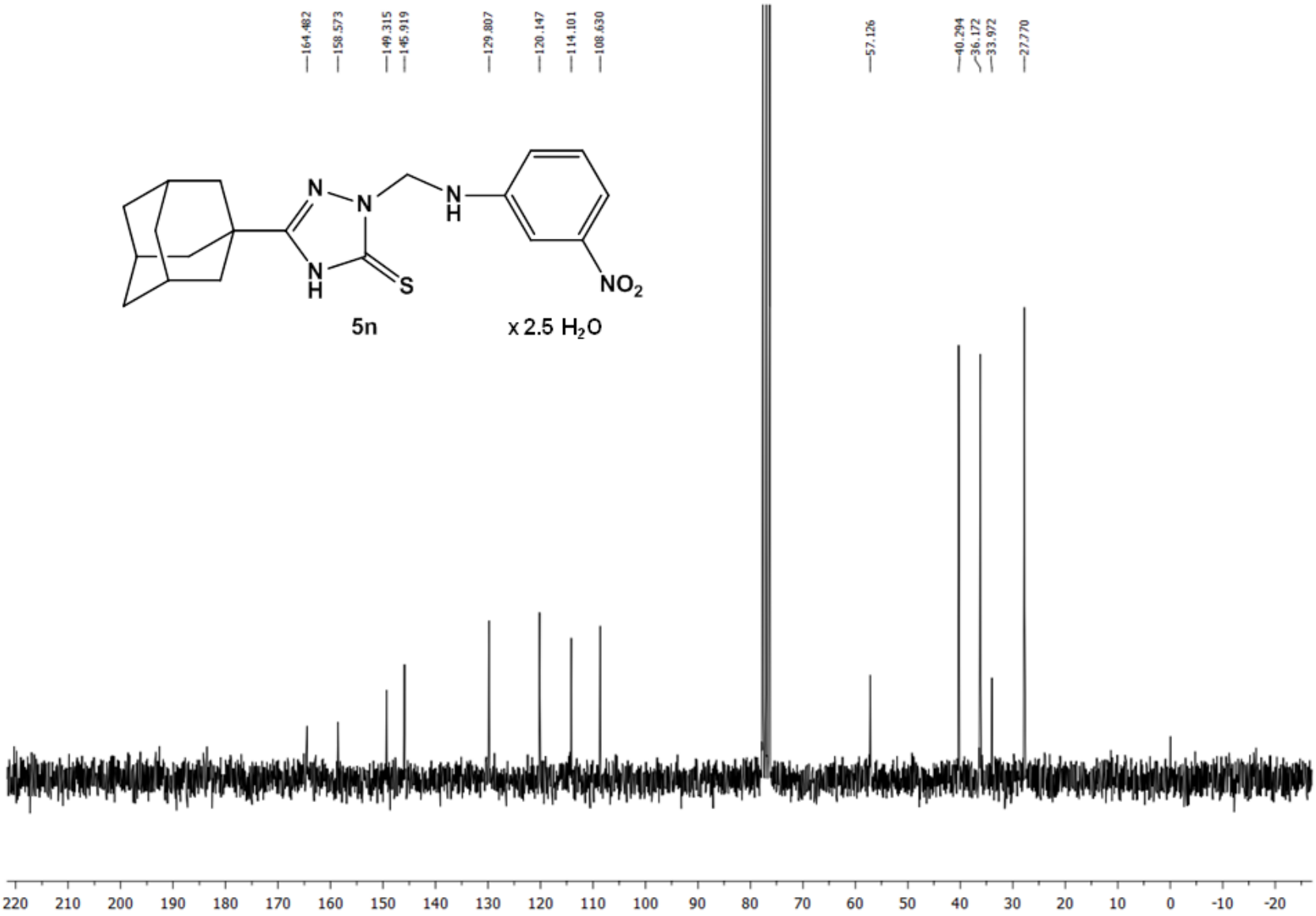

Figure S30: ^{13}C NMR spectrum of **5n** in $CDCl_3$ (50 MHz).

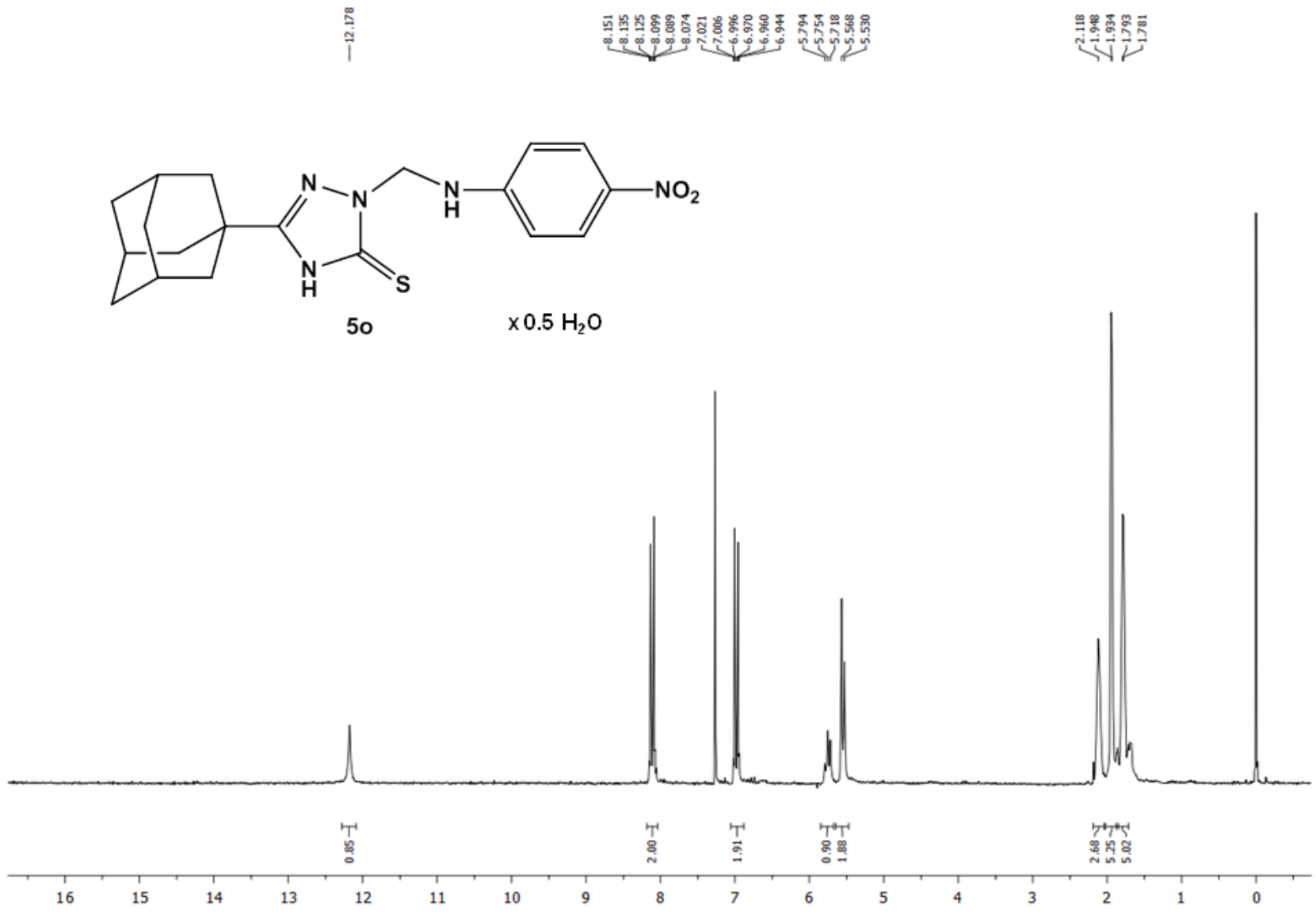

Figure S31: ^{1}H NMR spectrum of **5o** in $CDCl_3$ (200 MHz).

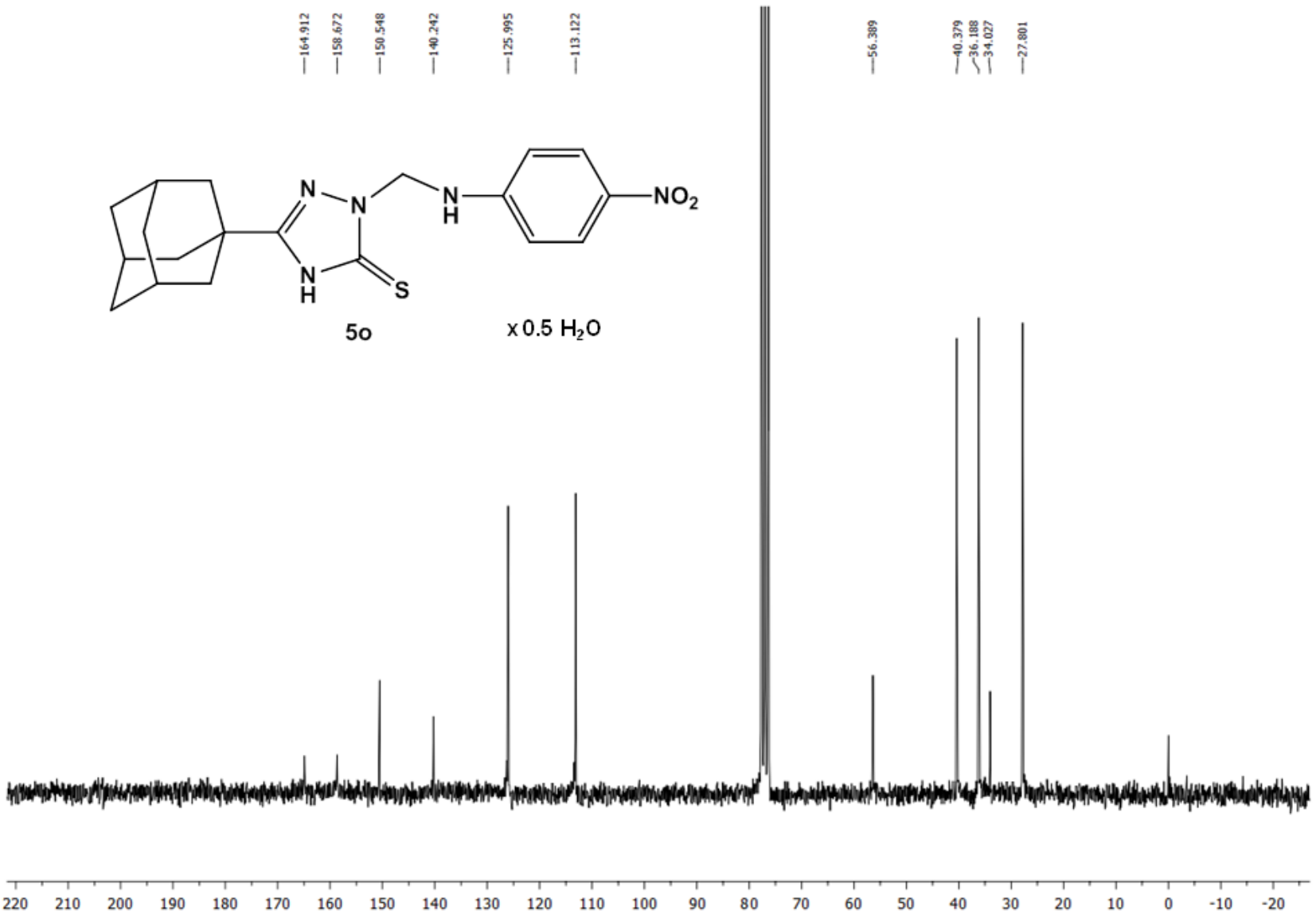

Figure S32: ^{13}C NMR spectrum of **5o** in $CDCl_3$ (50 MHz).

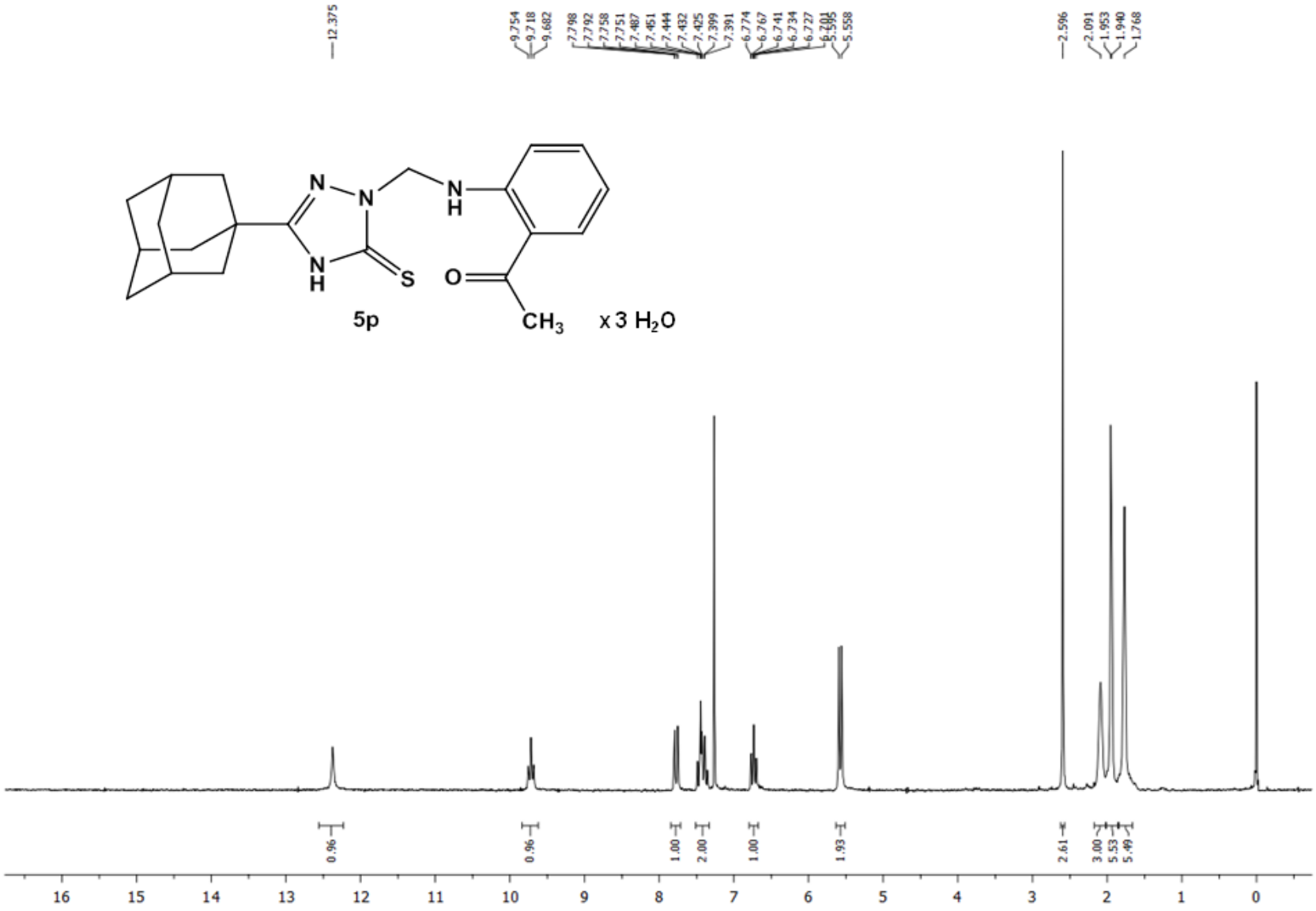

Figure S33: ^{1}H NMR spectrum of **5p** in $CDCl_3$ (200 MHz).

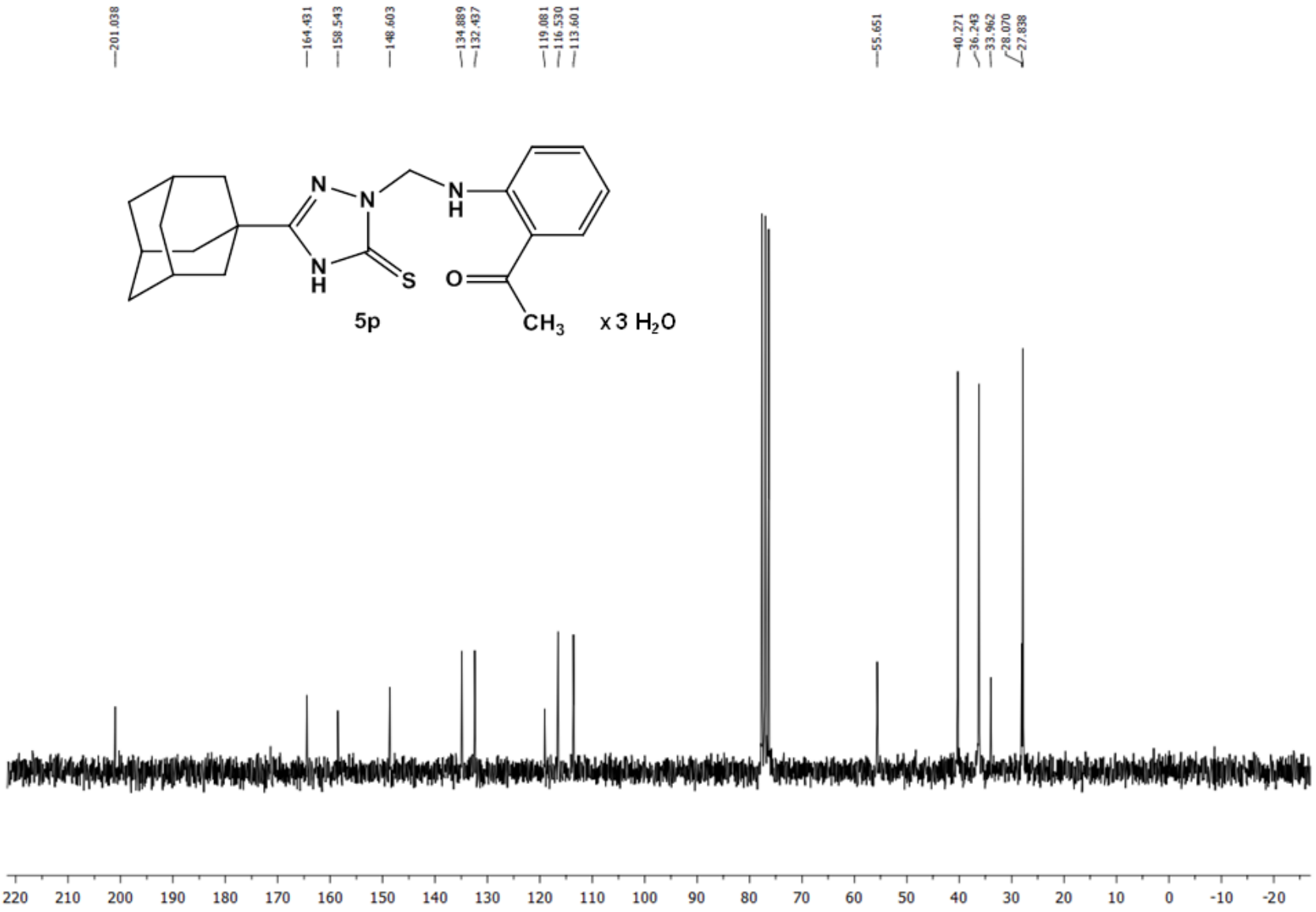

Figure S34: ^{13}C NMR spectrum of **5p** in $CDCl_3$ (50 MHz).

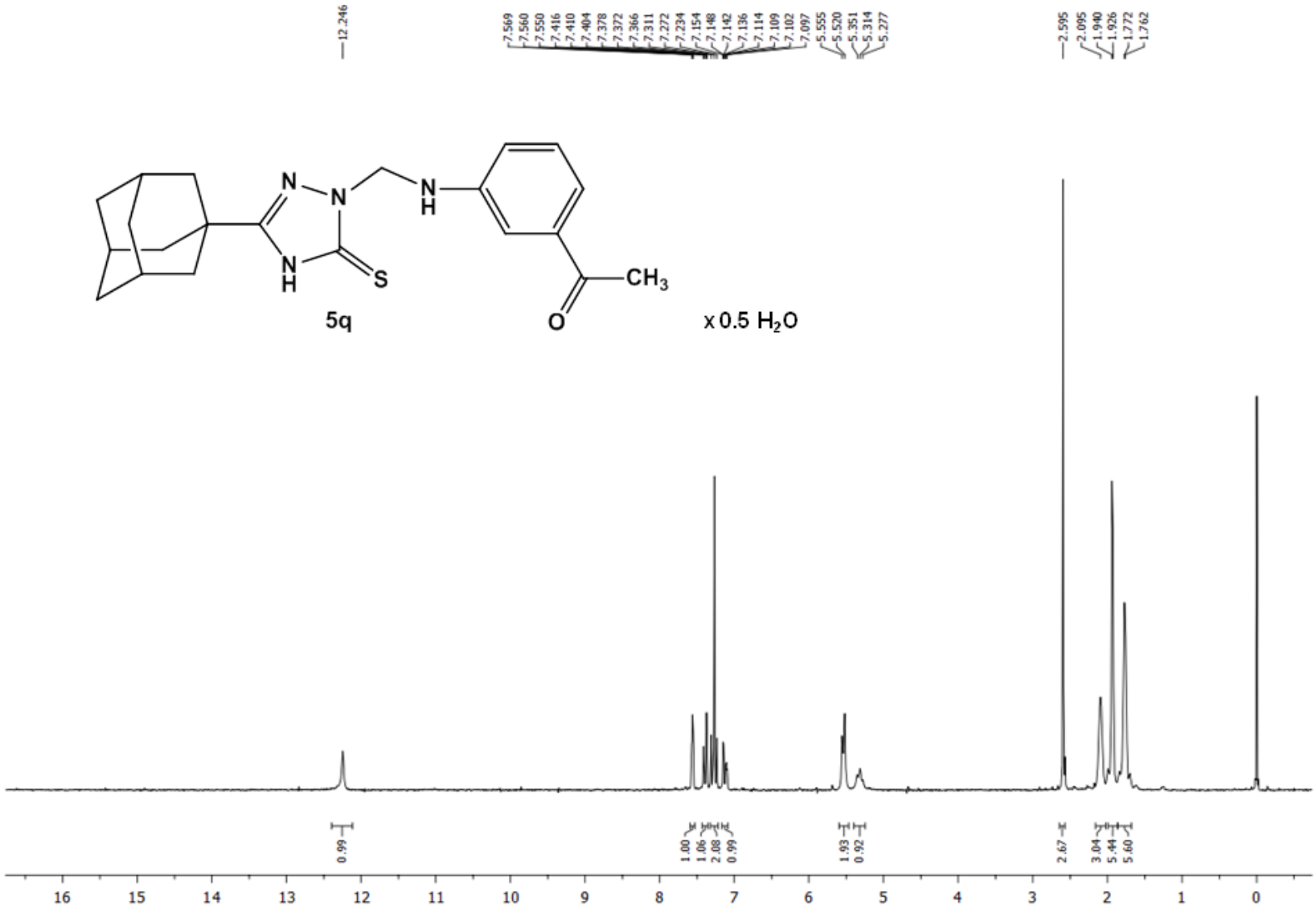

Figure S35: ^{1}H NMR spectrum of **5q** in $CDCl_3$ (200 MHz).

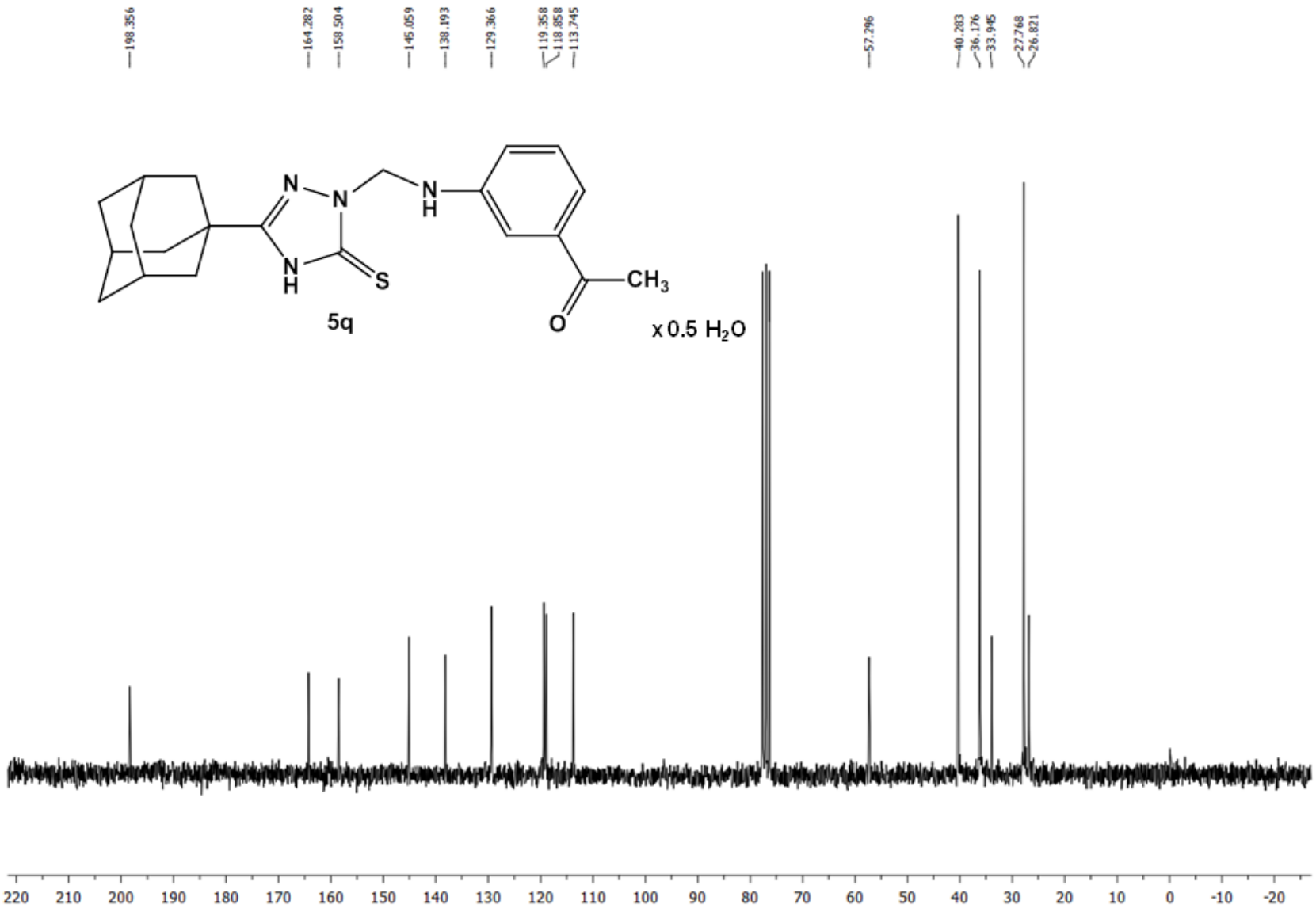

Figure S36: ^{13}C NMR spectrum of **5q** in $CDCl_3$ (50 MHz).

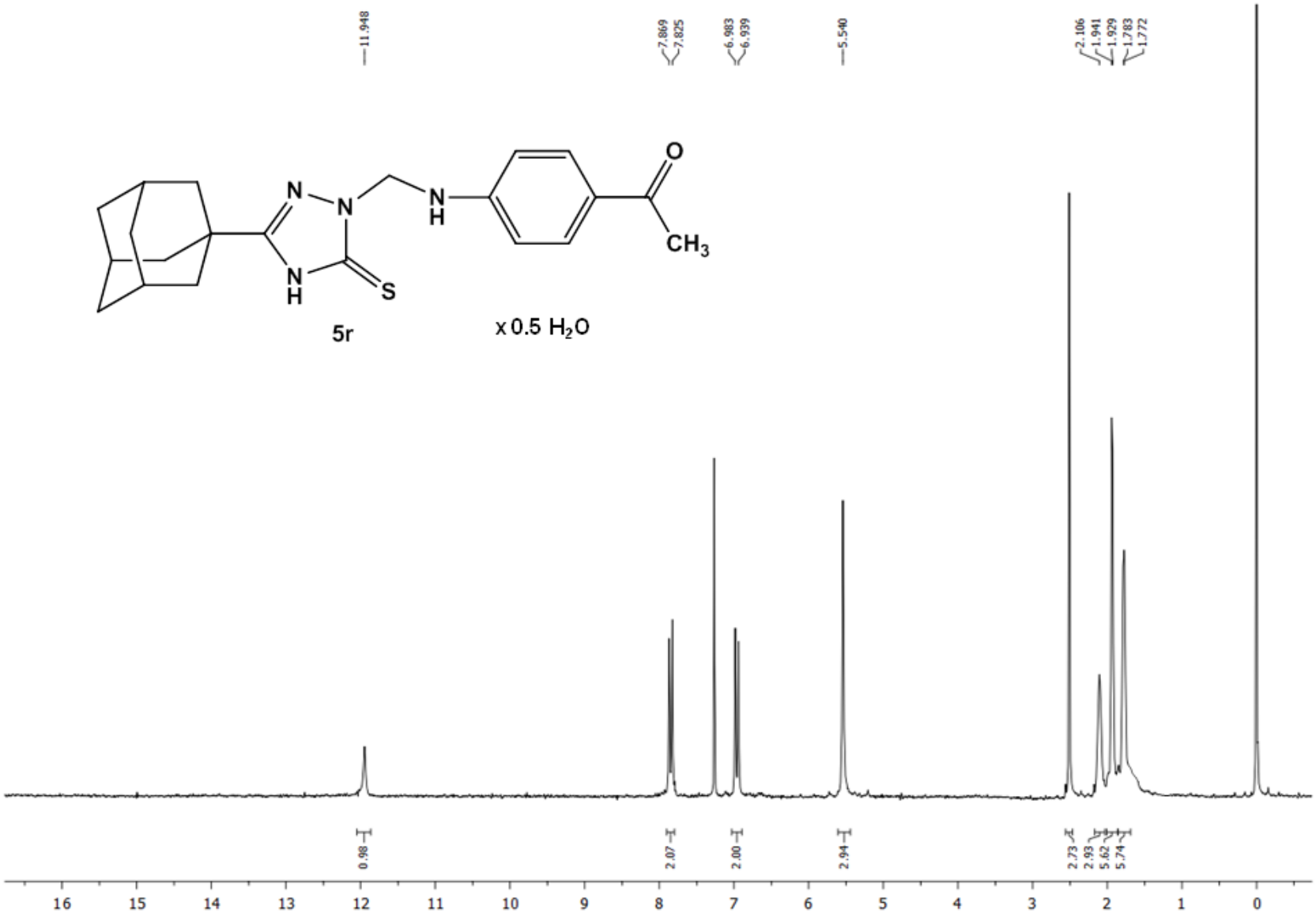

Figure S37: ^{1}H NMR spectrum of **5r** in $CDCl_3$ (200 MHz).

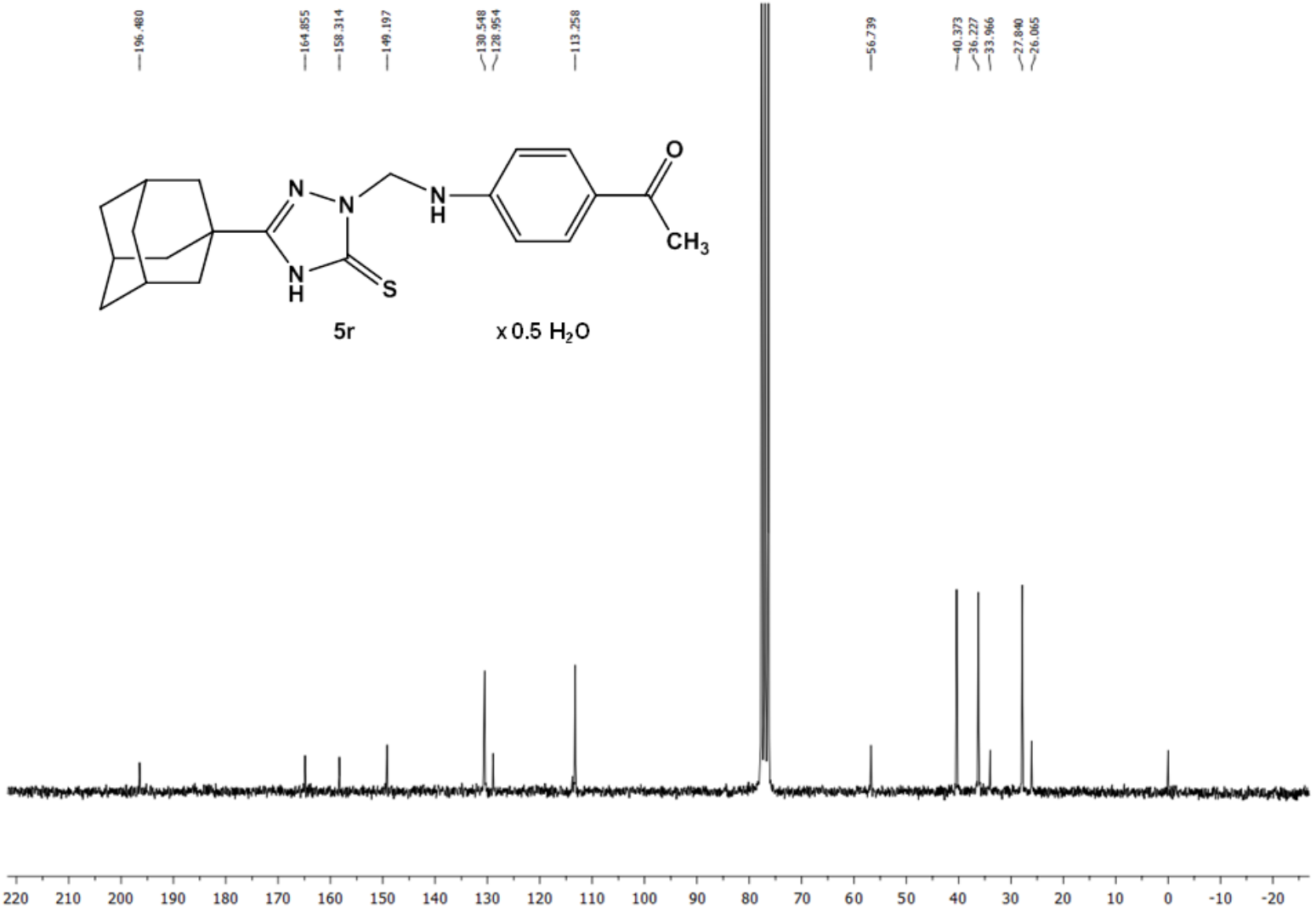

Figure S38: ^{13}C NMR spectrum of **5r** in $CDCl_3$ (50 MHz).

Crystal structure of compound 5e

The title compound crystallizes concomitantly as an orthorhombic (*Pbca*), and a monoclinic ($P2_1/n$) polymorph (these can be distinguished by their crystal habit). Structurally, two polymorphs differ in number of molecules in asymmetric unit and molecular packing (CIF files are deposited as CCDC 1465502–1465503). Namely, the orthorhombic polymorph crystalizes with one molecule in asymmetric unit, while the monoclinic polymorph crystallizes with two molecules, mutually related by non-crystallographic two-fold rotation axis. The three independent molecules in two polymorphic forms generally show structural similarity, and the differences are pronounced in conformations of side chains. The compound has V-shaped molecule (Figure 1, see article), with phenyl ring significantly inclined to the triazole ring. The dihedral angle between best planes through these rings are 61.67(11)° for orthorhombic form, and 82.98(11)° and 82.08(11)° for two molecules of the monoclinic form. Bond lengths in triazole rings are in their usual range; C1–S1 and C2–N1 bonds are double with lengths 1.678(2)–1.6928(19) Å and 1.298(2)–1.301(2) Å, respectively, while other bonds are classified as single between sp^2 hybridized atoms. Geometrical parameters of the triazole rings are similar to those found in structurally related compounds (Table S2).[1,2]

Additional structural difference between polymorphs is observed in the packing arrangements of their molecules (Figures S39 and S40). Namely, in the orthorhombic polymorph, two molecules are joined in a centrosymmetrical dimmer by pair of N3–H3···S1^{i} hydrogen bonds forming $R_2^2(8)$ motifs (symmetry code: (i) −*x*+2, −*y*+1, −*z*+1). Additionally, N4–H4···S1^{ii} hydrogen bond is present (symmetry code: (ii) *x*−1/2, −*y*+3/2, −*z*+1), which creates chain-type motif with the $C_1^1(6)$ descriptor. This results in further connection between the dimers so that a sheet of molecules is formed in the crystallographic *ab* plane. On the other hand, in the monoclinic polymorph the two crystallographically independent molecules are connected through the pair of N4*A*–H4*A*···N1*B* and N4*B*–H4*B*···N1*A* hydrogen bonds which results in formation of dimer motifs. These dimers are further connected by N3*A*—H3*A*···S1*B*^{i} and N3*B*—H3*B*···S1*A*^{ii} hydrogen bonds (symmetry codes: (i) *x*−1, *y*, *z*; (ii) *x*+1, *y*, *z*). All mentioned interactions are assigned with $D_1^1(2)$ descriptor in the first level network, whereas in the second level network they combine in two independent $R_2^2(10)$ and $R_2^2(8)$ motifs. It is interesting to note that these ring-motifs have non-crystallographic two-fold pseudo symmetry. As a result of combination of described hydrogen-bonding dimers, an infinite chain of molecules is formed parallel to the crystallographic *a* axis.

Crystal structure determination details and structural data

Diffraction measurements were performed on a Gemini S diffractometer (Oxford Diffraction) equipped with Sapphire CCD area detector. In all measurements a graphite monochromatized Mo *Kα* (0.71073 Å) radiation was used. Data collection strategy calculation, data integration, scaling and absorption correction were carried out with the *CrysAlisPRO*.[3] Structures were solved by dual-space methods by using the *SHELXT*,[4] and refined by full-matrix least-square methods on F^2 by using the *SHELXL*-2014.[5] The *ShelXle*[6] was used as a graphical user interface to the refinement procedures.

The non-H atoms were refined with anisotropic displacement parameters. In the case of monoclinic polymorph, the positional disorder of the adamantine cage was observed. The two positions of the substructure were refined using distance and ADP similarity restraints (see deposited CIF for details) together with refinement of the occupancy factor. Hydrogen atoms bonded to the carbon atoms were introduced in idealized positions and were refined using riding model. Hydrogen atoms bonded to nitrogen atoms were found by inspection of difference electron density maps; some of them are freely refined at isotropic level, while some are refined with distance restraints.

Additional geometrical analysis of refined structures and graphics preparing were made with the *PLATON*[7] and the *Mercury CSD 3.7*.[8]

A summary of the crystallographic data for crystal structures is given in Table S1. Crystallographic data have been deposited with the Cambridge Crystallographic Data Centre as Supplementary Publication Nos. CCDC 1465502–1465503. A copy of these data can be obtained, free of charge, *via* https://summary.ccdc.cam.ac.uk/structure-summary-form, or by emailing data_request@ccdc.cam.ac.uk.

Table S1: Experimental details

	Orthorhombic form	Monoclinic form
Chemical formula	$C_{19}H_{23}FN_4S$	$C_{19}H_{23}FN_4S$
M_r	358.47	358.47
Crystal system, space group	Orthorhombic, *Pbca*	Monoclinic, $P2_1/n$
Temperature (K)	567	294
a, *b*, *c* (Å)	8.7866 (2), 18.2502 (5), 23.2664 (6)	11.9693 (4), 20.9226 (11), 14.7933 (5)
α, β, γ (°)	90, 90, 90	90, 100.784 (3), 90
V (Å^3)	3730.91 (18)	3639.2 (3)
Z	8	8
Radiation type	Mo $K\alpha$	Mo $K\alpha$
μ (mm^{-1})	0.19	0.20
Crystal size (mm)	0.33 × 0.30 × 0.20	0.66 × 0.14 × 0.07
Diffractometer	Gemini S (Oxford Diffraction)	Gemini S (Oxford Diffraction)
Absorption correction	Analytical	Analytical
T_{min}, T_{max}	0.951, 0.965	0.927, 0.987
No. of measured, independent and observed [$I > 2\sigma(I)$] reflections	10911, 4353, 3044	17551, 8331, 4825
R_{int}	0.023	0.044
$(\sin \theta/\lambda)_{max}$ (Å^{-1})	0.681	0.685
$R[F^2 > 2\sigma(F^2)]$, $wR(F^2)$, S	0.049, 0.131, 1.02	0.053, 0.129, 1.01
No. of reflections	4353	8331
No. of parameters	316	467
No. of restraints	201	1
H-atom treatment	mixed	mixed
$\Delta\rho_{max}$, $\Delta\rho_{min}$ (e Å^{-3})	0.41, −0.36	0.23, −0.21

Table S2: Selected bond lengths and angles (Å, °)

Bond	Orthorhombic polymorph	Monoclinic polymorph	
		Molecule *A*	Molecule *B*
N1—N2	1.384 (2)	1.379 (2)	1.380 (2)
N1—C2	1.298 (2)	1.299 (2)	1.301 (2)
N2—C1	1.336 (2)	1.341 (2)	1.347 (2)
N2—C13	1.470 (2)	1.476 (2)	1.476 (2)
N3—C1	1.352 (2)	1.348 (2)	1.357 (2)
N3—C2	1.369 (2)	1.371 (2)	1.366 (2)
N4—C13	1.416 (3)	1.408 (3)	1.407 (3)
N4—C14	1.383 (3)	1.380 (3)	1.384 (3)
S1—C1	1.6928 (19)	1.6818 (19)	1.678 (2)
F1—C15	1.361 (3)	1.359 (3)	1.359 (3)
Angle			
C1—N3—C2	108.87 (15)	109.15 (15)	109.63 (15)
N2—C1—N3	104.11 (15)	103.68 (15)	103.05 (16)
N1—C2—N3	110.29 (16)	110.24 (16)	110.13 (16)
C2—N1—N2	104.48 (14)	104.30 (14)	104.49 (14)
C1—N2—N1	112.23 (14)	112.62 (14)	112.70 (15)

Table S3: Hydrogen-bond geometry (Å, º) for orthorhombic polymorph

D—H···*A*	*D*—H	H···*A*	*D*···*A*	*D*—H···*A*
N3—H3···S1^{i}	0.86 (2)	2.42 (2)	3.2722 (17)	176 (2)
N4—H4···S1^{ii}	0.78 (2)	2.74 (2)	3.447 (2)	151 (2)

Symmetry codes: (i) −*x*+2, −*y*+1, −*z*+1; (ii) *x*−1/2, −*y*+3/2, −*z*+1.

Table S4: Hydrogen-bond geometry (Å, º) for monoclinic polymorph

D—H···*A*	*D*—H	H···*A*	*D*···*A*	*D*—H···*A*
N3*A*—H3*A*···S1*B*^{i}	0.849 (19)	2.45 (2)	3.3010 (16)	174.2 (18)
N4*A*—H4*A*···N1*B*	0.78 (2)	2.47 (2)	3.180 (2)	151 (2)
N3*B*—H3*B*···S1*A*^{ii}	0.83 (2)	2.44 (2)	3.2624 (17)	170 (2)
N4*B*—H4*B*···N1*A*	0.81 (2)	2.62 (2)	3.290 (2)	142 (2)

Symmetry codes: (i) *x*−1, *y*, *z*; (ii) *x*+1, *y*, *z*.

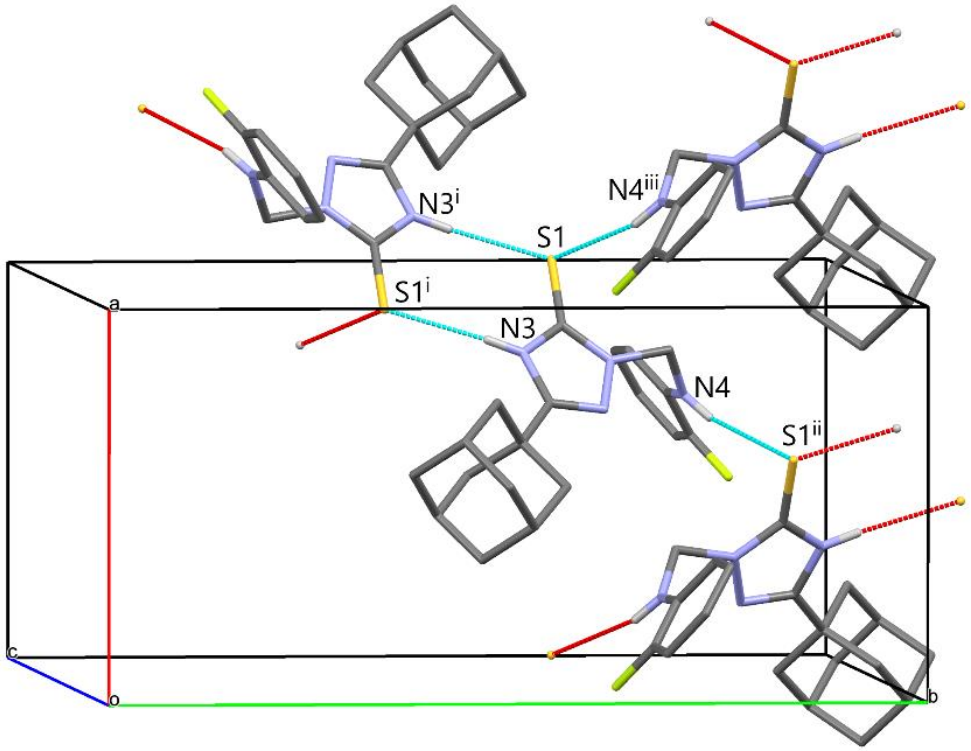

Figure S39: Hydrogen bonding in the orthorhombic form (see table S3 for symmetry operations).

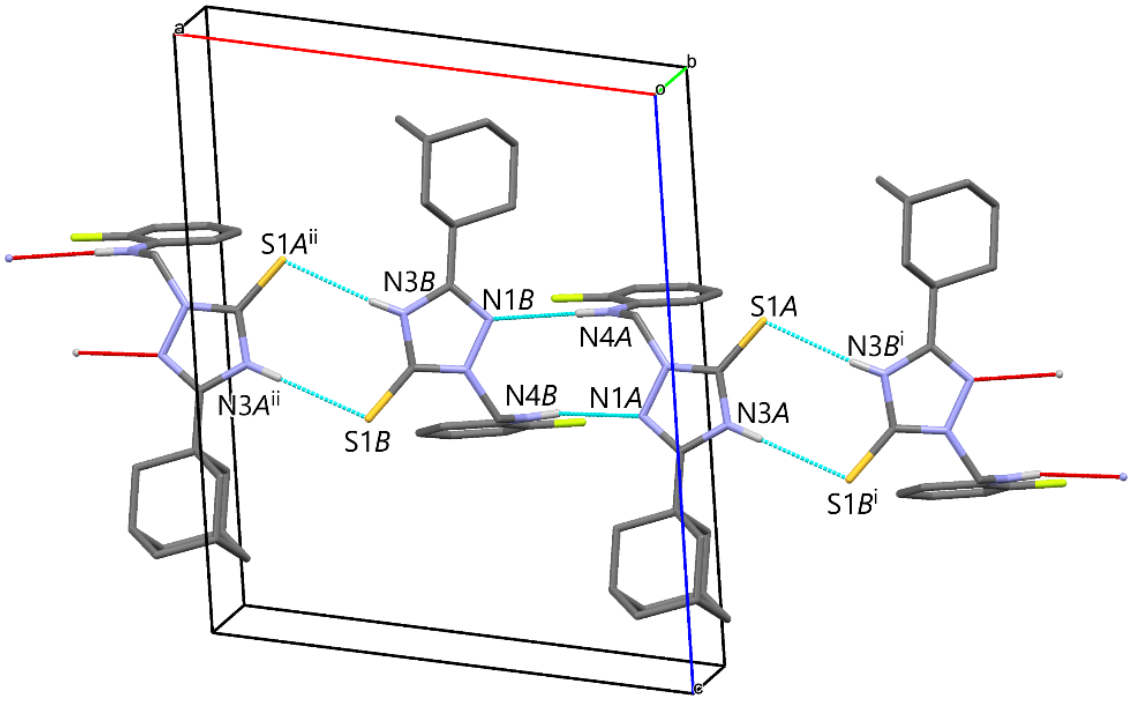

Figure S40: Hydrogen bonding in the monoclinic form (see table S3 for symmetry operations).

Biological experiments

Determination of cell survival

Briefly, 10 μL of MTT solution (5 mg/mL phosphate-buffered saline) was added to each well. Samples were incubated for a further 4 h at 37°C in a humidified atmosphere of 95% air/5% CO2 (v/v). Then 100 μL of 100 g/L sodium dodecyl sulfate was added to dissolve the insoluble product formazan resulting from conversion of the MTT dye by viable cells. The absorbance (A) at 570 nm was measured 24 h later. The number of viable cells in each well was proportional to the intensity of the absorbance of light, which was measured on a reader Multiskan EX Thermo Labsystems. To determine the cell survival (%), the A of a sample with cells grown in the presence of various concentrations of the investigated compounds was divided by the control optical density (the A of control cells grown only in nutrient medium) and multiplied by 100. In each experiment, the A of the blank was always subtracted from the A of the corresponding sample with target cells. IC_{50} is defined as the concentration of a compound inhibiting cell survival by 50% compared with a vehicle-treated control. As a positive control, cisplatin was used. All experiments were done in triplicate.

Molecular docking studies

Preparation of enzymes crystal structures

All of the selected complexes were loaded into UCSF Chimera v1.10.1 software[9] for Linux 64 bit architecture and visually inspected. For the experimental purposes preparation, complexes were initially superimposed to the **1F16** complex by means of the Matchmaker Chimera module. The proteins were improved by adding of hydrogen atoms using the embedded leap module of Amber 12 suite[10] and Amber parameters calculation by means of Antechamber using semiempirical QM method upon which the correct protonation at pH=7.4 was assigned to each amino acid residue. They were further energy minimized as follows: through the leap module they were solvated with water molecules (TIP3 model, SOLVATEOCT Chimera command) in a box extending 10 Å in all directions, neutralized with either Na^+ or Cl^- ions, and refined by a single point minimization using the Sander module of Amber suite with 1000 steps of the steepest-descent energy minimization and 4000 steps of conjugate-gradient energy minimization, with a non-bonded cuttoff of 5 Å. Prepared proteins were then separated in chains using the command line implementation of the Chimera split command which were used in further modeling.

Preparation of 5b structure

The structure of compound **5b** was generated using the Chemaxon's msketsh module[11] by means of molecular mechanics optimization upon which the correct protonation at pH 7.4 was assigned.

Preparation of homology modeled Bax-MOM complex

To the best of our knowledge there is no crystal structure of Bax immersed into the mitochondrial outer membrane (MOM). Therefore, the protein of interest was built using the homology modeling procedure as implemented in SwissModel automated web server.[12] The SwissModel Alignment Mode was used to prepare the conformationally changed Bax by submitting the human enzyme sequence (UniProt DataBase entry Q07812, 192 amino acids in sequence) and the Bax with C terminus truncated extracted from the **4BH8** crystal structure[13] to homology modeling protocol. Obtained homology modeled structure was finalized by Modeller software[14] implemented into UCSF Chimera by adding the missing residues and refining loops. Model was completed as the C terminal domain was inserted into the lipid membrane to create the complete membrane-aqueos system consisted of 192 amino acid residues, 128 DMPC molecules, 11 chlorine counter ions and 3655 water molecules. Transmembrane system was refined by a single point minimization using the Sander module of Amber suite with 100000 steps of the steepest-descent energy minimization and 40000 steps of conjugate-gradient energy minimization, with a non-bonded cuttoff of 5 Å.

AutoDock settings

AutoDock4.2 was used to perform the blind docking in this report. Prepared complexes were loaded into the AutoDockTools[15] and treated using the standard initiation protocol. Four subsequent molecular docking calculations were performed.

In the first docking experiment compound **5b** was docked into the Bax C terminal domain to generate Bax-**5b** complex. Docking was performed by setting up the center of Grid on Ser184. The xyz coordinates (in Ångströms) of the cuboid grid box used for the computation were Xmin/Xmax = -11.821/2.476, Ymin/Ymax = -17.574/-4.658, Zmin/Zmax = 4.839/21.167, with a spacing of 0.375 Å between the grid points, to embrace **5b** spanning 10 Å in all three dimensions. A total of 100 runs with RMS Cluster Tolerance of 0.5 Å were generated using the Lamarckian Genetic Algorithm, with default remaining run parameters.

For the purpose of the second and third docking experiments which implied the docking of Bax-**5b** into the Bcl-$_{XL}$ and Bcl-2 BH3 domains, Bax-**5b** was pre-aligned onto the chain B of Bcl-$_{XL}$ (PDB ID: **3PL7**)[16] and chain A of Bcl-2 (PDB ID: **2XA0**)[17], respectively, after which Bcl-$_{XL}$ chain A, Bcl-2 chain B, and chains C of both anti-apoptotic proteins, representing BH3 peptide, were removed from complexes. Afterwards, compound **5b** was re-docked into the Bax C terminus/ Bcl-$_{XL}$ chain B or Bax C terminus/ Bcl-2 chain A area using the same cuboid grid box and AutoDock parameters, allowing Asp98 and Ser184 to be flexible.

The final docking experiment was conducted on the C terminus of Bax-MOM system. Docking was performed by setting up the center of Grid on Ser184. The xyz coordinates (in Ångströms) of the cuboid grid box used for the computation were Xmin/Xmax = -9.023/8.052, Ymin/Ymax = -8.755/7.496, Zmin/Zmax = -8.280/13.149, with a spacing of 0.375 Å between the grid points, to embrace **5b** spanning 10 Å in all three dimensions. A total of 100 runs with RMS Cluster Tolerance of 0.5 Å were generated using the Lamarckian Genetic Algorithm, with default remaining run parameters.

Molecular dynamics simulations

The merged Bax-**5b**, Bax-**5b**- Bcl-$_{XL,}$ and Bax-**5b**-Bcl-2 complexes were used to perform explicit solvent molecular dynamics simulations. The parallelized Desmond Molecular Dynamics System and associated analysis tools, available within the Schrödinger suite 2009,[14] were used for this purpose. The models were prepared using the 'system builder' utility. The OPLS_2005 force field parameters were assigned for all the simulation systems. Each inhibitors-enzyme complex was placed in the centre of an orthorhombic box ensuring 10 Å solvent buffers between the solute and the boundary of simulation box in each direction. The TIP3 model was used to describe the water molecules. More, Na^+ and Cl^- ions were added at physiological concentration of 0.15 M to neutralize. The model systems were relaxed to 0.5 Å using the minimization protocol and subjected to a production phase, using the NPT ensemble and periodic boundary conditions for a period of 1.2 ns. The pressure control was used to maintain the pressure of the cell at 1.013 bar using the isotropic coupling method. The Nose-Hoover thermostat method was used to control the temperature at 310.15 K. Heavy atom-hydrogen covalent bonds were constrained using the SHAKE algorithm which allowed a 2-fs integration step to be used. The integration of the motion equation with RESPA multiple time step scheme was used in the simulations. Long-range electrostatic forces were computed using the smooth Particle-Mesh Ewald (PME) method. The cutoff distance for calculating short-range electrostatics and Lennard-Jones interaction was set to 9.0 Å. The trajectories and the energies were recorded at every 4.8 ps, respectively. The simulation quality analysis tool was used to analyze the trajectories obtaining RMSD and RMSF values, hydrogen bond distances, angles, and van der Waals interactions over the simulation trajectories.

MM-GBSA calculations and free energy decomposition

The binding free energy[18] of each system was calculated using *MM-GBSA* calculations according to the following equation (1):

$$\Delta G_{\text{bind}} = \Delta E_{\text{ele}} + \Delta E_{\text{vdw}} + \Delta G_{\text{solv}} - T\Delta S \qquad (1)$$

where ΔE_{ele} corresponds to the difference in electrostatic energy between the bound and unbound receptor-ligand states calculated using the OPLS_2005 force field, ΔE_{vdw} corresponds to the van der Waals energy contribution, while ΔG_{solv} is the corresponding contribution of the free energy of salvation calculated using the GB/SA continuum model. Embrace package implemented in MacroModel was used for the ΔE_{ele}, ΔE_{vdw}, and ΔG_{solv} calculations. The entropy change ΔS, was calculated utilizing the Rigid Rotor Harmonic Oscillator (RRHO) calculations. Applying this algorithm, the change in vibrational, rotational, and translational (VRT) entropy of the ligand binding was estimated. For the RRHO calculations, the representative complexes were pre-minimized using Desmond with explicit solvent retained; a 2000 steps LBFGS minimization (first 10 steps steepest descent) with residues beyond 15 Å of ligands restrained and a convergence criteria of 0.05 kcal $mol^{-1}Å^{-1}$ was used.

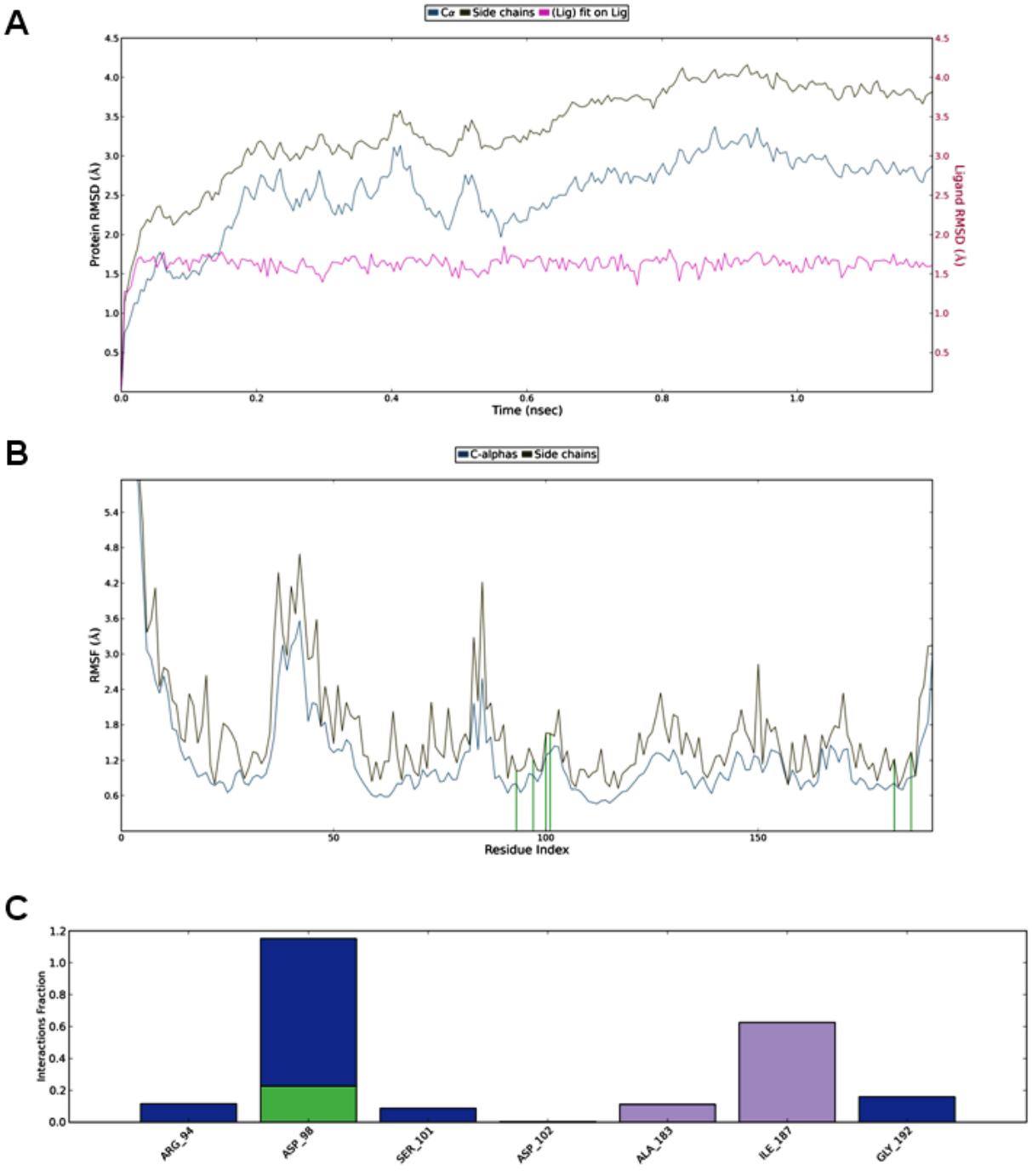

Figure S41: (A) Root Mean Square Deviations of Bax complexed with **5b**. (B) Root Mean Square Fluctuations of Bax complexed with **5b**. (C) Bax-**5b** interaction diagram. Green bars present hydrogen bonds, purple bars hydrophobic interactions, blue bars water bridges.

Molecular docking and molecular dynamics studies of Bax-5b-Bcl-$_{XL}$/Bax-5b-Bcl2 complexes formation

Mitochondrial dysfunction, in which IMS are released from the intermembrane space, is a critical step in the Bax-**5b**-mediated initiation of apoptosis[19] and is inhibited by Bcl-$_{XL}$ and Bcl-2.[20] Upon the activation, Bax-**5b** is hetero-dimerized with Bcl-$_{XL}$ and Bcl-2 in a way that C-terminal domain of pro-apoptotic protein is inserted in the α3-α4 hydrophobic groove of anti-apoptotic proteins.[17] Therefore, almost full flexible agonist-protein/protein molecular docking was further utilized to reveal the manner by which **5b** modulates the dimerisation process in the step (2) of the displacement model and alleviates the apoptotic event. Hence, Bax-**5b** complex, retrieved after the molecular dynamics stabilization, was docked into the Bcl-$_{XL}$ and Bcl2 α3-α4 groove (Figure S42).[17,20,21] During the second docking experiment, both Bax Ser184 and Asp98 were allowed to be flexible.

The **5b** was docked along with the Bax C-terminal helix in mainly hydrophobic environment of Bcl-$_{XL}$ and Bcl2, respectively. Within the lowest energy conformation, the agonist molecule adopted comparable pose to the one obtained after the molecular dynamics where RMSD values between the **5b-MD** and Bax-**5b**-Bcl-$_{XL}$/Bax-**5b**-Bcl2 **5b-BD** were 0.942 and 1.076 Å, respectively. The hydrogen bond between the 1,2,4-triazole-3(4*H*)-thione *N*4 HB donor and Bax Asp98-Met99 peptide bond carbonyl was as well established by molecular docking (d_{HB} = 2.363 Å within Bax-**5b**-Bcl-$_{XL}$, Figure S42A; d_{HB} = 2.368 Å within Bax-**5b**-Bcl2, Figure S42B). The 1,2,4-triazole-3(4*H*)-thione itself was in both complexes placed in front of Ser184 where sulfanylidene group was pointed towards Asp98 and involved in 4.188 Å long repulsive electrostatic interaction which forced the side chain of amino acid to be rotated for almost 90º away from α9 helix in comparison with the Bax crystal structure.[21] As for Bax-**5b**, in newly generated complexes there was no hydrogen bond between Asp98 and Ser184 inasmuch as in the obtained constellation, residue Asp 98, as former hydrogen bond donor, was 5.363 Å away from Ser 184. The Ser184 side chain hydroxyl group changed its orientation narrow to the imino nitrogen at position 4 of the 1,2,4-triazole-3(4*H*)-thione system to create another electrostatic attraction. Regarding the adamantly ring, it was, due to 1,2,4-triazole-3(4*H*)-thione transition, slightly allocated in comparison with the Bax-**5b** alignment towards Asp102 and was stabilized by hydrophobic attraction with Phe176 and Val180. The major difference in the alignment of **5b** between the Bax-**5b**-Bcl-$_{XL}$ and Bax-**5b**-Bcl2 was the positioning of 2-(*N*-(*o*-tolyl)aminoethyl scaffold. Within Bax-**5b**-Bcl-$_{XL}$ complex, the scaffold was tightly packed in sandwich-like conformation with the adamantly ring slightly touching the Bcl-$_{xL}$ surface due to hydrophobic interactions with anti-apoptotic protein Leu194 (Figure S42A). On the other side, within Bax-**5b**-Bcl2 the phenyl ring of the scaffold was immersed more deeply into anti-apoptotic protein surface where strong stabilization with Leu194 occurred (Figure S42B).

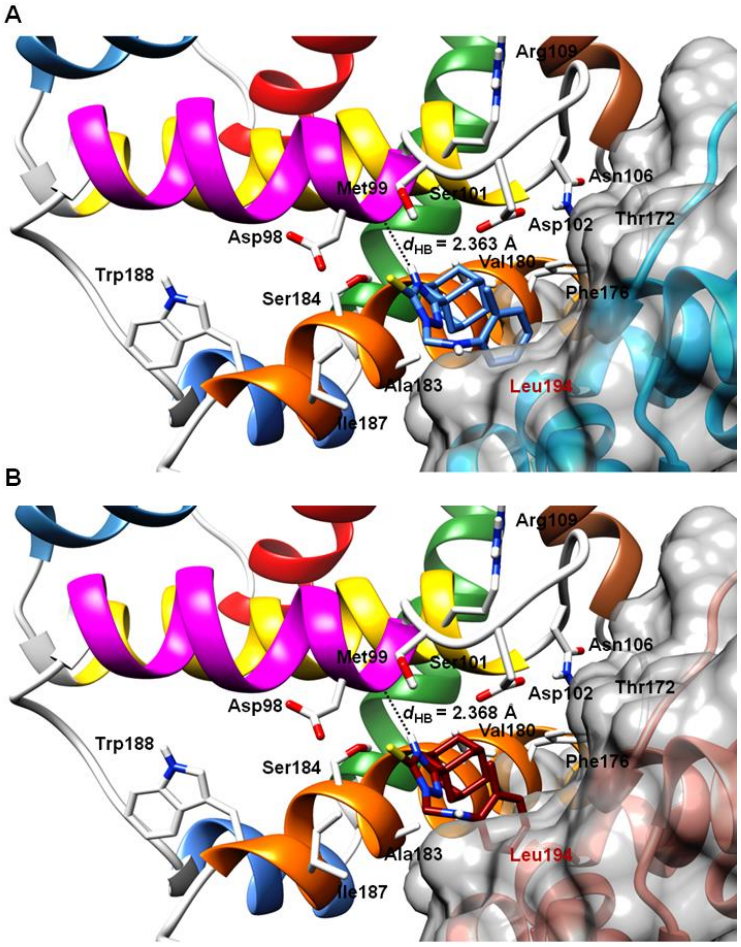

Figure S42: (A) The alignment of Bax-**5b** within the α3-α4 groove of Bcl-$_{XL}$ (for the clarity of presentation the Bcl-$_{XL}$ is depicted only blue ribbon in gray surface, **5b** is depicted in blue); **(B)** The alignment of Bax-**5b** within the α3-α4 groove of Bcl-2 (for the clarity of presentation the Bcl-$_{XL}$ is depicted only as red ribbon in gray surface, **5b** is depicted in dark red). The aminoacids belonging to Bcl-$_{XL}$ and Bcl-2 are labeled in red. (For interpretation of the references to colour in this figure legend, the reader is referred to the web version of this article.)

The stability of Bax-**5b**-antiapoptotic protein complexes was further on assessed trough molecular dynamics. The Bax-**5b**-Bcl-$_{XL}$ complex was stable after 1.0 ns of simulation by means of RMSD (Figure S43A) and RMSF values (range from 1.642 to 1.931 Å; Figure S43B). According to the binding affinity value (Table 2, ΔG_{bind} = -61.28 kcal/mol) **5b** was, along with the Bax, easily inserted into Bcl-$_{XL}$ remained stable due to the hydrophobic (Table 2, ΔE_{vdw} = -67.59±0.46 kcal/mol) and electrostatic interactions, too (Table 2, ΔE_{ele} = -34.39 kcal/mol). The most important result obtained from molecular dynamics was that the 1,2,4-triazole-3(4*H*)-thione *N*4 atom was during the period of simulation in 61% of time involved in hydrogen bonding with Asp98-Met99 backbone and 21% of time oriented towards Asp98 to make the same interaction

(Figure S43C). Established hydrogen bonds were the confirmation that 1,2,4-triazole-3(4*H*)-thione is the most important pharmacophore for the pro-apoptotic potential of **5b**. The adamantyl ring was stabilized by the interaction with Val80 and proximal hydrophobic residues, while the 2-(*N*-(*o*-tolyl)aminoethyl moiety was for the 43% of time engaged *via* the appertaining nitrogen donor in creating the hydrogen bond with Ser101. Therefore, the interference of *o*-tolyl with Bcl-$_{XL}$ Leu194 is not stabile and the functional group is more attracted with Ala183 and Ile187. However, even those hydrophobic interactions possess no strength to reduce the rotation of 2-(*N*-(*o*-tolyl)aminoethyl by which the amine nitrogen is oriented in vicinity of Ser101.

On the other hand, Bax-**5b**-Bcl-2 complex was relatively stable after 0.8 nm of simulation by means of RMSD (Figure S44A) and RMSF values (range from 1.679 to 1.846 Å; Figure S44B). According to the binding affinity value (Table 2, ΔG_{bind} = -60.42 kcal/mol) **5b** was, along with the Bax, also easily inserted into Bcl-$_{XL}$ and remained stable due to the hydrophobic (Table 2, ΔE_{vdw} = -67.41 kcal/mol) and electrostatic interactions, too (Table 2, ΔE_{ele} = -34.26 kcal/mol). As expected similar interactions were perceived for **5b** as in Bax-**5b**-Bcl-$_{XL}$ complex where the N4 of 1,2,4-triazole-3(4*H*)-thione for the 86% of time involved in Bax-**5b**-Bcl-$_{XL}$ hydrogen bond with Asp98-Met99 backbone (Figure S44C). However, there was no hydrogen bonding with between the **5b** and Ser101 most likely due to the low stabilization of 2-(*N*-(*o*-tolyl)aminoethyl moiety with Bax Ala183 and Ile 187.

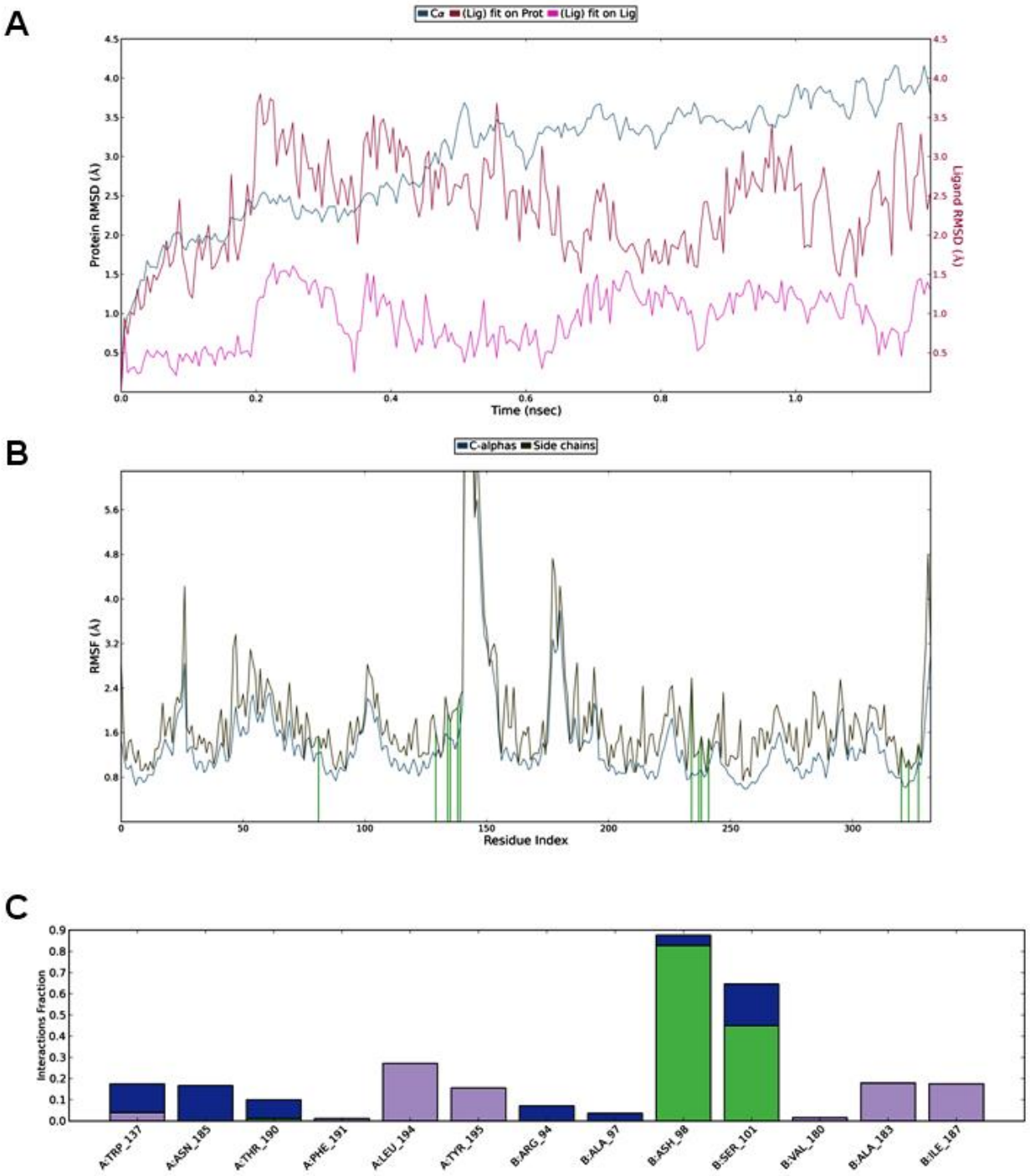

Figure S43: (A) Root Mean Square Deviations of Bax-**5b** complexed with Bcl-$_{XL}$. (B) Root Mean Square Fluctuations of Bax-**5b** complexed with Bcl-$_{XL}$. (C) Bax-**5b** interaction diagram. Green bars present hydrogen bonds, purple bars hydrophobic interactions, blue bars water bridges, Bcl-$_{XL}$ amino acids are labeled with A, Bax amino acids are labeled with B.

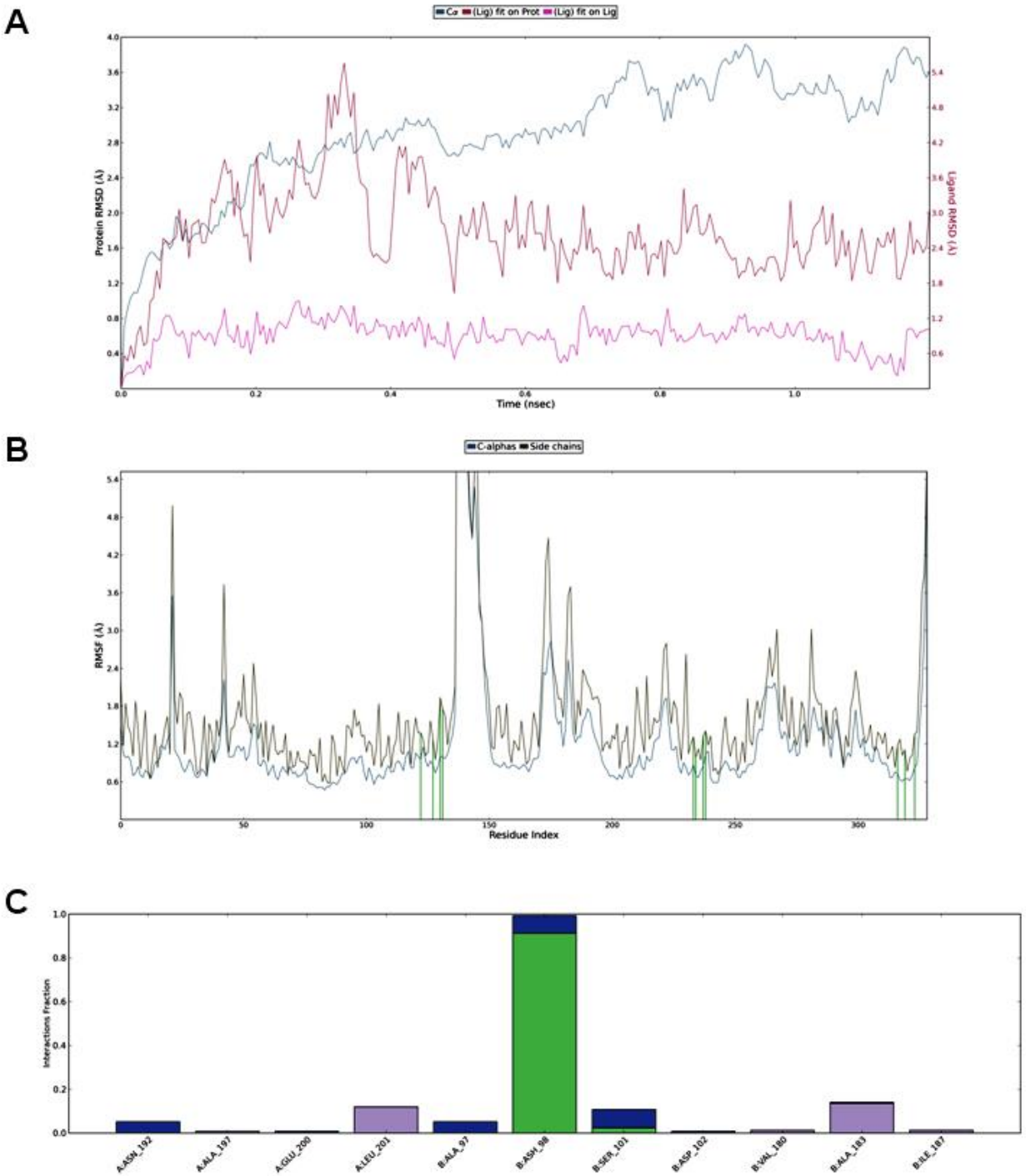

Figure S44: (**A**) Root Mean Square Deviations of Bax-**5b** complexed with Bcl-2. (**B**) Root Mean Square Fluctuations of Bax-**5b** complexed with Bcl-2. (**C**) Bax-**5b** interaction diagram. Green bars present hydrogen bonds, purple bars hydrophobic interactions, blue bars water bridges, Bcl-2 amino acids are labeled with A, Bax amino acids are labeled with B.

As proposed by the displacement model in the step 3), to initiate the apoptosis sensitizer BH3 proteins, like Bad, Noxa, Bik, Bmf, Hrk, and Bnip3, further displace Bax-**5b** from the antiapoptotic proteins to promote Bax-MOM permeabilization.[22] However, defining how Bax (or in this report Bax-**5b**) metamorphoses from an inert cytosolic monomer into the cytotoxic MOM-perforating oligomer has been deemed the "holy grail" of apoptosis research.[23] This pivotal step remains poorly understood, largely because no crystal structure of any activated form of Bax or Bax-agonist complex have been available. A progress was made with a recent crystallography studies which proved that Bax, truncated of α9 helix, undergoes homo-oligomerization after BH3 proteins are incorporated into the antiapoptotic canonical binding α3–α5 helixes groove.[13]

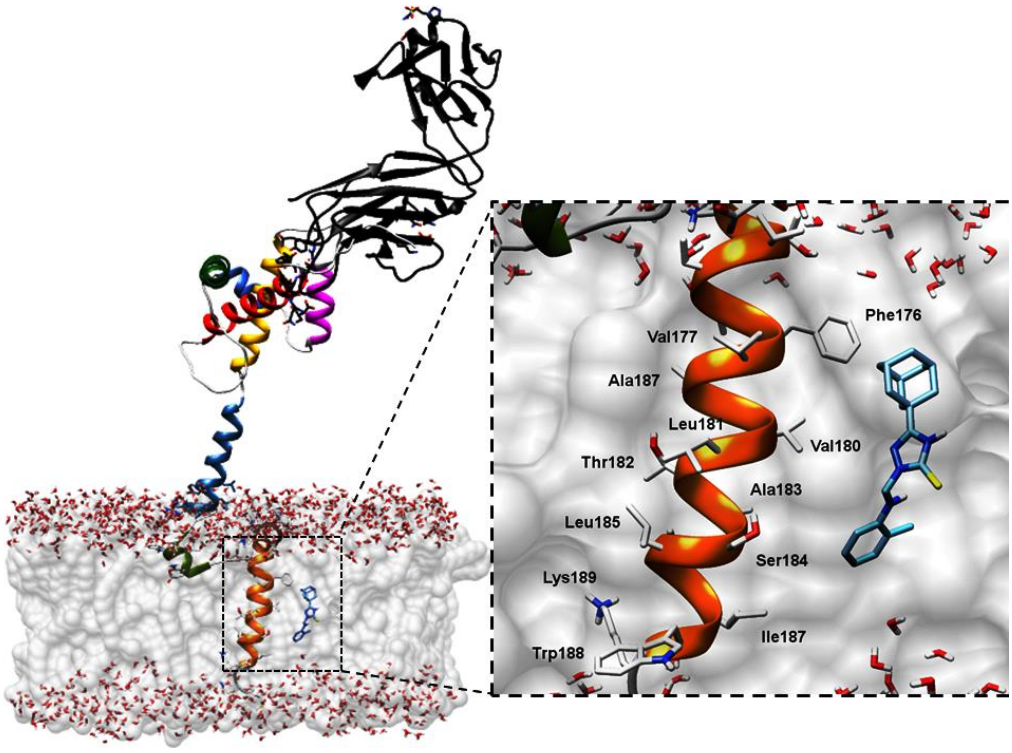

Figure S45: Homology modeled Bax immersed into the mitochondrial outer membrane (gray surface) and complexed with the monoclonal antibody 6A7 (black ribbons). The enlarged picture part represents the **5b** (depicted in blue) interference with the Bax α9 helix surrounded by lipid bylayer and water molecules. (For interpretation of the references to colour in this figure legend, the reader is referred to the web version of this article.)

Applying this finding to Bax-**5b**, the apoptotic event starts when the α9 helix is inserted into the mitochondrial outer membrane (step 4 of the displacement model). Prior to transformation helix 9 of Bax-**5b** is bound to the hydrophobic pocket in "cis," thus preventing helix 9 to insert into the MOM.[24] However, BH3 protein binding to the hydrophobic pocket

causes disruption of helix 9 interaction of with constitutive domain, making the C-terminus, along with the **5b** incorporated, available to interfere with the membrane. To reveal the role of **5b** during the membrane penetration, the C terminus of homology modeled Bax-**5b** in changed conformation was inserted in membrane environment to perform final docking experiment in this report (Figure S45). Within the lowest energy conformation, there were only hydrophobic interactions of limited strength between the **5b** and the α9 helix inasmuch as the average distance between the **5b** and C terminus was 5.361 Å. Not the single one of 100 generated conformations contained the strong attractive interactions between the agonist and the helix after which conclusion was made that the **5b** was prevented to interfere with the helix due to the strong stabilization in membrane hydrophobic environment. This practically means that **5b** has no influence on Bax penetration into the MOM and that it only protects the Ser184 from phosphorylation in order to facilitate the proapoptotic event.

Actual Bax conformational change (step 4 of the displacement model) occurs after the membrane penetration when the Bax α6–α8 domain (the "latch domain") is separated from the comprising helices α1–α5 region (the core domain).[13] The resulting process is the homo-oligomerization which occurs when the BH3 domain of one Bax-**5b** monomer is exposed and engages the of another activated Bax-**5b** monomer, forming "BH3-in-groove" dimers that multimerize by a separate interface.[25] The membrane disruption and the cytochrome c, OMI/HTRA2, SMAC/DIABLO, and endonuclease G (step 5 of the displacement model),[26] as well as the subsequent activation of capase-3 (step 6 of the displacement model, for the purpose of this study confirmed by western blotting) is controlled by monoclonal antibody 6A7 which binds to residues Pro13-Ile19, *i.e.* the portion of α1 Bax helix hidden in cytosolic form of Bax.[25] The epitope is exposed only transiently during the transition from monomer to dimer.

References

[1] H.-K. Fun, R. Kia, R. J. Samuel, K. Sujith, B. Kalluraya, *Acta Crystallogr. Sect. E* **2009**, *65*, o618.

[2] X.-D. Chen, H.-F. Wu, M. Du, *Chem. Commun.* **2008**, 1296.

[3] *CrysAlisPRO* Software system, Agilent Technologies UK Ltd., Oxford, 2014.

[4] G. M. Sheldrick, *Acta Crystallogr. Sect. A* **2015**, *71*, 3.

[5] G. M. Sheldrick, *Acta Crystallogr. Sect. C* **2015**, *71*, 3.

[6] C. B. Hübschle, G. M. Sheldrick, B. Dittrich, *J. Appl. Cryst.* **2011**, *44*, 1281.

[7] A. L. Spek, *Acta Crystallogr. Sect. D* **2009**, *65*, 148.

[8] C. F. Macrae, I. J. Bruno, J. A. Chisholm, P. R. Edgington, P. McCabe, E. Pidcock, L. Rodriguez-Monge, R. Taylor, J. van de Streek, P. A. Wood, *J. Appl. Crystallogr.* **2008**, *41*, 466.

[9] E. F. Pettersen, T. D. Goddard, C. C. Huang, G. S. Couch, D. M. Greenblatt, E. C. Meng, T. E. Ferrin, *J. Comput. Chem.* **2004**, *25*, 1605.
[10] D. A. Case, T. A. Darden, T. E. III Cheatham, C. L. Simmerling, J. Wang, R. E. Duke, R. Luo, R. C. Walker, W. Zhang, K. M. Merz, B. Roberts, S. Hayik, A. Roitberg, G. Seabra, J. Swails, A. W. Götz, I. Kolossváry, K. F. Wong, F. Paesani, J. Vanicek, R. M. Wolf, J. Liu, X. Wu, S. R. Brozell, T. Steinbrecher, H. Gohlke, Q. Cai, X. Ye, J. Wang, M.-J. Hsieh, G. Cui, D. R. Roe, D. H. Mathews, M. G. Seetin, R. Salomon-Ferrer, C. Sagui, V. Babin, T. Luchko, S. Gusarov, A. Kovalenko, P. A. Kollman, AMBER 12, University of California, San Francisco, 2012.
[11] Marvin Beans 15.4.27.0, 2015, ChemAxon (http://www.chemaxon.com).
[12] M. Biasini, S. Bienert, A. Waterhouse, K. Arnold, G. Studer, T. Schmidt, F. Kiefer, T. Gallo Cassarino, M. Bertoni, L. Bordoli, T. Schwede, *Nucleic Acids Res.* **2014**. *42*, 252.
[13] P. E. Czabotar, D. Westphal, G. Dewson, S. Ma, C. Hockings, W.D. Fairlie, E. F. Lee, S. Yao, A. Y. Robin, B. J. Smith, D. C. Huang, R. M. Kluck, J. M. Adams, P. M. Colman, *Cell* **2013**, *152*, 519.
[14] M. A. Marti-Renom, A. Stuart, A. Fiser, R. Sánchez, F. Melo, A. Sali, *Annu. Rev. Biophys. Biomol. Struct.* **2000**, *29*, 291.
[15] G. M. Morris, R. Huey, W. Lindstrom, M. F. Sanner, R. K. Belew, D. S. Goodsell, A. J. Olson, *J. Comput. Chem.* **2009**, *16*, 2785.
[16] P. E. Czabotar, E. F. Lee, G. V. Thompson, A. Z. Wardak, W. D. Fairlie, P. M. Colman, *J. Biol. Chem.* **2011**, *286*, 7123.
[17] B. Ku, C. Liang, J. U. Jung, B. H. Oh, *Cell Res.* **2011**, *21*, 627.
[18] J. H. Sng, V. J. Heaton, M. Bell, P. Maini, C. A. Austin, L. M. Fisher, *Biochim. Biophys. Acta* **1999**, *1444*, 395.
[19] M. Xin, R. Li, M. Xie, D. Park, T. K. Owonikoko, G. L. Sica, P. E. Corsino, J. Zhou, C. Ding, M. A. White, A. T. Magis, S. S. Ramalingam, W. J. Curran, F. R. Khuri, X. Deng, *Nat. Commun.* **2014**, *5*, 4935.
[20] J. Ding, Z. Zhang, G. J. Roberts, M. Falcone, Y. Miao, Y. Shao, X. C. Zhang, D. W. Andrews, J. Lin, *J. Biol. Chem.* **2010**, *285*, 28749.
[21] M. Suzuki, R. J. Youle, N. Tjandra, *Cell* **2000**, *103*, 645.
[22] M. Xin, R. Li, M . Xie, D. Park, T. K. Owonikoko, G. L. Sica, P. E. Corsino, J. Zhou, C. Ding, M. A. White, A. T. Magis, S. S. Ramalingam, W. J. Curran, F. R. Khuri, X. Deng, *Nat. Commun.* **2014**, *5*, 4935.
[23] R. J. Youle, A. Strasser, *Nat. Rev. Mol. Cell Biol.* **2008**, *9*, 47.
[24] A. Shamas-Din, J. Kale, B. Leber, D. W. Andrews, *Cold Spring Harb. Perspect. Biol.* **2013**, *5*, a008714.
[25] F. W. Peyerl, S. Dai, G. A. Murphy, F. Crawford, J. White, P. Marrack, J. W. Kappler, *Cell Death Differ.* **2007**, *14*, 447.
[26] T. Kuwana, L. Bouchier-Hayes, J. E. Chipuk, C. Bonzon, B. A. Sullivan, D. R. Green, D. D. Newmeyer, *Mol. Cell* **2005**, *17*, 525.